Copper Tin Sulfide thin film through Chemical Spray Pyrolysis: Material characterization and trials on device fabrication

Thesis submitted by

GINCY SUNNY

(University Registration Number : 4288)

in partial fulfillment of the requirements

for the award of the degree of

DOCTOR OF PHILOSOPHY

Under the guidance of

Dr. K. P. VIJAYAKUMAR

Thin Film Photovoltaic Division

Department of Physics

Cochin University of Science and Technology

Cochin - 682 022, Kerala, India

March 2019

Copper Tin Sulfide thin film through Chemical Spray Pyrolysis: Material characterization and trials on device fabrication

Ph.D. Thesis under the Faculty of Science

Author:
Gincy Sunny
(University Registration Number: 4288)
Thin Film Photovoltaic Division
Department of Physics
Cochin University of Science and Technology
Cochin - 682 022, Kerala, India.
Email: gincycusat@gmail.com

Supervisor:
Dr. K. P. Vijayakumar
Professor (Retd.)
Department of Physics
Cochin University of Science and Technology
Cochin - 682 022, Kerala, India.
Email:kpv@cusat.ac.in

Department of Physics
Cochin University of Science and Technology
Cochin - 682 022, Kerala, India.

March 2019

Dedicated to The Almighty, Family,
Teachers and Dear ones.....

DEPARTMENT OF PHYSICS
COCHIN UNIVERSITY OF SCIENCE AND TECHNOLOGY
COCHIN-682 022

Dr. K. P. Vijayakumar
(Supervising Guide)
Professor (Retd.)
Department of Physics
Cochin University of Science and Technology

Certificate

This is to certify that this thesis entitled "**Copper Tin Sulfide thin film through Chemical Spray Pyrolysis: Material characterization and trials on device fabrication**"is a bonafide record of the research work carried out by Ms. Gincy Sunny under my supervision in the Department of Physics, Cochin University of Science and Technology. The results embodied in this thesis or parts of it have not been presented for the award of any other degree.

I further certify that the corrections and modifications suggested by the audience during the pre-synopsis seminar and recommended by the Doctoral committee of Ms. Gincy Sunny are incorporated in the thesis.

Cochin - 22
25^{th} March 2019

Dr. K. P. Vijayakumar

Declaration

I hereby declare that the work presented in this thesis entitled "**Copper Tin Sulfide thin film through Chemical Spray Pyrolysis: Material characterization and trials on device fabrication**"is based on the original research work carried out by me under the supervision and guidance of Dr. K. P. Vijayakumar, Professor (Retd.), Department of Physics, Cochin University of Science and Technology, Cochin-682 022 and has not been included in any other thesis submitted previously for the award of any degree.

Gincy Sunny
Department of Physics,
CUSAT,
Cochin-22.

Cochin - 22
25^{th} March 2019

Acknowledgments

I would like to express my sincere gratitude to my supervising guide Dr. K. P. Vijayakumar for his valuable guidance given throughout my research work. I also express gratitude to Dr. Sudha Kartha for her inspiration and advice given throughout my research period.

I am thankful to Prof. Junaid Bushiri, Head of the Department and all former Heads of Physics department during the period of my research for providing the necessary facilities. Also, I am grateful to all the faculty members, office staffs of Department of Physics, and administrative office for all their help.

Financial support from MNRE (Ministry of New and Renewable Energy) and University Grant Commission for research fellowship are greatly acknowledged. I am thankful to Dr. Y Kashiwabara (Iwate University, Japan) and Dr. Rajeev Kumar (Department of Instrumentation, CUSAT) for their help during research work.

I am indebted to family and friends for their unconditional love and support.

Finally, I would like to thank everybody who was important to the successful realization of the thesis, as well as expressing my apology that I could not mention personally one by one.

Gincy Sunny

Preface

Environmental pollution and energy crisis are the major challenges of the 21st century. These major threats can be overcome by using renewable energy sources. In this scenario, solar energy is attention seeking one. Among the different solar energy conversion devices, solar cells are the elegant one. Even though solar energy is a clean and renewable source of energy, generally nonrenewable energy resources, such as petroleum and coal, are used to meet energy requirements nowadays. One of the major reason that hinders the widespread use of solar cells is its high cost. Currently, researchers focus on developing non-vacuum, simple, low cost and eco-friendly techniques for the production of photovoltaic devices. At present, the cost of the solar cell is high, making them economically uncompetitive with another conventional power source. The current photovoltaic industry mainly depends on silicon for solar cell fabrication. Even though silicon is abundant in the earth, the purification and the fabrication cost of silicon solar cell is very high. Vast research is going on to find a novel semiconducting material that is economical as well as eco-friendly.

The thesis describes the preparation condition and characterization of thin film solar cell deposited using chemical spray pyrolysis (CSP). CSP is a simple, low cost, non-vacuum, and reliable method for the thin film deposition. The research work is mainly focused on the absorber material used for solar cell fabrication. Here Copper Tin Sulfide (CTS) is used as absorber material for solar cell fabrication. CTS is one of the promising material for solar cell fabrication because of the optimum band gap and high absorption coefficient.

Chapter 1 Describes the importance of solar energy source among different energy sources. It includes the working of the solar cell, its origin, history, areas of application and its necessity in the present scenario. Some of the inorganic absorber materials currently used are mentioned in this chapter. Finally, we explain the reason for the selection of CTS as an absorber layer for the solar cell fabrication, followed by a short review on major highlights in the development of CTS based solar cells.

Chapter 2 Describes the deposition of CTS material using CSP deposition technique. The precursor solution for the spray, prepared by dissolving the salt of copper chloride, stannous chloride, and thiourea in demineralized water. In order to dissolve stannous chloride in demineralized water, 5% HCl is added. For obtaining device quality CTS thin film, the spray parameters should be optimized. A systematic variation of substrate temperature and copper concentration were done. From the characterization study, we optimize the substrate temperature and copper concentration. Solar cells were fabricated using the structure ITO/CTS/In_2S_3/Ag. From the J-V characteristic, the fabricated solar cell exhibit only dark junction without any light activity. The reason for this is due to the high thickness of the CTS layer so that the light cannot reach the junction between the absorber and the buffer layer. Thickness optimization of CTS layer is done, which results in light activity in the junction. The thickness variation is done through molarity variation of the CTS precursor solution and fine-tuning in the thickness of the CTS layer is also done by variation in the precursor solution volume.

Chapter 3 The device fabricated with stannous chloride precursor shows negligible efficiency due to the presence of HCl in the precursor solution. In order to avoid the presence of HCl, the stannous chloride precursor of tin is replaced by stannic chloride. The deposition condition and the characterization of CTS film with stannic chloride precursor are described in this chapter. The molarity, substrate temperature and spray rate of the precursor solution are also varied and structural, optical, electrical and morphological characterization was done. Solar cells were fabricated using the same structure ITO/CTS/In_2S_3/Ag and maximum efficiency of 0.84% was obtained.

Chapter 4 Deals with tuning the optoelectronic properties of the CTS film through variation in copper concentration, sulfur concentration, and tin concentration. In each case, the structural, optical, electrical, morphological and compositional properties were studied. Solar cells were fabricated with all the stoichiometric varied films and maximum efficiency was obtained for solar cell fabricated with copper: tin: the sulfur ratio of 1.6:0.4:12. Further improvement of the cell properties is done by introducing a thin layer of ZnO between ITO and CTS layer. But some difficulty observed with high resistance of ZnO

and it is overcome by doping ZnO with Al and solar cell fabricated with structure ITO/ZnO:Al/CTS/In_2S_3/Ag attained a maximum efficiency of 1.93%.

Chapter 5 CTS is one of the novel absorber material, the research work on CTS based solar cell is in its embryonic stage so we did not know which structure is better for solar cell fabrication (ITO/CTS/In_2S_3/Ag or ITO/In_2S_3/CTS/Ag) for the optimization of this, solar cells were fabricated with superstrate structure. The optimization of the top electrode, buffer layer, copper to the tin ratio of CTS layer, the thickness of In_2S_3 layer, the ratio of In_2S_3 layer and thickness of the CTS layer were done. For band structure tuning, ZnO:Al layer is introduced between the ITO and In_2S_3 layer which improved the efficiency of the solar cell up to 0.63%. On comparing the solar cell parameters of superstrate structure with ITO/CTS/In_2S_3/Ag, the superstrate structure shows less efficiency in all trials.

Chapter 6 Summarizes the main results and conclusions consolidated. The future outlook has also been discussed.

List of Figures

List of Tables

List of Abbreviations

AFM ..... Atomic force microscopy

CBD ..... Chemical Bath Deposition

CTS ..... Copper tin sulfide

CdTe ..... Cadmium telluride

GaAs ..... Gallium arsenide

CIGS ..... Copper Indium Gallium Selenide

CSP ..... Chemical spray pyrolysis

FF ..... Fill factor

FTO ..... Fluorine doped tin oxide

$\mathbf{I_{SC}}$ ..... Short circuit current

ITO ..... Tin doped indium oxide

$\mathbf{J_{SC}}$ ..... Short circuit current density

PLD ..... Pulsed Laser Deposition

PV ..... Photovoltaic

RMS ..... Root mean square

SEM ..... Scanning electron microscopy

SLG ..... Soda Lime Glass

TCO ..... Transparent conducting oxide

$\mathbf{V_{OC}}$ ..... Open circuit voltage

XPS ..... X-ray Photo electron spectroscopy

XRD ..... X-ray diffraction

Contents

Chapter 1

Introduction

Contents

1.1 Introduction

The rapid increase in world population and industrialization result in tremendous increase of energy usage and hence demand for energy is also growing. Current energy production mainly depends on nonrenewable energy; almost 85% of current energy is contributed by fossil fuels. Main reason for dependence on fossil fuel is simple process required for the production of heat and electricity from it; also the transport of fuel from one place to another can be done easily. Fossil fuel makes life easier; however it has very dangerous negative effects such as air pollution, acid rain, climate change etc. Also the demand for fossil fuel causes all over very high hike in the price that results in unbalanced economy in several countries. For the development of any country, energy resources play a crucial role. Search for new energy sources has to overcome problems of scarcity as well as environmental issues. Surely a transformation is required from current unsustainable energy to a sustainable one. The requirements of ideal energy source are: it should be environmentally friendly, energy supplied by nature, renewable source of energy, it is thus free and abundant, no noise, no moving part, no emission, no use of fuel and water for production, least maintenance requirement, long lifetime and modular custom-made energy can be sized for any application from watch to a multi-megawatt (say for a city).

Solar energy is one of the promising energy sources that full fill the condition of ideal energy source. Solar energy production can be generally classified into two: photothermal and photovoltaic. In photothermal technology, heat energy from the sun is trapped or light energy from the sun is converted in to heat

and that heat may be used directly or transformed into electricity. In the photovoltaic technique, photon energy is directly converted into electricity without any moving parts. Photovoltaic (PV) cells or solar cells are used for the conversion of light energy into electricity. Here we focus on photovoltaic conversion for energy production.

1.2 History of solar cell

- 1839: Alexandre-Edmond Becquerel (French physicist-father of nuclear Physicist Henry Becquerel) discovered photovoltaic effect in an experiment with electrolytic cell. The electrolytic cell consisted of electrodes, immersed in an electrolyte (silver chloride dissolved in an acidic solution). As a result of illuminating the cell, it produced current and voltage; hence initially photovoltaic effect was known as Becquerel effect [1].

- 1873: Willoughby Smith (English engineer) discovered the photoconductivity of selenium [2]. 1876: William Grylls Adams and Richard Evans Day observed electricity production when selenium was exposed to light [3].

- 1883: Charles Fritts invented the first solid-state solar cell using selenium and achieved an efficiency of 1-2%.

- 1887: Heinrich Hertz observed that irradiating metal surface with ultraviolet rays produce more power compared to the intensity of visible light [4].

- 1905: Albert Einstein publishes the theory of photoelectric effect named "On a Heuristic Viewpoint Concerning the Production and Transformation of Light" and for this contribution, he received the noble prize in 1921.

- 1916: Physicist Robert Millikan experimentally verified Einstein's theory of photoelectric effect.

- 1940: Russell Ohl discovered that a junction formed with n and p-type semiconductor exposed to bright light will produce an electric current.

- 1954: Physicists at Bell Labs (Daryl Chapin, Calvin Fuller, and Gerald Pearson) created the first practical photovoltaic silicon solar cell. This discovery of a silicon-based solar cell made a remarkable role in solar cell history.

- 1958: Vanguard, the first solar-powered space satellite was launched.

Regardless of the research made in solar cell technology, usage of solar cell for domestic application was strictly restricted due to its high price as compared to the conventional fuel. But the oil crisis in early 1970s made it clear for the first time that fossil fuel will become more expensive in the future and this leads to a very frantic search for new energy sources, forcing even oil Companies to invest for photovoltaic research. The huge research in the area of solar cell resulted in improvement of the technology due to which we can find a steep reduction in price (from hundreds of US $ to less than a Dollar), wonderful enhancement in (silicon) solar cell efficiency and development of very eco-friendly and earth abundant compound semiconductors for new cells, making this very useful technology affordable for common people.

1.3 Applications of solar cell

Nowadays, solar cells are used by people living even in remote spots and also in major cities. PV systems can be mainly categorized into the following groups: On-grid, Off-grid, and Hybrid solar system.

1.3.1 On-grid

In the case of On-grid or Grid-tie solar systems, PV system is connected to utility grid. Now a days grid-tie system is common in residential and commercial buildings, as there is no need for batteries. Moreover, as PV system is linked to the common electricity grid, any additional solar power produced is directly sent to the electricity grid and the customer gets credit for the energy produced.

1.3.2 Off-grid

An off-grid system (also known as a Stand-Alone Power System - SAPS) remains single home system not connected to the common electricity grid. In comparison with on grid system, the off-grid system required battery to store the power produced. An off-grid solar system is to be planned and designed properly so that it will produce sufficient power all over the year and have sufficient battery capacity. Additional cost of batteries makes off-grid systems more expensive than on-grid systems. Main application of the off-grid system is in remote areas that are far away from the common electricity grid. Similarly, areas under construction must require a power supply and the off-grid PV systems is a good choice. Electricity crisis occurs with natural calamities; disasters like floods, earthquakes, tsunami, and tornadoes destroy common electricity generation from hydropower, thermal and nuclear system and also destroy the distribution systems. In these situations, portable PV systems can offer short-term solutions for light, communication, water and food systems. Many scientific experiments which are set up in the regions far away from the utility power supply usually avail power from PV systems.

1.3.3 Hybrid

Currently market for hybrid solar system is growing rapidly. Modern hybrid systems use both off -grid and on - grid in one configuration. This means that excess energy produced in the day time is stored for consuming it in night. When battery stored energy is depleted, the grid act as backup, permitting consumers to have the best of both off the grid and on a grid systems.

1.4 Basic concepts of solar cell

Solar panels are composed of assembly of individual PV (solar) cells. The solar cell is the electrical device that converts light energy into electricity without any moving part. For this initially we must enhance the energy of carriers and then the carriers should be separated. Generally, semiconducting material is used for cell fabrication. Since a major portion of light energy (sunlight and other artificial light) is in visible range, and the material used for solar cell

fabrication should absorb radiation in this range; hence cells are fabricated using semiconductors which have strong absorption in the visible region. Some of the examples for semiconducting materials used for solar cells fabrication are silicon, copper sulfide, cadmium sulfide, gallium arsenide, indium sulfide, indium phosphide, copper indium selenide, copper indium sulfide etc. When light is incident on such a semiconducting material, electron hole pairs are created due to the absorption of light; but recombination also takes place with each other within a short interval of time either by radiative or non-radiative methods so that collection of charge carriers is not possible. Charge separation in semiconductor can be done by applying an external electric field to the semiconductor; but it is not worth in the case of the solar cell. Another method, in order to separate the charge carriers, is to create an asymmetry in electronic energy structure (band structure) in the semiconductor. Band structure modification can be done either by making junction with metal or with another semiconductor. Different kinds of semiconductor junctions are used for fabricating solar cells. These are mainly classified into Schottky junction and a p-n junction. In Schottky junction, a semiconductor is in contact with metal and in p-n junction, two layers of semiconductors with different types of majority carriers are in contact. Generally, p-n junctions are used for solar cell fabrication.

1.4.1 p-n junction

When p-type semiconductor and an n-type semiconductor are in direct contact with each other the boundary or interface between the semiconductor materials, is known as a p-n junction. The p-type semiconductor contains large quantity of free holes, and n-type semiconductor contains huge quantity of free electrons in the conduction band The free electrons on n-type semiconductor closer to the junction first migrate to the p-type semiconductor because of the higher concentration of free electrons in the n-type region than that of the p-type region. The electrons entering to the p region will combine with holes; the recombination of electron-hole pair results in negative ions in the p-type region near to the junction. Similarly migration of electron makes immobile positive ions near to the junction in the n-region. Once formation of the sufficiently dense ion layers takes place in both the n-type and p-type regions, there will be no further diffusion of charges from n-type to p-type or

vice-versa. The potential formed at the junction blocking further diffusion of charge carriers is known as Barrier Voltage. There are no free charge carriers in potential barrier region, making either sides of the junction completely depleted from free carriers and hence this area nearby the p-n junction is known as Depletion Region. Thickness of the depletion layer depends on doping concentration. The p-n junction performs very different way from single material. Schematic diagram of the p-n junction, potential difference at the junction shown in Figure 1.1.

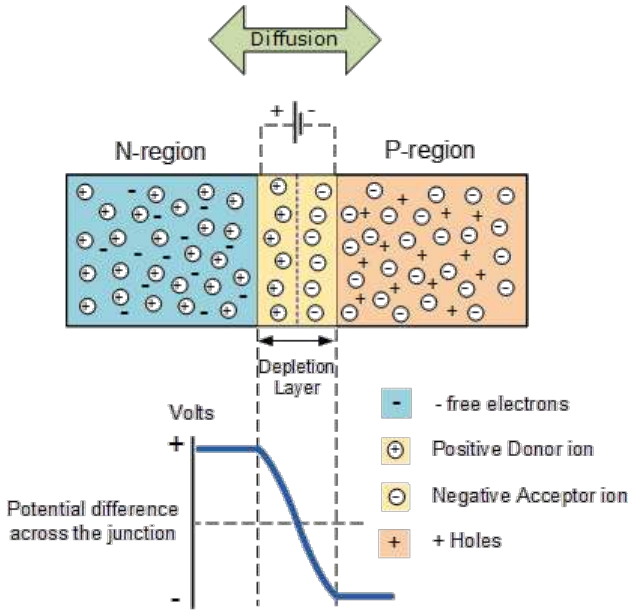

Figure 1.1: p-n junction [5]

1.4.2 Working principle of solar cell

When a p-n junction is illuminated through the absorber side, light enters into the absorber, probably reaching up to the junction. Major part of the photons entering the absorber will be absorbed createing electron-hole pairs. The barrier potential at the junction helps the charge separation, enabling free electrons created in the absorber and depletion regions move rapidly to the n side. In the same way, the holes created in absorber and depletion regions move to the p side of the p-n junction. This movement of newly created carrier to either side increases electron/hole concentrations in n/p

regions. The movement of photogenerated carrier set up a voltage and can flow through the connected external load resulting in current through the load.

1.4.3 The equivalent circuit of a solar cell

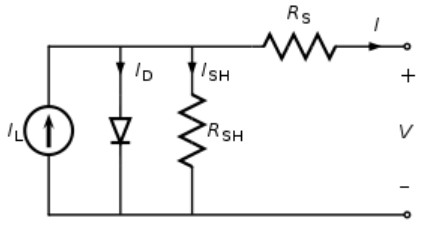

Figure 1.2: The equivalent circuit of a solar cell

In order to analyze behavior of a solar cell, an electrically equivalent model is usually used (Figure 1.2) [6] [7]. This is a theoretical circuit that holds all the electrical behaviors of a cell constructed by using well defined ideal electrical components. In the equivalent circuit, ideal solar cell is represented as current source and a diode is connected in parallel with it; but in practical case, no ideal solar cell exists! Hence resistance components (viz., Shunt resistance and Series resistance) are added to the model and the resulting equivalent circuit shown in the Figure1.2. Characteristic equation: The current produced using the solar cell (the output current) is equal to

$$\mathrm{I} = \mathrm{I_L} - \mathrm{I_D} - \mathrm{I_{SH}} \tag{1.1}$$

where

$I =$ output current
$I_L =$ light generated current
$I_D =$ diode current
$I_{SH} =$ shunt current

By the Shockley diode equation, the current diverted through the diode is:

$$I_D = I_0 \left[\exp\left(\frac{qV_j}{nkT} \right) - 1 \right] \tag{1.2}$$

where

$I_0 =$ reverse saturation current
$n =$ diode ideality factor (1 for an ideal case)
$q =$ charge of the electron
$k =$ Boltzmann's constant
$T =$ absolute temperature
$V_j =$ voltage across both diode and the shunt resistor (R_{SH})

V_j can be expressed as

$$V_j = V + IRs \tag{1.3}$$

where

$V =$ output voltage
$I =$ output current
$R_S =$ series resistance

By Ohm's law, the current through the shunt resistor can be expressed as

$$I_{SH} = \frac{V_j}{R_{SH}} \tag{1.4}$$

where, R_{SH} = shunt resistance.

Substituting all these into equation (1.1) (the characteristic equation of a solar cell). Then the output current through the solar cell

$$I = I_L - I_0 \left\{ \exp\left[\frac{q\,(V + IR_S)}{nkT} \right] - 1 \right\} - \frac{V + IR_S}{R_{SH}} \tag{1.5}$$

1.5 Solar cell Performance parameters

Solar cell performance can be analyzed by measuring four performance parameters i.e., open circuit voltage (V_{OC}), short circuit current density (J_{SC}), fill factor (FF) and efficiency (η).

1.5.1 Open circuit voltage (V_{OC})

The maximum voltage that is obtainable from a solar cell is the open circuit voltage (V_{OC}). It is the output voltage of the cell when no external current flows. Otherwise, the open-circuit voltage may be assumed as the voltage that requires a solar cell to stop the light generated current. V_{OC} is influenced by light generated current and considering the shunt resistance of the solar cell

as high the final term in equation (1.5) can be neglected. Then V_{OC} is given by(1.6).

$$V_{OC} \approx \frac{nkT}{q} \ln \left[\frac{I_L}{I_0} + 1 \right] \tag{1.6}$$

Therefore, for higher value of V_{OC}, value of % should be lower. Meanwhile,I_0 depends on the recombinations in the solar cell; higher value of band gap leads to lower recombination. The dependence of V_{OC} on bandgap is shown in Figure 1.3. So V_{OC} is actually a measure of the amount of recombination in the device. Surface and bulk recombinations are main factors that retard V_{OC} of a solar cell. An upper border for the open circuit voltage of a solar cell is the band gap and the lower values may be due to the sub band recombination processes in the cell.

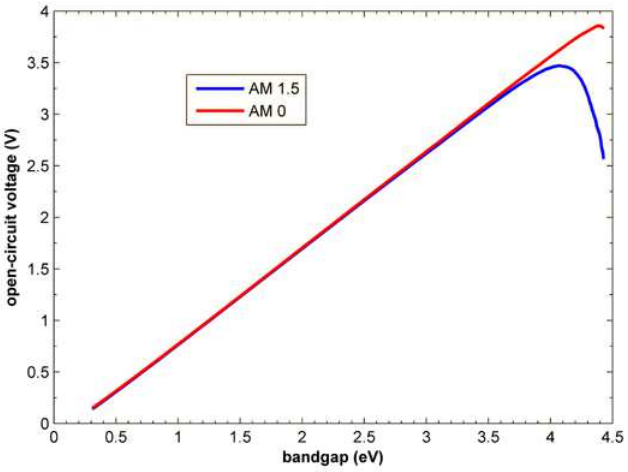

Figure 1.3: Dependence of V_{oc} on bandgap [8]

1.5.2 Short circuit current (I_{SC})

Short circuit current (I_{SC}) is the maximum current obtained from a solar cell when terminals of the solar cell are short-circuited. Short circuit current depends on a number of parameters like area of the solar cell, number of photons incident, optical properties of the material used for cell fabrication, minority carrier lifetime etc. This is determined by the spectrum of incident light and area of the solar cell. Generally, short circuit current density (J_{SC})

of the solar cell is analysed to eliminate dependence of the I_{SC} on area of the solar cell.

Band gap of the material has critical role in determining J_{SC} of a solar cell. Material with higher bandgap only absorbs less number of photons as compared to low band gap materials. Figure 1.4 shows the relationship between the J_{SC} and the band gap. J_{SC} increases with a reduction in band gap energy.

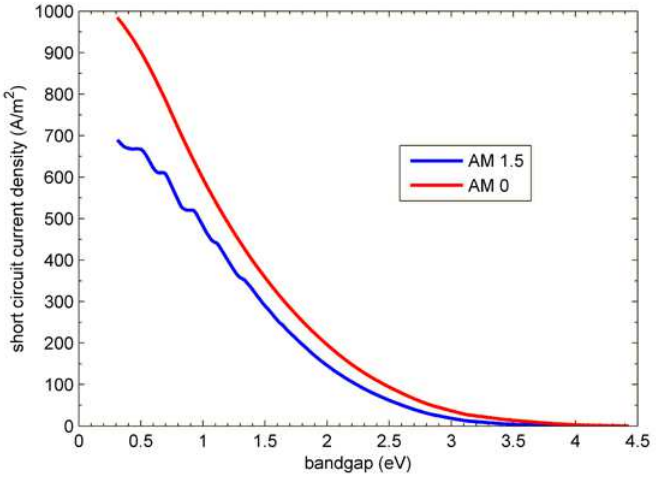

Figure 1.4: The relationship between the J_{sc} and the band gap [9]

1.5.3 Fill factor (FF)

Fill Factor (FF) determines quality of the solar cell. It is the ratio of maximum power (P_{MAX}) to the theoretical power (P_T). The theoretical power is product of open circuit voltage and short circuit current. For ideal case, maximum power and theoretical power are the same and the fill factor is 100%; in that case, the I-V curve is a perfect rectangle. But in practical case, I-V curve is not perfect rectangle and hence fill factor always less than 100%. FF explains graphically as the squareness of the I-V curve of the solar cell.

$$FF = \frac{P_{MAX}}{P_T} = \frac{I_m \cdot V_m}{I_{SC} V_{OC}} \tag{1.7}$$

Fill factor of a solar cell depends on the parasitic resistance (the series and

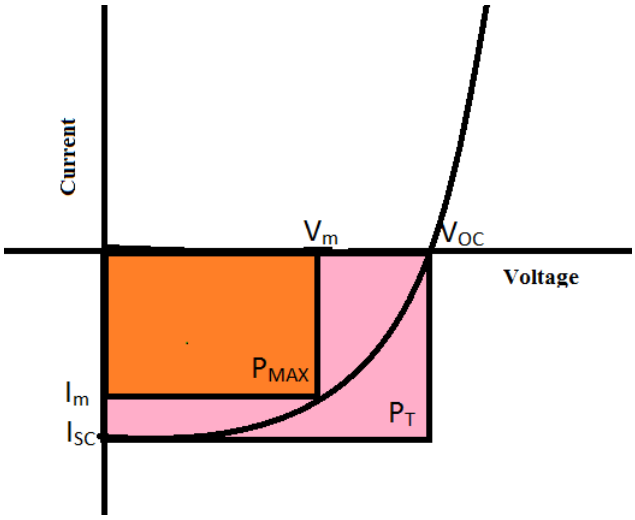

Figure 1.5: I-V characteristics of solar cell

shunt resistance). Series resistance is the total of resistances due to all elements that arise in the path of the current flow. Series resistance of the ideal solar cell is zero. With an increase in the series resistance, voltage drop also increases within the cell and this result in a deviation of I-V curve as shown in Figure 1.6. Low shunt resistance is providing an alternate path for light

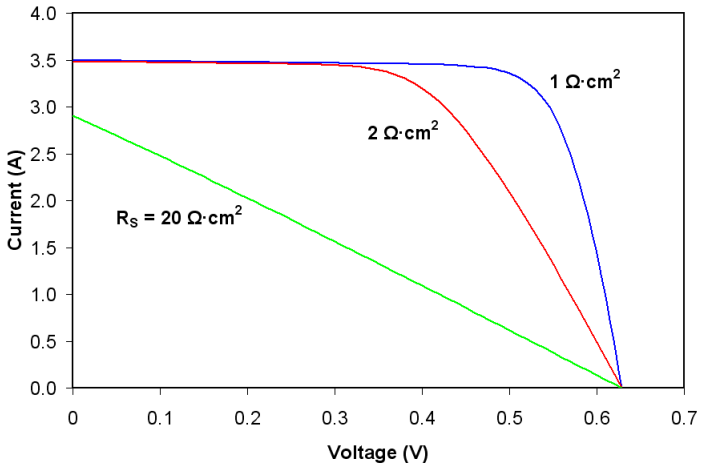

Figure 1.6: Deviation of I-V curve with series resistance [10]

generated current which reduces the output power of the solar cell. For an ideal solar cell, the shunt resistance should be infinite. The I-V curve starts to fall towards the origin as shunt resistance decreases (Figure 1.7).

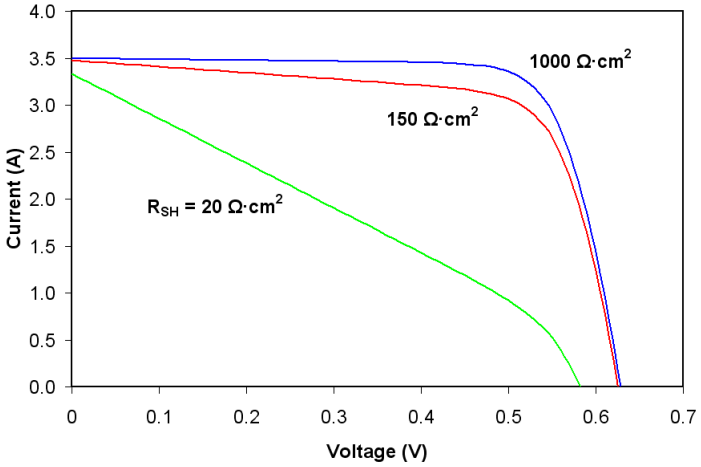

Figure 1.7: Deviation of I-V curve with shunt resistance [10]

1.5.4 Efficiency of the solar cell

Efficiency of a solar cell is ratio of output energy to energy input (light). The performance of different solar cells is compared by analyzing the efficiency of the solar cell. Cell efficiency depends on some external parameters like incident light spectrum and intensity and temperature at which measurement of the solar cell is done. Therefore, solar cell analysis is done at standard test condition (STC). The conditions for STC: a solar cell is analysed under AM1.5 conditions and temperature of 25 °C.

The I-V curve of solar cell is shown in the Figure 1.5 and the maximum power point can be obtained from the curve. At V_{OC} maximum voltage is obtained from the cell; but the current is zero. This results in zero output power. Similarly, at I_{SC} maximum current is obtained from the solar cell; but the voltage at this point is zero. Hence that also leads to zero output power. Hence maximum power point lies in between I_{SC} and V_{OC}. Maximum power point is obtained by fitting rectangle with maximum area in the I-V curve as shown in Figure1. 5. Maximum power point is denoted by Pm with Vm and Im as the corresponding voltage and current. Then the efficiency of the solar cell can be defined as

$$\eta = \frac{\text{output power}}{\text{input power}} \times 100 \tag{1.8}$$

$$\eta = \frac{V_m I_m}{P_{in}} \times 100 \tag{1.9}$$

$$\eta = \frac{\mathrm{V_{OC}} \cdot \mathrm{I_{SC}} \cdot \mathrm{FF}}{\mathrm{P_{in}}} \times 100 \tag{1.10}$$

1.6 Different materials used for solar cell fabrication

Current PV market mainly depends on silicon-based solar cell. Almost 90% of solar modules are produced from crystalline silicon (multicrystalline and monocrystalline silicon) while the rest part is made up of thin-film technologies. Silicon is one of the abundant materials in the earth crust, but the purification cost of silicon for solar cell fabrication is very high that leads to high cost of the solar cell. For thin film solar cells, minimum material is required for cell fabrication and also most of the thin film solar cells are made up of material which is abundant in the earth crust. The heart of thin film solar cell is the absorber layer which is responsible for the absorption of light and conversion of light into free carrier. Different types of absorber materials are used for industrial thin film solar cell fabrication. The major industrially successful solar cells are listed below

1.6.1 Cadmium Telluride (CdTe)

A thin film of CdTe absorbs the sunlight and converts into electricity. Huge research is done on CdTe because the band gap ($\sim$ 1.5 eV) is optimum for solar cell absorber layer. Solar cell is usually fabricated by making heterojunction between p-type CdTe and n-type cadmium sulfide (CdS) and the cell is completed by introducing top and bottom electrical contacts. The main advantage of CdTe based solar cell is that the manufacturing cost is much lower than silicon-based cells. It is the second top material used for solar cell fabrication and more than half of thin film technology depends on CdTe PV technology. CdTe has some disadvantages too; Cadmium is one of the top toxic materials and Tellurium is scarce. In February 2016, First Solar declared that CdTe cells had reached maximum conversion efficiency 22.1%.

1.6.2 Gallium Arsenide (GaAs)

Gallium arsenide (GaAs) is the most commonly used III-V compound semiconductor for PV applications. This material has direct band gap (1.43 eV) and high electron mobility. Single junction GaAs solar cell devices reached efficiency almost close to 29%. The main advantage of GaAs solar cell is its flexibility and lightweight in comparison with Si solar cell. It shows high resistant to the radiation damage so that GaAs is much suitable for space applications. The main disadvantage of this solar cell is its high cost.

1.6.3 Copper Indium Gallium Selenide (CIGS)

It is a compound semiconductor material of I-III-VI_2 group and is composed of copper, indium, gallium, and selenium with chemical formula of $CuIn_xGa_{(1-x)}Se_2$; the band gap can be varied from 1 to 1.7 eV with stoichiometric variation. This material shows high absorption coefficient ($>10^5$/cm). Comparison with CdTe solar cell, CIGS solar cell is environment-friendly. But it has some disadvantage like high cost of Indium in comparison with Si and CdTe solar cell. Another difficulty is that the cell required encapsulation; otherwise moisture can damage the cell [11].

1.6.4 Silicon solar cell

Silicon is an abundant and non-toxic material. Four major types of Si based solar cells are available in the market; crystalline silicon cells, amorphous silicon cells, amorphous/microcrystalline and thin-film polycrystalline silicon cells.

1.7 Emerging photovoltaics

Till now CdTe, CIGS, GaAs and a-Si thin film materials are extensively studied and solar cells based on these materials are commercially developed. CdTe and GaAs solar cells are not widely used due to environmental (toxicity) and economic issues. Hence, huge research is done related to CIGS and this material considered as a substitute material to Si. However production technique of CIGS is more complicated than that of CdTe.

In order to collect more energy from the sun, we must discover novel material for the absorption of light, with low-cost deposition techniques. Huge research was done to find out such novel absorber material that has properties such as nontoxicity, low cost, high absorption coefficient, optimum band gap etc. Main research on the inorganic absorber material is done in chalcogenide compounds. Binary absorber material similar to CdTe like SnS, SnS_2, Sb_3Se_3, ZnP, MnS etc are presently considered to be very important. Major advantage of these materials over CdTe compound is that these are environment-friendly and earth-abundant materials [12] [13]. Works on materials related/similar to CIGS resulted in development of much complicated materials like $Cu_2ZnSn(S,Se)_4$ (CZTS). In CZTS the costly indium and gallium are replaced by low-cost zinc and tin. In 2013 CZTS solar cell achieved record efficiency of 12.6% [14]. Huge research was done by different groups to improve the efficiency of CZTS thin film [15, 16]. But the record efficiency stays constant, probably due to Cu/Zn cationic sublattice disorder. Further, to avoid cationic disorder, researchers tried to shift to the quaternary materials that do not contain both Cu and Zn like $Ag_2ZnSn(S,Se)_4$ (AZTS) , $BaCu_2Sn(S,Se)_4$ (BCTS), $Cu_{10}Zn_2Sb_4Se_{13}$ etc [17] [18]. But the deposition of quaternary compound with correct stoichiometry without impurity phase is very difficult. Then massive research was done in the ternary compound $Cu_{10}Te_4S_{13}$, $CuSbSe_2$, $CuInS_2$, $CuInSe_2$, CZS, Cu_2SnS_3 etc [19–23]. Among the different ternary compounds, Cu_2SnS_3 (CTS) is one of the promising materials that shows almost the same properties of CZTS. CTS is p-type semiconductor with optical band gap of 0.92 - 1.8 eV and high absorption coefficient (>104), which are the optimum conditions for solar cell fabrication. Deposition of CTS film can be done by using physical, chemical and physiochemical methods [24] [25]. First CTS based solar cell was fabricated by Kuku and Fakolujo in 1987. CTS film was deposited with evaporation method and Schottky junction cell was fabricated with Al electrode. The cell showed efficiency of 0.11% with V_{OC} of 100 mV, J_{SC} of 1.36 mA/cm^2 and FF of 0.48 [26]. As the first CTS based solar cell fabricated in 1987, people identified its importance recently and intense research has already started on this material

1.8 Review on CTS based solar cell

1.8.1 Physical method

A variety of physical methods are used for CTS thin film deposition such as sputtering [27–36] E-beam evaporation [37] [38], vacuum evaporation [39–45], solid state reaction [46–48], pulsed laser deposition [49, 50] and ball milling [51]. Optoelectronic and structural properties, of CTS material and its photovoltaic cell efficiency are related to the deposition technique.

1.8.1.1 Sputtering

In thin film deposition using sputtering, surface of target material is bombarded with high-velocity ions leading to ejection of surface atoms from it and these atoms condense on the substrate surface. In CTS film deposition DC (direct current) and RF (radio frequency) magnetron sputtering techniques are commonly used. Yuchen Dong et al [29], deposited CTS films over the SLG and Mo-coated glass, using RF sputtering. In this work, they used metallic targets and after depositing metallic films, sulfurisation was done to convert the metallic film to CTS They optimised sulfurisation time by varying from 5 to 30 minutes. XRD and Raman analyses indicate that all samples had cubic phase with polycrystalline nature and maximum crystallinity was obtained for samples which were given 20-minute sulfurisation. Increased sulfurisation time improved crystallinity of the films which caused decrease in band gap (from 1.02 to 0.98 eV); transmittance also decreased with sulfurisation time. Solar cells were fabricated with the structure SLG/Mo/CTS/CdS/i-ZnO/AZO. The solar cell parameters improved with increase in sulfurisation time and this may be due to improved crystallinity and morphology of the film, leading to reduction in recombination losses through grain boundaries. The best performance was obtained from the cell fabricated using CTS thin film sulfurized at 20 minutes. (efficiency of 0.20%, V_{OC} of 197 mV, J_{SC} of 3.60 mA/cm^2 and FF of 26.1%). The device with sulfurisation time 30 minute resulted in rough surface formation which decreased V_{OC} and hence the PCE.

Dong et al. [28] also studied consequence of variation of sulfurisation temperature on properties of sputtered CTS thin films. Sulfurisation was done in an environment of elemental sulfur vapour for 20 min and sulfurisation temperature was varied from 400 to 550 °C. From XRD and Raman studies, samples were proved to be with cubic phase for all sulfurisation temperatures. Sulfurisation temperature has important role in determining composition of the film. With the increase in sulfurisation temperature, Cu/Sn ratio increased from 1.34 to 1.86;. Optical band gap increased with increase in sulfurisation temperature (from 0.92 eV to 0.99 eV). Solar cell was fabricated with structure SLG/Mo/CTS/CdS/ i-ZnO/ZnO: Al; with variation in sulfurisation temperature from 450 to 550 °C, PCE increased from 0.08% to 0.28%. The highest PCE was obtained for the film sulfurized at 550 °C (PCE of 0.28% with, FF of 26, V_{OC} of 183 mV and J_{SC} of 5.45 mA/cm^2). The same authors could later enhance the cell efficiency to 0.76% by optimizing preheating time [35].

Chierchia et al [32] deposited CTS film using targets CuS and SnS. In this study, both Cu/Sn ratio and sulfurisation temperature were varied. Cu/Sn ratio variation was achieved by changing source power of CuS keeping SnS source power fixed. XRD and Raman results indicated monoclinic structure with band gap of 0.92 eV in both sulfurisation temperatures at 520 and 560 °C. From SEM image, it was clear that sample at lower sulfurisation temperature (520 °C) was dense and void free; but at higher sulfurisation temperature sample developed large grains with higher voids/ pinhole density. Solar cells (with structure SLG/Mo/CTS/CdS/ZnO/ZnO: Al/Al) were fabricated using all samples. The cell fabricated with CST films sulfurized at 520 °C showed maximum conversion efficiency of 3.05% with J_{SC} 26.2 mA/cm^2 and V_{OC} 243 mV.

CTS thin films were deposited by Mingrui He et al [52] using RF sputtered Cu-Sn metallic film which was annealed in sulfur environment at 580 °C for 10 minutes. Here impact of Cu deposition time (from 2812 s to 3212 s) on optoelectronic, structural and photovoltaic properties of CTS thin films was studied. XRD and Raman analysis indicated monoclinic phase of CTS film. The band gap showed slight increase with increase in copper deposition time. Among solar cells fabricated with different copper deposition time, a solar cell

with copper deposition time of 2812 s had better cell performance (efficiency of 2.39%, FF of 40%, V_{OC} of 208 and J_{SC} of 28.92 mA/cm^2).

1.8.1.2 Electron beam evaporation

In Electron Beam or E-Beam Evaporation method, the target material is bombarded with high energy electron beam and it vaporizes the target material; then it condenses to form a thin film on the substrate surface. In electron beam evaporation, rate of film deposition can be 1nm to few micrometers per minute

Chino et al. [53] deposited Cu/Sn metallic films on glass substrates by using e-beam evaporation. In this study, sulfurisation temperature was varied as 450, 500, 550, and 580 °C. Sulfurization was done for two hours and then allowed to cool naturally. XRD analysis showed the peak corresponding to tetragonal phase for lower sulfurisation temperature and cubic and monoclinic phases appeared at higher sulfurisation temperature. Optical band gap energy of the films was obtained in the range 0.96 - 1.00 eV. Solar cells were fabricated with the structure glass/ Mo/CTS/CdS/ZnO: Al/Al and influence of the sulfurisation temperature on cell parameters were studied. Solar cell efficiency increased from 0.03 to 2.54 with increase in sulfurisation temperature. The solar cell with better conversion efficiency of 2.54% was obtained from CTS sulfurized at 580 °C, (V_{OC} of 211 mV, J_{SC} of 28.0 mA/cm^2, and FF of 0.43).

In another work by Naoya Aihara et al. [54], effect of Cu/Sn ratio on properties of the CTS film was studied. In tin-rich region, the sample showed monoclinic phase with band gap 0.92-0.99eV. Solar cells were fabricated with structure SLG/Mo/ CTS/CdS/ZnO: Al/Al using these CST films. Among these, the cell having CTS thin film with Cu/Sn ratio of 1.77 had better cell parameters (V_{OC} of 242 mV, J_{SC} of 28.9 mA/cm^2, FF of 0.417 and conversion efficiency of 2.92%). Same authors [38]also studied the role of sulfurisation temperature on the properties of CTS film; here sulfurisation temperature was varied from 500 to 580 °C. Photovoltaic parameters of the solar cell showed increasing nature with increase in sulfurisation temperature. High photovoltaic

parameters were obtained from the cell which used CTS film with sulfurisation temperature of 580 °C (V_{OC} 244mV, J_{SC} of 29 mA/cm^2, FF of 0.39, and conversion efficiency of 2.7%).

Cu-Sn alloy films were deposited by Zeguo Tang et al. [37] with Cu/Sn ratio of 1.72 and sulfurized in H_2S atmosphere with different temperatures, 100, 200, 300, 400, 500, and 550 °C; heater of the furnace was turned off and samples were cooled to room temperature. Binary phases of Cu_2S, SnS_2, and SnS were produced at lower temperature (300 °C), and Cu_2S was located at the surface and SnS_2 and SnS phases were found at bottom of the film. The final phase of CTS was produced at interface of Cu_2S and SnS film when temperature of furnace further increased to 400 °C. SnS evaporation occurred at this temperature and the evaporation rate increased with increase in temperature; this was reduced by sulfurisation in a closed space. Solar cells were fabricated with the structure Al/ZnO: Al/ZnO/CdS/CTS/Mo/SLG using both lamp furnace and sealed glass ampoule; efficiency of 0.7% could be achieved in lamp furnace while efficiency of 1.2% was achieved in sealed glass ampoule.

1.8.1.3 Vacuum evaporation

Vacuum evaporation is a common method for thin film deposition. It involves heating of target material in closed chamber at low pressure (10^{-6} Torr). Heating of target material results in escape of atoms/molecules from the target surface which hits substrate and stick on it.

Kuku et al [26], first time reported CTS based solar cell (Schottky junction) with the efficiency of 0.11%. In this study CTS film was deposited by vacuum evaporation of CTS power (prepared by melting of stoichiometric Cu, Sn, and S mixture).

CTS films were deposited by Ayaka Kanai et al [42], using co-evaporation of Cu, Sn, and S and in this work, they studied on the role of annealing temperature on photovoltaic properties of CTS films with Cu/Sn ratio of 1.7 and 1.8; for this films (having ratio of 1.7) were annealed at temperatures of 520, 540, and 560 °C, while those having ratio of 1.8 were annealed at 560, 570, and 580 °C. In both Cu/Sn ratios (1.7 and 1.8) XRD and Raman

analysis confirmed monoclinic phase of CTS. Solar cells were fabricated using structure SLG/Mo/CTS/CdS/ZnO:Al/Al with all the samples and the cell with CST film having Cu/ Sn ratio of 1.8 and annealed at 570 °C showed the best cell performance with V_{OC} of 248 mV, J_{SC} of 33.5 mA/cm^2, FF of 44 and efficiency of 3.66

The same authors [55] also studied role of Cu/Sn ratio on the photovoltaic properties. Here Cu/Sn ratio was varied by altering source temperatures of Cu and Sn. Among the solar cell fabricated with different Cu/Sn ratios, the maximum efficiency was exhibited by the cell having Cu/Sn ratio of 1.87 and it showed V_{OC} of 258 mV, J_{SC} of 35.6 mA/cm^2, FF of 0.467, and efficiency of 4.29%

Mitsuki Nakashima et al [45] deposited stacked Sn/Cu precursors on Mo/SLG by sequential evaporation of Sn and Cu. In this study, the Cu/Sn mole ratio was changed from 2/1.0 to 2/1.5 and after deposition, the stacked Sn/Cu film crystallized due to annealing in mixed atmosphere sulfur/tin for 30 min at 570 °C. Structural analysis indicated that the fabricated films had monoclinic structure. Grain size of the films increased with increase in tin molar ratio up to 1.2; further increase in tin concentration resulted in decrease in grain size. Solar cells were fabricated with structure Al/ZnO: Ga/ZnO/CdS/CTS/Mo/SLG and the cell with better cell parameters was obtained for Cu/Sn mole ratio of 2/1.2. It exhibited V_{OC} = 247.5 mV and J_{SC} = 5.75 mA/cm^2, FF = 0.30 and efficiency = 0.43%. Same authors [44] used stacked NaF/Sn/Cu precursor coated on Mo (deposited on glass substrate by the sequential evaporation of Sn and Cu elements and NaF) for another set of studies. The molar ratio of Cu and Sn was kept at 1.0 and 0.6 respectively and the NaF/Cu mole ratio alone was changed from 0 to 0.12. The deposited NaF/Sn/Cu precursor was placed in vacuum-sealed glass ampoule with elemental sulfur and tin shots. It was crystallized by annealing in a mixed atmosphere of tin and sulfur vapours for 30 min at 570 °C. From the structural analysis (XRD and Raman) these films were found to have monoclinic structure and grain size decreased with increase in NaF/Cu mole ratio. Solar cells were fabricated with structure of Al/ZnO: Ga/ZnO/CdS/CTS/Mo/SLG and highest conversion efficiency was obtained for NaF/Cu molar ratio of 0.075 (V_{OC} = 283 mV, J_{SC} = 37.3 mA/cm^2, FF = 0.439, and efficiency (η) = 4.63%).

1.8.1.4 Pulsed laser deposition (PLD)

In PLD, high power laser beam is focused towards target material causing vaporization of target material. The material vaporized from the target gets deposited over substrate and the process can occur in ultrahigh vacuum.

In yet another work by Vanalakar et al [50], pellet of CTS was used as target, which was produced by hot-pressing of powered Cu_2S and SnS_2 with1:1 molar ratio. As-deposited thin films were annealed at various temperatures as 200 °C, 300 °C and 400 °C in furnace for 1 hour in H_2S+N_2 atmosphere. From the structural analysis, films annealed at 400 °C showed maximum crystallinity with cubic structure. Solar cells fabricated using the CTS film (CTS:400) with the structure SLG/Mo/CTS/CdS/i-ZnO/AZO/Al, showed J_{SC} of 11.90 mA/cm^2, V_{OC} of 260 mV, (FF) of 24%, and efficiency (η) of 0.82%.

1.8.1.5 Ball milling

It is one of the simple, inexpensive nonvacuum physical technique most commonly used for mechanical alloying. It contains a hollow cylindrical shell with partially filled balls. The cylindrical shell can rotate around horizontal axis or at small angle to the horizontal axis. In this cylinder, the chosen material is placed along with balls and friction between the material and the ball result in fine powder of the material.

Qinmiao Chen et al, [51] produced CTS powder using ball milling with powders of copper, tin and sulfur at the molar ratio 2:1:3. For the film deposition, the power was dissolved in propylene glycol and made as paste; this was deposited over the substrate by employing doctor blade method. Annealing temperature of the samples was varied from 350 to 500 °C. Cell was fabricated by depositing the paste on the prepared FTO glass/TiO_2/In_2S_3 substrates and got the highest efficiency of 1.11% for the sample annealed at 400 °C. The efficiency further increased by modification of the p-n junction interface. Interface modifications were done by depositing additional layer of In_2S_3 (with low deposition temperature) which improved the efficiency up to 1.92%.

Takeshi Nomura et al [56] produced CTS powder by ball milling of elemental Cu, Sn, and S; in this study molar ratio of copper was varied in such a way that $Cu_{(2-x)}SnS_3$ with x = 0.0, 0.1, 0.2, and 0.3 was obtained. Then the mixed powders were post-heated at different temperatures in N_2 gas atmosphere. For CTS film fabrication the powder was dissolved in ethylene glycol monophenyl ether and films were deposited by employing screen-printing technique. High-pressure sintering at 6 MPa and annealing for 10 min at 575 °C with S powder in 1% H_2S/N_2 atmosphere was done to enhance compact microstructure and crystallinity. Using the device structure of Ag/ITO/i-ZnO/CdS/CTS/Mo/SLG, cells were fabricated. Among the different cells, the cell with x = 0.1 showed maximum photovoltaic efficiency of 1.03%. In order to find the role of post-heating on the photovoltaic properties, they prepared $Cu_{1.9}SnS_3$ powder and post-heated at various temperatures (300 °C to 600 °C). The post-heating at 300 °C resulted in maximum efficiency of 1.38% with V_{OC} of 182mV, J_{SC} of 21.7 mA/cm^2, and FF of 0.35%.

1.8.2 Chemical method

A variety of chemical methods are used for CTS thin film deposition such as chemical bath deposition [57], chemical spray pyrolysis [58–63], electrode deposition [64, 65], Dip coating [66], Spin coating [67, 68]and SILAR method [69, 70]. Comparing with physical methods these are low-cost deposition techniques; but only a few reports are there on cell fabrication using chemical method.

1.8.2.1 Chemical bath deposition (CBD)

In CBD process, deposition of thin film takes place on solid substrate surface when it is immersed in the precursor solution maintained at the correct temperature. Jianmin Li et al [57] deposited CTS thin film by annealing stacked layer of SnS/Cu deposited using CBD. In this work stack order (SnS/Cu or Cu/SnS), composition and annealing temperature (500 to 600 °C) were optimized. Characterisation studies proved that the film had monoclinic structure with band gap of 0.87 eV. Solar cell fabricated using the structure Al/AZO/ZnO/CdS/CTS/Mo/SLG exhibited efficiency of 0.96 with (V_{OC} = 157 mV, J_{SC} = 19.20 mA/cm^2, and FF = 31.9%).

1.8.2.2 Electrodeposition

Electrodeposition is a common technique used for metallic thin film coatings. Conductive material is dipped in solution containing salt of the metal to be deposited and applying a constant electric current to electrode results in deposition of the thin metallic film.

Berg et al [71] deposited CTS thin films by electrodeposition. Initially, Cu and Sn were deposited sequentially in a sandwich order (Mo/Cu/Sn/Cu/Sn) using basic Cu and acidic Sn solutions. In order to convert the metal stack into the desired compound, the stacked precursor was annealed at 550 °C for 2 hours in N_2+H_2 atmosphere along with elemental sulfur and SnS powder. Structural analysis made it clear that the fabricated film has monoclinic structure and band gap of 0.93 eV (obtained from photoluminescence (PL) studies). Solar cell fabricated with the configuration of glass/Mo/CTS/CdS/ZnO/ZnO: Al/Al: Ni, had J_{SC} 17.1 mA/cm^2, V_{OC} 104 mV, FF 0.30% and efficiency 0.54%.

Koike et al [65] deposited CTS films through electrodeposition of Cu/Sn precursors followed by sulfurisation. The precursors Cu-Sn were deposited onto the glass substrates coated with Mo and after the deposition, sulfurisation was done at 580 °C for 2 hours in sulfur and N_2 atmosphere. In this work, major aim was to analyse effect of variation of Cu/Sn ratio on the properties of CTS film. All the films had tetragonal phase of CTS film and at higher copper concentration, the phase of Cu_4SnS_4 was also present. Solar cell was made with the structure glass/Mo/CTS/CdS/ZnO: Al/Al and the best cell showed V_{OC} of 249 mV J_{SC} of 29.3 mA/cm^2, FF of 0.39 and efficiency of 2.84%.

1.8.2.3 Dip coating

Solid substrate is immersed in a liquid (solution of the coating material) and lifted out of the solution at a predetermined speed; evaporation of liquid takes place, forming thin film on the substrate.

Devendra Tiwari et al [66] deposited tetragonal CTS film by employing dip coating using solution of Cu-Sn-thiourea complexes in methanol. The dip-coated films were then thermolyzed at 200 °C in the air. Characterization studies proved that the film had tetragonal structure with band gap of 1.12eV. Morphological studies (AFM and SEM) disclosed that the deposited CTS films were compact with low roughness. Solar cell was fabricated with structure graphite/CTS/ZnO/ITO/SLG; the best cells depicted efficiency of (PCE) of 2.10% with V_{OC} of 0.816 V,(It is the highest V_{OC} reported for CTS based solar cell), J_{SC} of 6.14 mA/cm^2 and fill factor FF 0.42%.

1.8.2.4 Spin coating

This technique is used for deposition of thin film over flat substrate surface. For deposition of a thin film, small quantity of coating solution is dropped on the center of substrate. Then the substrate is rotated at optimized speed in order to get uniform film.

Jun Han et al [68] deposited CTS thin film using spin-coating method with hydrazine solution. The film was initially baked at 80 °C for 5 min in order to evaporate hydrazine. Then the film was again baked at 425 °C for 2 min to eliminate excess S. Finally it was annealed at 600 °C with different quantities of sulfur for 20 min and the annealing temperature was also optimized. The CTS film with sulfur addition and annealing had monoclinic phase with band gap of 0.88 eV. Solar cell constructed with structure Mo/Cu_2SnS_3/CdS/ZnO/AZO/Au exhibited V_{OC} of 199 mV, J_{SC} of 14.2 mA/cm^2, FF of 27.4% and conversation efficiency of 0.78%.

J J Chaudhari et al deposited [72] CTS thin films using spin coating method; after deposition the film was dried in air for 10 min at 300 °C to remove the solvent. These films were sulfurized in S_2(S)+Ar atmosphere at 520 °C for 60 min. Structural analysis showed that both as deposited and sulfurized films had tetragonal structure. Band gap of the as deposited film was 1.45eV and that of the sulfurized film was 1.01 eV. Solar cell was fabricated using sulfurized CTS film with structure SLG/FTO/ZnO/CTS/Al and the cell showed efficiency of 1.12 with J_{SC} of 11.6 mA/cm^2, V_{OC} of 0.276 V and fill factor (FF) of 35%

1.9 Aim of the present work

The literature survey evidently illustrates that the research on fabrication of solar cells with CTS thin films is relatively few. A major portion of studies on CTS based cells was done on devices fabricated using vacuum based techniques. Major aim of the present work is to deposit CTS thin films of good opto-electronic properties, using low-cost deposition technique, (viz., Chemical Spray Pyrolysis (CSP)), and try junction fabrication using these films.

References

[1] https://en.wikipedia.org/wiki/Edmond_Becquerel.

[2] W. Smith, "Effect of Light on Selenium During the Passage of An Electric Current," *Nature*, vol. 7, p. 303, feb 1873.

[3] W. G. Adams and R. E. Day, "The action of light on selenium," *Proceedings of the Royal Society of London*, vol. 25, no. 171-178, pp. 113–117, 1877.

[4] H. Hertz, "Ueber einen einfluss des ultravioletten lichtes auf die electrische entladung [on an effect of ultra-violet light upon the electrical discharge]," *Annalen der Physik*, vol. 267, no. 8, pp. 983–1000, 1887.

[5] https://www.electronics-tutorials.ws/diode/diode_2.html.

[6] J. Nelson, *The Physics of Solar Cells*. World Scientific Publishing Co., 2003.

[7] https://en.wikipedia.org/wiki/Theory_of_solar_cells.

[8] https://www.pveducation.org/pvcdrom/solar-cell-operation/open-circuit-voltage.

[9] https://www.pveducation.org/pvcdrom/solar-cell-operation/short-circuit-current.

[10] https://en.wikipedia.org/wiki/Theory_of_solar_cells.

[11] D. J. Coyle, "Life prediction for cigs solar modules part 1: modeling moisture ingress and degradation," *Progress in Photovoltaics: Research and Applications*, vol. 21, no. 2, pp. 156–172, 2013.

[12] J. A. Andrade-Arvizu, M. Courel-Piedrahita, and O. Vigil-Galán, "Sns-based thin film solar cells: perspectives over the last 25 years," *Journal of Materials Science: Materials in Electronics*, vol. 26, pp. 4541–4556, Jul 2015.

[13] X. Liu, C. Chen, L. Wang, J. Zhong, M. Luo, J. Chen, D.-J. Xue, D. Li, Y. Zhou, and J. Tang, "Improving the performance of sb2se3 thin film solar cells over 4% by controlled addition of oxygen during film deposition," *Progress in Photovoltaics: Research and Applications*, vol. 23, no. 12, pp. 1828–1836, 2015.

[14] W. Wang, M. T. Winkler, O. Gunawan, T. Gokmen, T. K. Todorov, Y. Zhu, and D. B. Mitzi, "Device characteristics of cztsse thin-film solar cells with 12.6% efficiency," *Advanced Energy Materials*, vol. 4, no. 7, p. 1301465, 2014.

[15] M. Ravindiran and C. Praveenkumar, "Status review and the future prospects of czts based solar cell a novel approach on the device structure and material modeling for czts based photovoltaic device," *Renewable and Sustainable Energy Reviews*, vol. 94, pp. 317 – 329, 2018.

[16] S. Zhuk, A. Kushwaha, T. K. Wong, S. Masudy-Panah, A. Smirnov, and G. K. Dalapati, "Critical review on sputter-deposited cu2znsns4 (czts) based thin film photovoltaic technology focusing on device architecture and absorber quality on the solar cells performance," *Solar Energy Materials and Solar Cells*, vol. 171, pp. 239 – 252, 2017.

[17] D. Shin, B. Saparov, T. Zhu, W. P. Huhn, V. Blum, and D. B. Mitzi, "Bacu2sn(s,se)4: Earth-abundant chalcogenides for thin-film photovoltaics," *Chemistry of Materials*, vol. 28, no. 13, pp. 4771–4780, 2016.

[18] E. Chagarov, K. Sardashti, A. C. Kummel, Y. S. Lee, R. Haight, and T. S. Gershon, "Ag2znsn(s,se)4: A highly promising absorber for thin film photovoltaics," *The Journal of Chemical Physics*, vol. 144, no. 10, p. 104704, 2016.

[19] A. Zakutayev, "Brief review of emerging photovoltaic absorbers," *Current Opinion in Green and Sustainable Chemistry*, vol. 4, pp. 8 – 15, 2017. 4 Novel materials for energy production and storage 2017.

[20] M. S. Sreejith, D. R. Deepu, C. S. Kartha, K. Rajeevkumar, and K. P. Vijayakumar, "Tuning the properties of sprayed cuzns films for fabrication of solar cell," *Applied Physics Letters*, vol. 105, no. 20, p. 202107, 2014.

[21] M. Santhosh, D. Deepu, C. S. Kartha, K. R. Kumar, and K. Vijayakumar, "All sprayed ito-free cuins2/in2s3 solar cells," *Solar Energy*, vol. 108, pp. 508 – 514, 2014.

[22] D. Abou-Ras, N. Schfer, T. Rissom, M. N. Kelly, J. Haarstrich, C. Ronning, G. S. Rohrer, and A. D. Rollett, "Grain-boundary character distribution and correlations with electrical and optoelectronic properties of cuinse2 thin films," *Acta Materialia*, vol. 118, pp. 244 – 252, 2016.

[23] K. J. Tiwari, V. Vinod, A. Subrahmanyam, and P. Malar, "Growth and characterization of chalcostibite cusbse2 thin films for photovoltaic application," *Applied Surface Science*, vol. 418, pp. 216 – 224, 2017. Asian Consortium on Computational Materials Science - Theme Meeting on First Principles Analysis and Experiment: Role in Energy Research.

[24] A. Lokhande, R. Chalapathy, M. He, E. Jo, M. Gang, S. Pawar, C. Lokhande, and J. H. Kim, "Development of cu2sns3 (cts) thin film solar cells by physical techniques: A status review," *Solar Energy Materials and Solar Cells*, vol. 153, pp. 84 – 107, 2016.

[25] A. Lokhande, K. Gurav, E. Jo, C. Lokhande, and J. H. Kim, "Chemical synthesis of cu2sns3 (cts) nanoparticles: A status review," *Journal of Alloys and Compounds*, vol. 656, pp. 295 – 310, 2016.

[26] T. A. Kuku and O. A. Fakolujo, "Photovoltaic characteristics of thin films of cu2sns3," *Solar Energy Materials*, vol. 16, no. 1, pp. 199 – 204, 1987.

[27] P. Zhao and S. Cheng, "Influence of sulfurization temperature on photoelectric properties cu2sns3 thin films deposited by magnetron sputtering,"

Advances in Materials Science and Engineering, vol. 2013, p. 4 Pages, 2013.

[28] Y. Dong, J. He, L. Sun, Y. Chen, P. Yang, and J. Chu, "Effect of sulfurization temperature on properties of cu2sns3 thin films and solar cells prepared by sulfurization of stacked metallic precursors," *Materials Science in Semiconductor Processing*, vol. 38, pp. 171 – 176, 2015.

[29] Y. Dong, J. He, X. Li, W. Zhou, Y. Chen, L. Sun, P. Yang, and J. Chu, "Synthesis and optimized sulfurization time of cu2sns3 thin films obtained from stacked metallic precursors for solar cell application," *Materials Letters*, vol. 160, pp. 468 – 471, 2015.

[30] R. Bodeux, J. Leguay, and S. Delbos, "Influence of composition and annealing on the characteristics of cu2sns3 thin films grown by cosputtering at room temperature," *Thin Solid Films*, vol. 582, pp. 229 – 232, 2015. E-MRS 2014 Spring Meeting, Symposium A, Thin-Film Chalcogenide Photovoltaic Materials.

[31] P. A. Fernandes, P. M. P. Salomé, and A. F. da Cunha, "A study of ternary cu2sns3and cu3sns4thin films prepared by sulfurizing stacked metal precursors," *Journal of Physics D: Applied Physics*, vol. 43, p. 215403, may 2010.

[32] R. Chierchia, F. Pigna, M. Valentini, C. Malerba, E. Salza, P. Mangiapane, T. Polichetti, and A. Mittiga, "Cu2sns3 based solar cell with 3% efficiency," *physica status solidi c*, vol. 13, no. 1, pp. 35–39, 2016.

[33] S. Sato, H. Sumi, G. Shi, and M. Sugiyama, "Investigation of the sulfurization process of cu2sns3 thin films and estimation of band offsets of cu2sns3-related solar cell structure," *physica status solidi c*, vol. 12, no. 6, pp. 757–760, 2015.

[34] H. Zhang, M. Xie, S. Zhang, and Y. Xiang, "Fabrication of highly crystallized cu2sns3 thin films through sulfurization of sn-rich metallic precursors," *Journal of Alloys and Compounds*, vol. 602, pp. 199 – 203, 2014.

[35] Y. Dong, J. He, X. Li, Y. Chen, L. Sun, P. Yang, and J. Chu, "Study on the preheating duration of cu2sns3 thin films using rf magnetron sputtering technique for photovoltaics," *Journal of Alloys and Compounds*, vol. 665, pp. 69 – 75, 2016.

[36] P. A. Fernandes, P. M. P. Salom, and A. F. da Cunha, "Cuxsnsx+1 (x = 2, 3) thin films grown by sulfurization of metallic precursors deposited by dc magnetron sputtering," *physica status solidi c*, vol. 7, no. 34, pp. 901–904, 2010.

[37] Z. Tang, K. Kosaka, H. Uegaki, J. Chantana, Y. Nukui, D. Hironiwa, and T. Minemoto, "Investigation on evaporation and suppression of sns during fabrication of cu2sns3 thin films," *physica status solidi (a)*, vol. 212, no. 10, pp. 2289–2296, 2015.

[38] N. Aihara, A. Kanai, K. Kimura, M. Yamada, K. Toyonaga, H. Araki, A. Takeuchi, and H. Katagiri, "Sulfurization temperature dependences of photovoltaic properties in cu2sns3-based thin-film solar cells," *Japanese Journal of Applied Physics*, vol. 53, p. 05FW13, apr 2014.

[39] V. Robles, J. Trigo, C. Guilln, and J. Herrero, "Copper tin sulfide (cts) absorber thin films obtained by co-evaporation: Influence of the ratio cu/sn," *Journal of Alloys and Compounds*, vol. 642, pp. 40 – 44, 2015.

[40] U. Chalapathi, Y. Jayasree, S. Uthanna, and V. S. Raja, "Effect of annealing on the structural, microstructural and optical properties of co-evaporated cu2sns3 thin films," *Vacuum*, vol. 117, pp. 121 – 126, 2015.

[41] T. S. Reddy, R. Amiruddin, and M. S. Kumar, "Deposition and characterization of cu2sns3 thin films by co-evaporation for photovoltaic application," *Solar Energy Materials and Solar Cells*, vol. 143, pp. 128 – 134, 2015.

[42] A. Kanai, H. Araki, A. Takeuchi, and H. Katagiri, "Annealing temperature dependence of photovoltaic properties of solar cells containing cu2sns3 thin films produced by co-evaporation," *physica status solidi (b)*, vol. 252, no. 6, pp. 1239–1243, 2015.

[43] N. Aihara, K. Tanaka, H. Uchiki, A. Kanai, and H. Araki, "Donor-acceptor pair recombination luminescence from monoclinic cu2sns3 thin film," *Applied Physics Letters*, vol. 107, no. 3, p. 032101, 2015.

[44] M. Nakashima, J. Fujimoto, T. Yamaguchi, and M. Izaki, "Cu2sns3thin-film solar cells fabricated by sulfurization from NaF/cu/sn stacked precursor," *Applied Physics Express*, vol. 8, p. 042303, apr 2015.

[45] M. Nakashima, T. Yamaguchi, H. Itani, J. Sasano, and M. Izaki, "Cu2sns3 thin film solar cells prepared by thermal crystallization of evaporated cu/sn precursors in sulfur and tin atmosphere," *physica status solidi c*, vol. 12, no. 6, pp. 761–764, 2015.

[46] X. an Chen, H. Wada, A. Sato, and M. Mieno, "Synthesis, electrical conductivity, and crystal structure of cu4sn7s16and structure refinement of cu2sns3," *Journal of Solid State Chemistry*, vol. 139, no. 1, pp. 144 – 151, 1998.

[47] M. Onoda, X. an Chen, A. Sato, and H. Wada, "Crystal structure and twinning of monoclinic cu2sns3," *Materials Research Bulletin*, vol. 35, no. 9, pp. 1563 – 1570, 2000.

[48] S. Fiechter, M. Martinez, G. Schmidt, W. Henrion, and Y. Tomm, "Phase relations and optical properties of semiconducting ternary sulfides in the system cusns," *Journal of Physics and Chemistry of Solids*, vol. 64, no. 9, pp. 1859 – 1862, 2003. 13th International Conference on Ternary and Multinary Compounds.

[49] R. B. Ettlinger, A. Cazzaniga, S. Canulescu, N. Pryds, and J. Schou, "Pulsed laser deposition from zns and cu2sns3 multicomponent targets," *Applied Surface Science*, vol. 336, pp. 385 – 390, 2015. E-MRS 2014 Spring Meeting. Symposium J. Laser Interaction with Advanced Materials: Fundamentals and Applications.

[50] S. Vanalakar, G. Agawane, A. Kamble, C. Hong, P. Patil, and J. Kim, "Fabrication of cu2sns3 thin film solar cells using pulsed laser deposition technique," *Solar Energy Materials and Solar Cells*, vol. 138, pp. 1 – 8, 2015.

[51] Q. Chen, X. Dou, Y. Ni, S. Cheng, and S. Zhuang, "Study and enhance the photovoltaic properties of narrow-bandgap cu2sns3 solar cell by pn junction interface modification," *Journal of Colloid and Interface Science*, vol. 376, no. 1, pp. 327 – 330, 2012.

[52] M. He, A. Lokhande, I. Y. Kim, U. Ghorpade, M. Suryawanshi, and J. H. Kim, "Fabrication of sputtered deposited cu2sns3 (cts) thin film solar cell with power conversion efficiency of 2.39 %," *Journal of Alloys and Compounds*, vol. 701, pp. 901 – 908, 2017.

[53] K. Chino, J. Koike, S. Eguchi, H. Araki, R. Nakamura, K. Jimbo, and H. Katagiri, "Preparation of cu2sns3 thin films by sulfurization of cu/sn stacked precursors," *Japanese Journal of Applied Physics*, vol. 51, p. 10NC35, oct 2012.

[54] N. Aihara, H. Araki, A. Takeuchi, K. Jimbo, and H. Katagiri, "Fabrication of cu2sns3 thin films by sulfurization of evaporated cu-sn precursors for solar cells," *physica status solidi c*, vol. 10, no. 78, pp. 1086–1092, 2013.

[55] A. Kanai, K. Toyonaga, K. Chino, H. Katagiri, and H. Araki, "Fabrication of cu2sns3thin-film solar cells with power conversion efficiency of over 4%," *Japanese Journal of Applied Physics*, vol. 54, p. 08KC06, jul 2015.

[56] T. Nomura, T. Maeda, and T. Wada, "Fabrication of cu2sns3solar cells by screen-printing and high-pressure sintering process," *Japanese Journal of Applied Physics*, vol. 53, p. 05FW01, jan 2014.

[57] J. Li, C. Xue, Y. Wang, G. Jiang, W. Liu, and C. Zhu, "Cu2sns3 solar cells fabricated by chemical bath depositionannealing of sns/cu stacked layers," *Solar Energy Materials and Solar Cells*, vol. 144, pp. 281 – 288, 2016.

[58] Z. Jia, Q. Chen, T. W. Jin Chen, Z. Lia, and X. Dou, "The photovoltaic properties of novel narrow band gap cu 2 sns 3 films prepared by a spray pyrolysis method," *RSC Advances*, vol. 5, p. 2888528891, 2015.

[59] U. Chalapathi, Y. Jayasree, S. Uthanna, and V. Sundara Raja, "Effect of annealing temperature on the properties of spray deposited cu2sns3 thin films," *physica status solidi (a)*, vol. 210, no. 11, pp. 2384–2390, 2013.

[60] M. Adelifard, M. M. B. Mohagheghi, and H. Eshghi, "Preparation and characterization of cu2sns3ternary semiconductor nanostructures via the spray pyrolysis technique for photovoltaic applications," *Physica Scripta*, vol. 85, p. 035603, feb 2012.

[61] Y.-X. Guo, W.-J. Cheng, J.-C. Jiang, and J.-H. Chu, "The effect of substrate temperature, cu/sn ratio and post-annealing on the phase-change and properties of cu2sns3 film deposited by ultrasonic spray pyrolysis," *Journal of Materials Science: Materials in Electronics*, vol. 27, pp. 4636–4646, May 2016.

[62] V. V. Brus, I. S. Babichuk, I. G. Orletskyi, P. D. Maryanchuk, V. O. Yukhymchuk, V. M. Dzhagan, I. B. Yanchuk, M. M. Solovan, and I. V. Babichuk, "Raman spectroscopy of cu-sn-s ternary compound thin films prepared by the low-cost spray-pyrolysis technique," *Appl. Opt.*, vol. 55, pp. B158–B162, Apr 2016.

[63] M. Bouaziz, M. Amlouk, and S. Belgacem, "Structural and optical properties of cu2sns3 sprayed thin films," *Thin Solid Films*, vol. 517, no. 7, pp. 2527 – 2530, 2009. Thin Film Chalogenide Photovoltaic Materials (EMRS, Symposium L).

[64] N. R. Mathews, J. Tamy Benítez, F. Paraguay-Delgado, M. Pal, and L. Huerta, "Formation of cu2sns3 thin film by the heat treatment of electrodeposited sns–cu layers," *Journal of Materials Science: Materials in Electronics*, vol. 24, pp. 4060–4067, Oct 2013.

[65] J. Koike, K. Chino, N. Aihara, H. Araki, R. Nakamura, K. Jimbo, and H. Katagiri, "Cu2sns3 thin-film solar cells from electroplated precursors," *Japanese Journal of Applied Physics*, vol. 51, p. 10NC34, oct 2012.

[66] D. Tiwari, T. K. Chaudhuri, T. Shripathi, U. Deshpande, and R. Rawat, "Non-toxic, earth-abundant 2tetragonal films direct-coated from single metal-organic precursor solution," *Solar Energy Materials and Solar Cells*, vol. 113, pp. 165 – 170, 2013.

[67] B. Xu, Y. Zhao, A. Sun, Y. Li, W. Li, and X. Han, "Direct solution coating of pure-phase cu2sns3 thin films without sulfurization," *Journal of Materials Science: Materials in Electronics*, vol. 28, pp. 3481–3486, Feb 2017.

[68] J. Han, Y. Zhou, Y. Tian, Z. Huang, X. Wang, J. Zhong, Z. Xia, B. Yang, H. Song, and J. Tang, "Hydrazine processed cu2sns3 thin film and their application for photovoltaic devices," *Frontiers of Optoelectronics*, vol. 7, pp. 37–45, Mar 2014.

[69] H. Guan, H. Shen, C. Gao, and X. He, "Structural and optical properties of cu2sns3 and cu3sns4 thin films by successive ionic layer adsorption and reaction," *Journal of Materials Science: Materials in Electronics*, vol. 24, pp. 1490–1494, May 2013.

[70] Z. Su, K. Sun, Z. Han, F. Liu, Y. Lai, J. Li, and Y. Liu, "Fabrication of ternary cusns sulfides by a modified successive ionic layer adsorption and reaction (silar) method," *J. Mater. Chem.*, vol. 22, pp. 16346–16352, 2012.

[71] D. M. Berg, R. Djemour, L. Gtay, G. Zoppi, S. Siebentritt, and P. J. Dale, "Thin film solar cells based on the ternary compound cu2sns3," *Thin Solid Films*, vol. 520, no. 19, pp. 6291 – 6294, 2012.

[72] J. J. Chaudhari and U. S. Joshi, "Fabrication of high quality cu2sns3 thin film solar cell with 1.12% power conversion efficiency obtain by low cost environment friendly sol-gel technique," *Materials Research Express*, vol. 5, p. 036203, mar 2018.

Chapter 2

Preparation and characterization of CTS film using Stannous Chloride precursor

Contents

2.1 Introduction

Currently, intense research is going on for developing low cost, nontoxic, eco-friendly thin film solar cells. Cu_2SnS_3 (CTS) is one such promising material for solar cell fabrication due to its optimum optoelectronic properties; deposition of thin films of this material can be done rather easily with physical and chemical methods [1–10]. Among devices prepared using different deposition methods, devices with vacuum evaporated CTS absorber have obtained maximum conversion efficiency of 4.63% [11]. The cost reduction of the solar cell can be achieved if the cell fabrication can be done through non-vacuum methods [12, 13]. Among the different non-vacuum deposition methods Chemical Spray Pyrolysis (CSP) is one of the simple, low-cost deposition techniques [14, 15].

CSP technique was first introduced by Chamberlin in 1966 [16]. In CSP technique metal salt solution is sprayed onto the preheated substrate surface; the optimum substrate temperature will result in pyrolysis of the solution and the constituents in the solution react to form the required chemical compound, which is coated on the substrate surface. Comparing with other deposition technique, spray pyrolysis has some advantages such as simplicity of technique and good reproducibility; again, this is a vacuum-free technique and scalable for industrial applications. Moreover doping at any desired concentration is possible in this technique. In spite of these advantages, the CSP technique has some disadvantages too. Selection of chemical salt and solvent should be in such a way that the undesired chemical compounds formed during the

deposition are volatile at the deposition temperature. Moreover, the selection of substrate is important; it should be able to withstand the deposition temperature and should not react with spray solution.

The objective of the present work is concerned with the deposition of CTS films through CSP technique and to modify its properties so as to make it suitable for fabricating thin film solar cells. As it is solution based deposition technique, the composition of sprayed films can be tailored by adjusting the composition of the precursor solution [17]. In the case of high vacuum method, the composition variation can be achieved by adjusting the deposition time of the respective source. But in the case of CSP technique, the deposition time is more related to thickness than the composition of the films. On the other hand, spray parameters such as the substrate temperature, the precursors, spray rate etc. are strongly connected with the final properties of the sprayed films [18–21]. Before deposition of solar cell, we should have an imperative knowledge of how structural, optical, compositional, morphological and electronic properties of the CTS material varied with deposition conditions. Only a few research work reported in CTS film deposition using CSP technique [22].

In 2009, for the first time, Bouaziz et al. [23], reported deposition of CTS thin film using the CSP technique. For the fabrication of CTS film initially, SnS_2 film was deposited using spraying solution (a mixture of water and methanol) containing thiourea (0.6 M) and stannic chloride (0.2 M) at a substrate temperature of 280 °C. Cu_2S film was deposited over the SnS_2 film again through spraying solution (a mixture of water and methanol) containing thiourea and copper chloride at a substrate temperature of 300 °C. Here nitrogen gas used as a carrier gas. The solution spray rate and gas flow rates were fixed as 4 cm^3/min and 4 L/min respectively and afterward, the deposited bi-sprayed films (SnS_2/Cu_2S) were annealed in the sulfur atmosphere at 550 °C for 2hours. Characterizations studies indicated the formation of greenish-gray colored film crystallized mainly in Cu_2SnS_3 phase having a cubic structure with E_g (band gap) of 1.15 eV. Amlouk et al. [24], prepared SnS_2 film using the same deposition condition as that used by Bouaziz et al., and above the SnS_2 film, a copper thin film (thickness 200 nm) was deposited using thermal evaporation under vacuum less than 10^{-4} mbar. Then, the bilayer film (SnS_2/Cu) was annealed with sulfur (99.98% of purity) in Pyrex ampoule at

pressure less than 10^{-2} mbar for 2 hours, at a temperature of 550 °C ; this resulted in the formation of cubic structured Cu_2SnS_3 films with E_g of 1.75eV.

Adelifard et al. [25], fabricated Cu_2SnS_3 by single spray, using precursor solution containing copper acetate (0.1 M), stannous chloride and thiourea (0.3 M). Deposition temperature was 285 °C. In the two reports cited earlier nitrogen used as carrier gas but here compressed air was used as the carrier gas. Spray deposition parameters such as the volume of spray solution, spray rate, nozzle-to-substrate distance and rotation speed of hot plate were kept at 100 ml, 7 ml/min, 30 cm and 50 rpm, respectively. Here various Sn/Cu (0.0 to 1.0) molar ratios were used for film deposition and characterization studies indicated that with Sn/Cu ratio increased, sulfur and tin deficiency improved along with a decrease of copper content; CuS hexagonal structure, gradually changed to of Cu_2SnS_3 triclinic phase, while band gap changed from 2.57 to 1.58 eV. Electrical resistivity increased from about 2.1×10^{-4} to 8.5 Ωcm.

Chalapathi et al. [26], prepared the samples using cupric chloride, stannic chloride and thiourea dissolved in double distilled water as the precursor solution. Substrate temperature was 360 °C, spray rate 12 ml/min and the deposited films were annealed in sulfur atmosphere at different temperatures. From the structural analysis, both tetragonal and monoclinic CTS phases were found to be present; as-deposited and samples annealed in lower temperature were having tetragonal phase. On increasing annealing temperature, monoclinic phase dominated, shifting the Eg from 1.65 to 0.93 eV (on annealing at 5000 °C). Same author [27], also study the role of Cu/Sn concentration on the properties of the film. Prepared CTS films with different Cu/Sn ratio (copper-rich, stoichiometric and copper poor). Deposited films were annealed in sulfur atmosphere structural characterization revealed the formation of monoclinic phase whose crystallite size increased with an increase in Cu/Sn ratio and also band gap changed from 0.99 to 0.90 eV.

Another group [28] prepared CTS films using precursors copper chloride, stannous chloride and thiourea in which they varied Cu/Sn ratio as well as substrate temperature. The samples prepared with varied Cu/Sn ratio (at 350 °C) showed tetragonal phase only. After fixing Cu/Sn ratio, variation in substrate temperature resulted in enhancement of Cu/Sn ratio up to 375 °C,

and this decreased thereafter. Again these films had tetragonal structure up to 350 °C on further increasing the temperature (375 °C) it changed to cubic. However, at 400 °C; the structure again changed to monoclinic phase. CTS thin film deposited at the substrate temperature of 350 °C and Cu concentration of 0.02 M had the better crystallinity with crystallite size of 38.3 nm and lowest resistivity (around 11.6×10^{-2} Ωcm); band gap value was 1.16 eV.

Brus et al. [29], reported CTS thin film deposition on bare and molybdenum (Mo) coated glass substrates at a temperature of 288 °C, spray rate of 5ml/min and compressed air used as carrier gas; precursors were copper chloride, stannic chloride and thiourea. Films were deposited with different sulfur concentrations and thicknesses. Structural analysis proved presence of both Cu_2SnS_3 and Cu_3SnS_4 phases; with an increase in the thickness, $Cu_{(2-x)}S$ phase increased (Eg 1.89 eV). Electrical analysis showed two shallow acceptor levels - Ev $\sim$ 0.07 eV at T $<$ 334 K and Ev $\sim$ 0.1 eV at T $>$ 334 K.

Guo et al. [7], deposited CTS thin films with different Cu/Sn precursor ratio and substrate temperatures using the precursors copper chloride, tin chloride and thiourea (dissolved in distilled water) with the spray rate of 5 ml/min. Dominant phase of CTS film changed from tetragonal phase to monoclinic phase on reducing Cu/Sn ratio or increasing substrate temperature. With increasing Cu/Sn ratio (1.4 to 2.2) E_g of CTS films changed from 1.87 to 1.03 eV, making the resistivity minimum ($\sim 3.5\times10^{-3}$ Ωcm). Annealing in sulfur atmosphere increased crystallinity and sulfur content of the film.

2.2 Preparation of precursor solutions for CTS film - Present work

Choice of solvent for the preparation of precursor solution is very important because it affects the properties of the films [30]. In comparison with other solution based technique such as spin and dip coating, for spray technique, precursor solution should have low viscosity so that atomization process to procedure small droplets is possible. Different types of solvents have been used in CSP technique; among these water or short-chain alcohols are better

choice. Here we used demineralized water as solvent. Major factor that decides selection of solutes are cost, purity, toxicity, solubility in the selected solvent and not to react with other solutes in the solvent to form precipitate. Usually metal salts are in form of chlorides, acetates or nitrates; here we used chloride based metal salt since it has high solubility in water (>70 g/100mL). Film deposition was done using precursors copper chloride ($CuCl_2.2H_2O$), stannous chloride ($SnCl_2.2H_2O$) and thiourea (CH_4N_2S) for Cu, Sn and S respectively and these were dissolved in demineralized water.

Stock solution of one molar $CuCl_2.2H_2O$ was prepared by dissolving 17.048 g of $CuCl_2.2H_2O$ in 100 ml demineralized water. Using the same way, we prepared the stock solution of thiourea by dissolving 7.612 g of CH_4N_2S in 100 ml demineralized water. But on dissolving stannous chloride in water some difficulty was observed. Solubility of $SnCl_2.2H_2O$ in water is 83.9 g/100 ml (3.72 M) at 0 °C. The preparation of the precursor solution for the deposition of CTS film takes place at room temperature and the molarity of the precursor solution much less than that of 3.72 M. Either an increase in temperature of solution from 0 °C or decrease in the molarity of the precursor solution hydrolysis takes place. By trial and error method we observed that by adding few milliliters (5% of stock solution volume (100 ml)) of HCl to the $SnCl_2.2H_2O$ powder and make up to 100 ml by using demineralized water. This stock solution is used for the preparation of precursor solution of desired molarity. From this stock solution we can make precursor solution of preferred molarity by using the equation

$$m_1 v_1 = m_2 v_2 \tag{2.1}$$

where
m_2= molarity of the precursor solution used for deposition of the film,
v_2= volume of the precursor solution used for deposition of the film,
m_1= molarity of the stock solution and
v_1 = required volume of stock solution to prepare the precursor solution for spray.

2.2.1 Experimental

Our aim was to deposit Cu_2SnS_3 (CTS) film so copper to tin ratio in the aqueous solution was kept two. But the concentration of thiourea was kept

greater than requirement, in order to compensate for the possible loss due to the volatile nature of sulfur at higher temperature [31]. The precursor solution was sprayed over the substrate maintained at a temperature of 285 °C [25], with a molarity of 0.015 M, spray rate of 3 ml/min and compressed air used as the carrier gas. The deposition result in a uniform thin film of gray color with a greenish tinge.

2.2.2 Structural studies

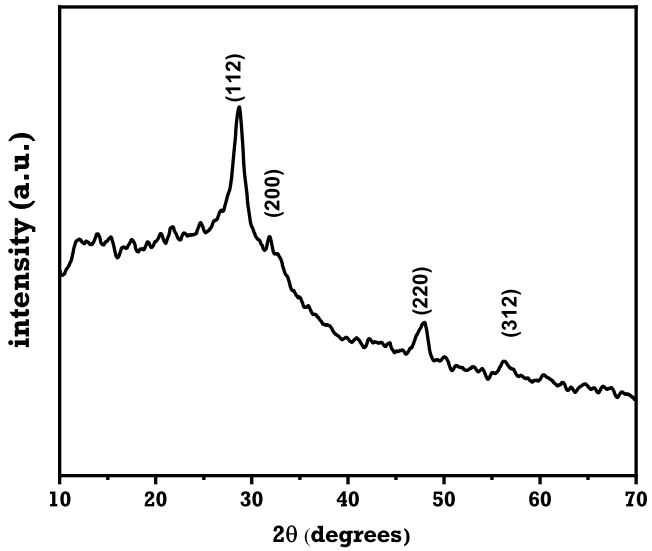

Figure 2.1: XRD pattern of CTS thin film

X-ray diffraction analysis was done in order to get the information about crystalline structure of the samples. Each crystalline material gives a unique diffraction pattern, as its fingerprint and this is explained using the Braggs diffraction condition (2).

$$n\lambda = 2d\sin\theta \tag{2.2}$$

where n: order of diffraction, λ: wavelength of the incident monochromatic radiation, d: interplanar spacing and θ is glancing angle. The grain size (D) can be obtained by the Debye-Scherrer formula:

$$\mathrm{D} = \frac{\mathrm{k}\lambda}{\beta\cos\theta} \tag{2.3}$$

where k is constant called the shape factor and equal to 0.9, β is Full Width at Half Maximum (FWHM), θ is Bragg's angle and λ is wavelength of the incident radiation.

For the present study XRD measurements of the sample were carried out using Rigaku X-ray diffractometer, having Cu K (λ =1.5418 Å) line with Ni filter, operated at 30 kV and 20 mA. X-ray diffraction pattern of the sample is shown in Figure 2.1. All the peaks are in good agreement with the characteristic peaks of Cu_2SnS_3 with tetragonal structure (ICDD card number- 089-4714). Additional XRD lines are not observed suggesting that the deposited CTS film has no other impurity phases.

2.2.3 Electrical properties

Hall measurement technique can give lot of information such as mobility, carrier concentration, conductivity type, resistivity etc. Electrical characterization of the sample was carried out at room temperature using Ecopia (model No HMS-5300; magnetic field= 0.57 T and current measurement can be done in the range of 1nA - 20 mA.). For Hall measurements, the samples were cut into a square shape with an area of 0.5 cm^2 and silver electrode coated at the vertex. Hall measurement indicated that the sample was p-type with resistivity, mobility and carrier concentration as 5.9×10^{-3} Ωcm, 2.44×10^{-1} cm^2/Vs and 4.33×10^{21} cm^{-3} respectively which is good agreement with the reported result [32].

2.2.4 Optical properties

The optical absorption spectrum of the CTS sample was recorded using UV-Vis -NIR spectrophotometer (JASCO V-570 model), in the range 190 - 2500 nm. Optical absorption coefficient and band gap are related by

$$h\nu\alpha = A\,(h\nu - E_g)^n \tag{2.4}$$

where
A is a constant; h is the Plank's constant; E_g is band gap; α is absorption coefficient, ν is incident beam frequency and n is a constant equal to 1/2 for direct and 2 for indirect gap.

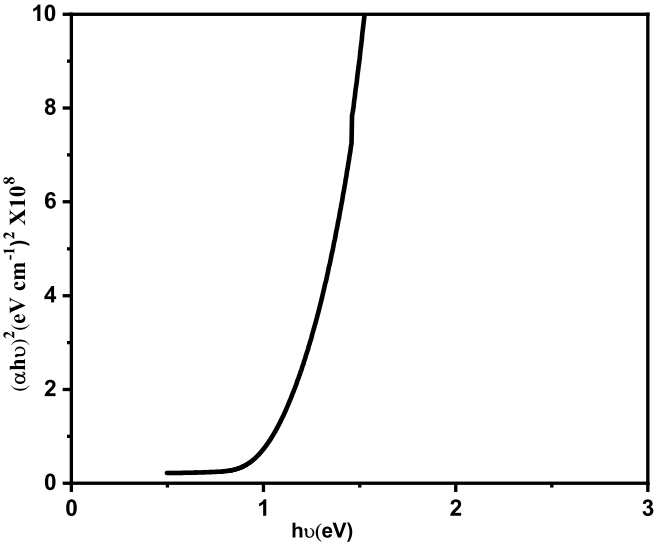

Figure 2.2: Tauc plot of CTS thin film

Band gap was calculated by plotting $(\alpha h\nu)^2$ versus $h\nu$ (Tauc plot) and extrapolating the linear portion of the curve. Figure 2.2 shows the Tauc plot of CTS film with band gap of 1.2 eV. The sample exhibited an absorption coefficient $> 10^4$ cm^{-1} in the visible region. The values obtained from the optical characterization are in good agreement with the reported results [32] [25].

2.3 Effect of substrate temperature

In CSP deposition technique, each material has its own characteristic substrate temperature at which samples having good adhesion without any pinhole and good surface quality. In order to find the optimum substrate temperature, CTS films were deposited with substrate temperature varying from 250 to 350 °C, in steps of 25 °C where Cu:Sn:S ratio, spray rate, molarity and volume of solution sprayed were 1.6:0.8:10, 3 ml/min, 0.015 M and 30 ml respectively. Here substrate temperature alone was varied from 250 °C to 350 °C in steps of 25 °C and these samples were named as CTS 250, CTS 275, CTS 300, CTS 325, and CTS 350.

2.3.1 Structural properties

XRD analysis of all these samples was done and results are depicted in Figure 2.3. All the samples had diffraction peaks corresponding to (112), (220), and (312) planes, which were characteristics peaks of CTS films (tetragonal structure) with preferential orientation along (112) plane [26]. On closely analyzing the XRD peaks, it can be seen that intensity increases up to the substrate temperature of 325 °C. Increasing substrate temperature further resulted in the decrease in peak intensity. At lower substrate temperature (up to 325 °C) film growth is dominant but on increasing substrate temperature further, possibly evaporation is taking place; this may be the reason for the decline in intensity of XRD peaks. From the XRD analysis, it is also clear that there is no other phase in this temperature range.

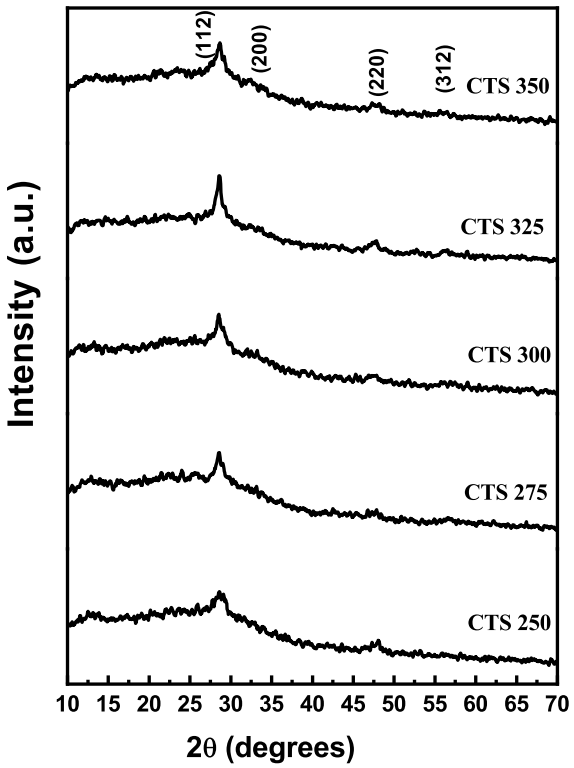

Figure 2.3: XRD pattern of CTS thin film with different substrate temperature

Table 2.1: Electrical characterization of CTS film with various substrate temperature

Sample Name	Carrier Concentration (cm^{-3})	Resistivity (Ωcm)	Mobility (cm^2/Vs)
CTS 250	1.20×10^{21}	1.33×10^{-2}	0.39
CTS 275	1.71×10^{21}	7.37×10^{-3}	0.5
CTS 300	9.53×10^{20}	9.37×10^{-3}	0.7
CTS 325	1.08×10^{21}	5.89×10^{-3}	1
CTS 350	2.04×10^{21}	6.17×10^{-3}	0.5

2.3.2 Electrical properties

Hall measurement data of the sample are depicted in Table 2.1. All CTS samples exhibited p-type conductivity irrespective of substrate temperature. Compared to the other samples, CTS 250 had the highest electrical resistivity and this might be due to improper film formation at the lower temperature. XRD analysis also indicated the same result. Slightly better mobility and lower resistivity was obtained for samples deposited at 325 °C.

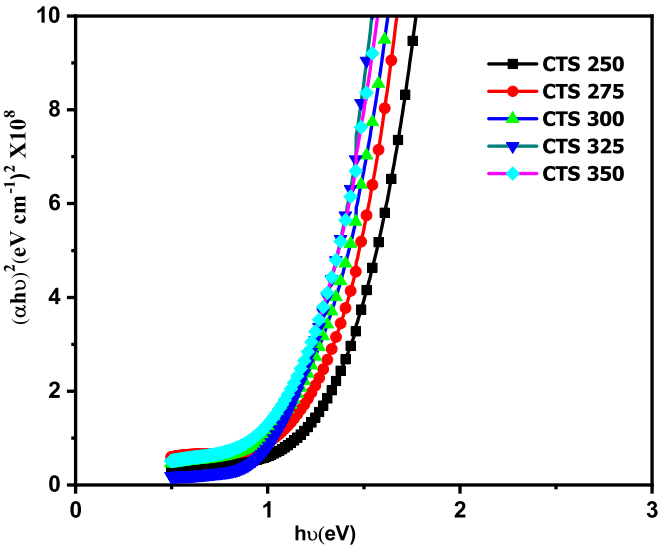

Figure 2.4: Tauc plot of CTS thin film prepared at various substrate temperatures

2.3.3 Optical properties

Optical band gap (E_g) can be found from the graph of $(\alpha h\nu)^2$ versus ($h\nu$) (Figure 2.4). Optical band gap has slight variation with substrate temperature; band gap decreased from 1.35 to 1.2 eV as substrate temperature varied from 250 to 375. This may be due to the increased crystallinity of the film.

2.4 Effect of Copper concentration

To study the role of Copper concentration on the properties of the film, the copper concentration varied from 1 to 2 keeping concentrations of tin and thiourea constant. The samples were named as CTS 1, CTS 1.2, CTS 1.4, CTS 1.6, and CTS 2. In this study, substrate temperature, molarity and spray rate were fixed at 325 °C, 0.015 M and 3 ml/min. and the films were deposited using the same precursors i.e., copper chloride ($CuCl_2.2H_2O$), stannous chloride ($SnCl_2.2H_2O$) and thiourea ($SC(NH_2)_2$) for copper, tin and sulfur respectively [33].

2.4.1 Structural analysis

XRD analysis was done on all these samples (CTS 1 to CST2). (Figure 2.5) The sample exhibited polycrystalline nature with tetragonal structure having peaks corresponding to the planes (112), (200), (220) and (312 having preferential orientation along (112) plane. With an increase in copper concentration, the peak intensity also increased.

2.4.2 Electrical properties

Electrical properties of the samples are tabulated in Table (2.2). Hall measurement data revealed the p-type nature of the deposited films. Another important information obtained from the electrical study is that the resistivity is decreasing (by one order) with increase in Copper concentration.

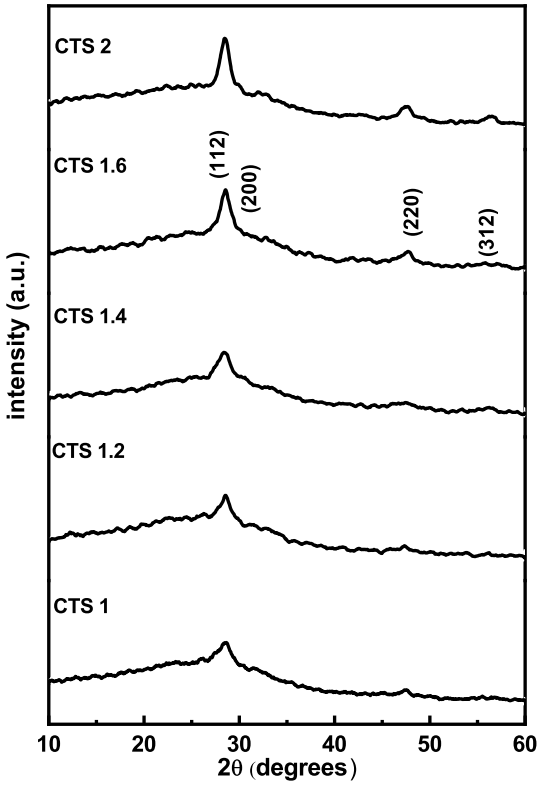

Figure 2.5: XRD pattern of CTS thin film prepared with different Copper concentration

Table 2.2: Electrical properties of copper varied films

Sample Name	Carrier Concentration (cm^{-3})	Resistivity (Ωcm)	Mobility (cm^2/Vs)
CTS 1	2.31×10^{20}	6.9×10^{-2}	0.4
CTS 1.2	5.4×10^{20}	1.6×10^{-2}	0.8
CTS 1.4	5.8×10^{20}	1.3×10^{-2}	0.8
CTS 1.6	1.08×10^{21}	5.89×10^{-3}	1
CTS 2	7×10^{21}	4.8×10^{-3}	0.9

2.4.3 Optical studies

In order to understand the role of copper concentration on the optical properties of the CTS film, we analysed absorption spectra. From the Tauc plot

(Figure 2.6) the band gap shows a decreasing tendency with an increase in copper concentration. A similar case was observed by Acevedo et al. [34] for CIS film and by Raja et al. [35] for CZTS film. The absorption spectra did not give any information about the secondary phase formation.

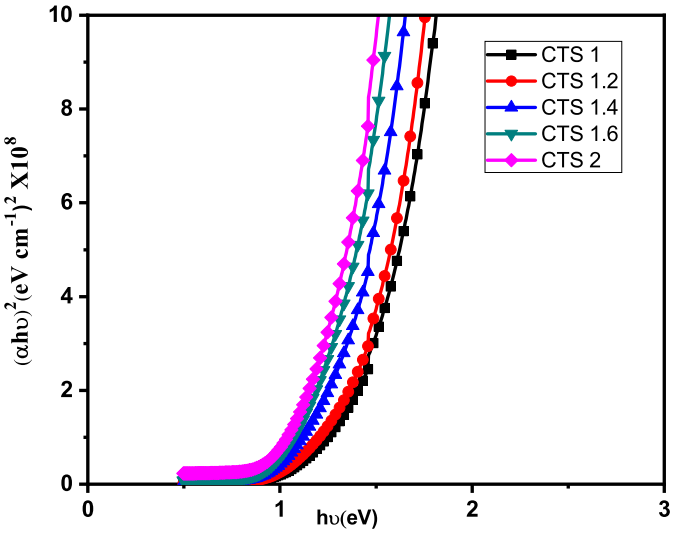

Figure 2.6: Absorption spectra of CTS thin film with different copper concentration

However, with all the good qualities for samples with enhanced copper concentration, there was a problem for the precursor solution when the copper concentration goes above 1.6; the precursor solution became turbid and precipitated after some time. In the case of large scale/ industrial fabrication (of solar cells), the precursor solution should withstand storage for a long interval of time and hence this problem of precipitation has to be overcome. For this, we did several trials and when we increased the thiourea concentration slightly high (from 10 to 12), the precipitation disappeared. But to know if there is any variation in the properties of the film with the increased sulfur concentration, we deposited CTS film with copper:tin:sulfur ratio of 1.6:0.8:12 keeping spray rate, substrate temperature and volume of spray as 3 ml/min, 325 °C and 30 ml respectively and the sample named as A. From the structural characterization sample A it was observed that the sample had the same tetragonal structure (Figure 2.7). The optical band gap was also the same as that in the earlier case (1.2 eV). From the electrical characterization resistivity, mobility and carrier concentration were found to be 9.61×10^{-3} Ωcm,

0.8 cm^2/Vs and 8.00×10^{20} cm^{-3} respectively on comparing with earlier case (sample CTS 1.6) there is only a slight variation in electrical properties. Hence from these studies, it was observed that there was no considerable variation in optoelectronic properties of the film with increased sulfur concentration.

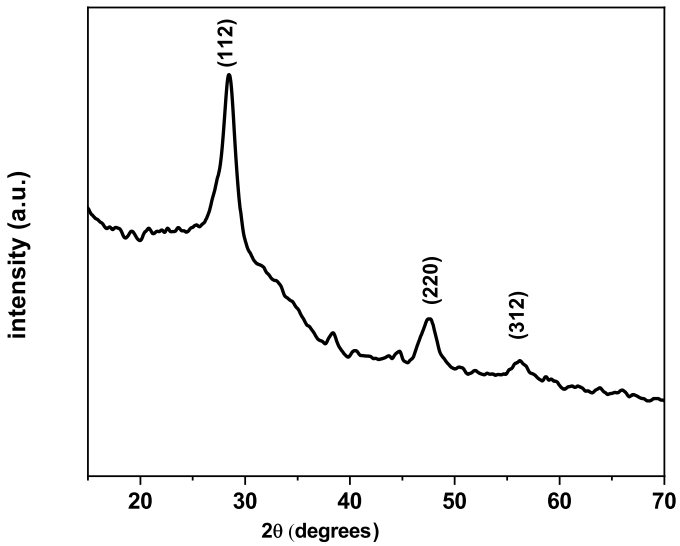

Figure 2.7: XRD pattern of sample A

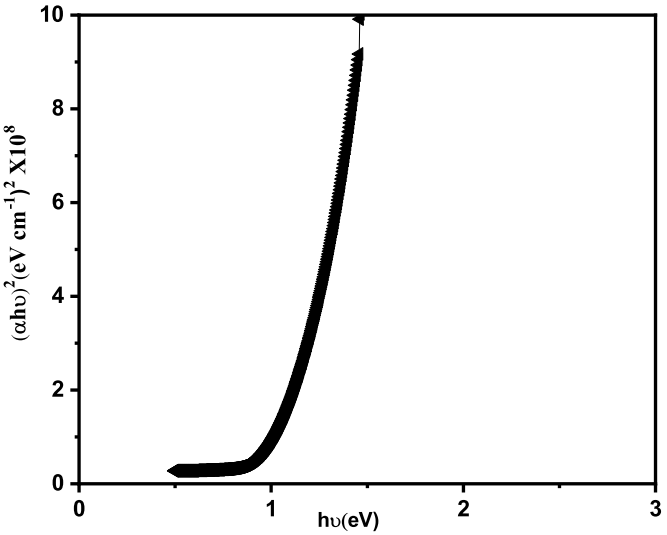

Figure 2.8: Tauc plot of sample A

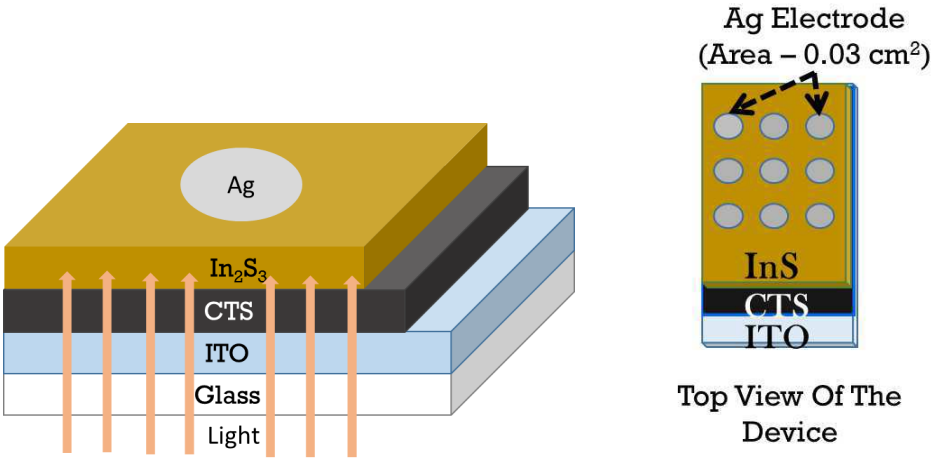

(a) *(b)*

Figure 2.9: Schematic diagram of solar cell fabricated

2.5 Solar cells fabrication

The structure of the solar cell fabricated is shown in Figure 2.9. Glass plates coated with Tin-doped Indium Oxide (ITO) (thickness 200 nm, sheet resistance 12 Ω/cm; Geomatec, Yokohama, Japan) were used as the substrates; here the ITO served as bottom electrode. We fabricated heterojunction using CTS as an absorber layer and n-type In_2S_3 as buffer layer. Here In_2S_3 (In_2S_3) had been selected as buffer layer due to its large band gap and non-toxicity. More importantly, the deposition is done with same CSP technique. Furthermore, the deposition conditions for In_2S_3 layer well optimized by our group for the fabrication of Copper Indium Sulfide(CIS) based solar cells [36] [37] [38]. Here we used $InCl_3$ and thiourea as precursors for the deposition of In_2S_3 film. Indium to sulfur ratio was taken as 1.2:12, substrate temperature was 350 °C and spray rate of 4 ml/min. Metallic silver films were deposited over the In_2S_3 layer using vacuum evaporation technique as the top electrode. An array of nine electrodes (as shown in Figure 2.9) with each one having area of 0.05 cm^2 and thickness of 50nm. Light was admitted from ITO side and J-V characteristic analysis was done by using Photo Emission Tec SS550AAA solar simulator (illumination - 100 mW/cm^2) and National Instruments Source Measure Unit.

As shown in Figure 2.9 an array of nine electrodes were deposited on the sample and each electrode acted as a single solar cell, four such devices were fabricated for error analysis(for each copper concentration). But none of these samples had any light activity; the possible reason might be due to the high thickness of the CTS films used. Hence we systematically reduced thickness of the film by reducing the volume of spray solution. However, even after reducing the volume of spray solution to 3 ml (the minimum possible volume that can be sprayed with spray rate of 3 ml/min), we did not get any light activity. Hence further reduction in thickness of the films could not be done with reduction of volume of precursor solution. Another possible method to reduce the thickness of the film was by reducing the molarity of the precursor solution and we resorted to that.

2.6 Effect of variation of molarity

Before cell fabrication, we first checked if there was any variation in opto-electronic properties of the CTS films with molarity variation; for this, the molarity of the solution was varied from 0.015 to 0.005 in steps of 0.0025 and CTS samples were prepared. Here copper: tin: sulfur ratio was taken as 1.6:0.8:12, the substrate temperature, spray rate and the precursors were same as in the earlier case. Here the samples were named as CTS 0.015, CTS 0.0125, CTS 0.01, CTS 0.0075, and CTS 0.005. All these films were characterized using structural, optical and electrical measurements. Table 2.3 demonstrations how to make a precursor solution with different molarity that maintains the same Cu:Sn:S ratio.

2.6.1 Structural properties

XRD patterns of CTS films deposited with different molarities are shown in Figure 2.10. Well distinct peaks corresponding to the (112), (200), (220) and (312) planes of tetragonal CTS could be observed. But for samples prepared using solution having very low molarity (CTS 0.005) the peaks were not clearly visible; this might be due to the very low thickness of the film. However on increasing the volume of spray to 75 ml the XRD pattern (Figure 2.11) very

Table 2.3: Preparation of precursor solution with different molarity

Molarity of spray solution (30ml)	Amount of 1M copper chloride solution added to the spray solution (ml)	Amount of 1M tin chloride solution added to the spray solution (ml)	Amount of 1M thiourea solution added to the spray solution (ml)
CTS 0.005	0.24	0.12	1.8
CTS 0.0075	0.36	0.18	2.7
CTS 0.01	0.48	0.24	3.6
CTS 0.0125	0.6	0.3	4.5
CTS 0.015	0.72	0.36	5.4

clear with all the peaks corresponding to the tetragonal structure of CTS sample.

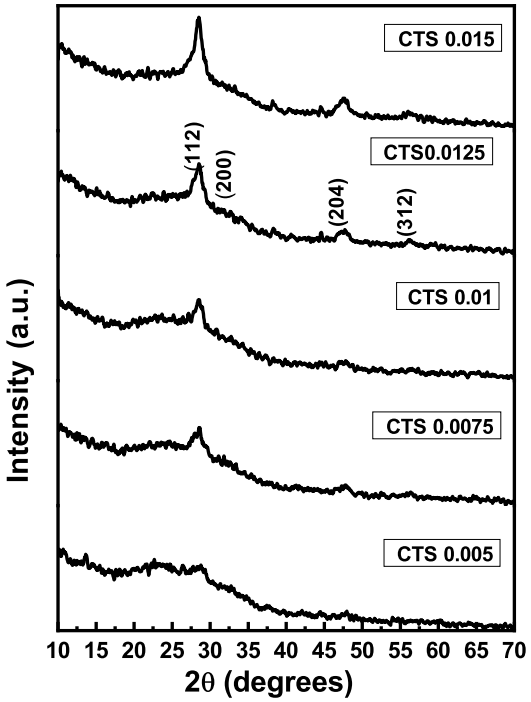

Figure 2.10: XRD pattern of CTS thin film with different molarities.

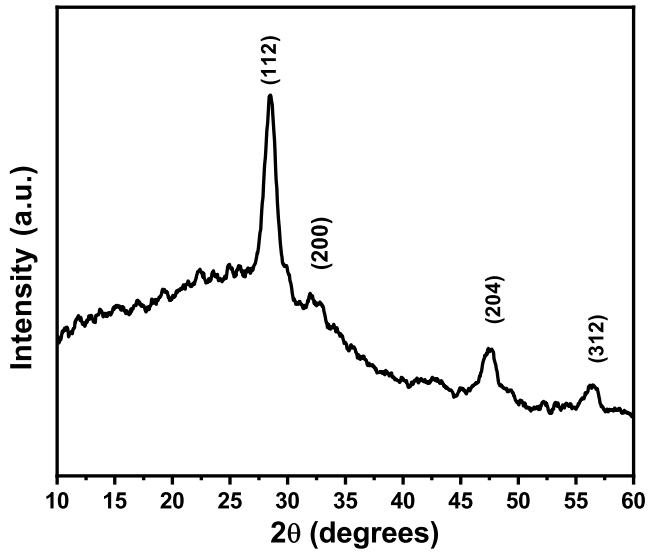

Figure 2.11: XRD pattern of sample CTS 0.005 when volume of spray solution was enhanced to 75 ml

2.6.1.1 Structural analysis using Raman spectra

In order to understand details of the structure of these films, (viz., samples 0.015 M to 0.005 M) Raman analysis was also done (using JobinYvon Horiba LABRAM-HR in the back scattering mode), at room temperature, on samples CTS 0.015, CTS 0.01and CTS 0.005. The results are shown in Figure 2.12. From this study, it was observed that Raman shift at 337 cm^{-1} and 294 cm^{-1} corresponding to the tetragonal structure of CTS. Raman analysis also confirmed that additional peaks due to the secondary phases such as SnS (shift at 160 cm^{-1}, 190 cm^{-1}, 220 cm^{-1}), SnS_2 (shift at 315 cm^{-1}), $Cu_{(2-x)}S$ (shift at 472 cm^{-1}) were not present.

2.6.2 Optical and electrical studies

Optical band gaps of the CTS film with molarity variation are shown in Figure 2.13 and from this, it is clear that there are no variations in band gap with molarity change of the precursor solution. Hall measurement data of these samples (given in Table 2.4) proved that there are no considerable variations due to change in molarity of the precursor solution.

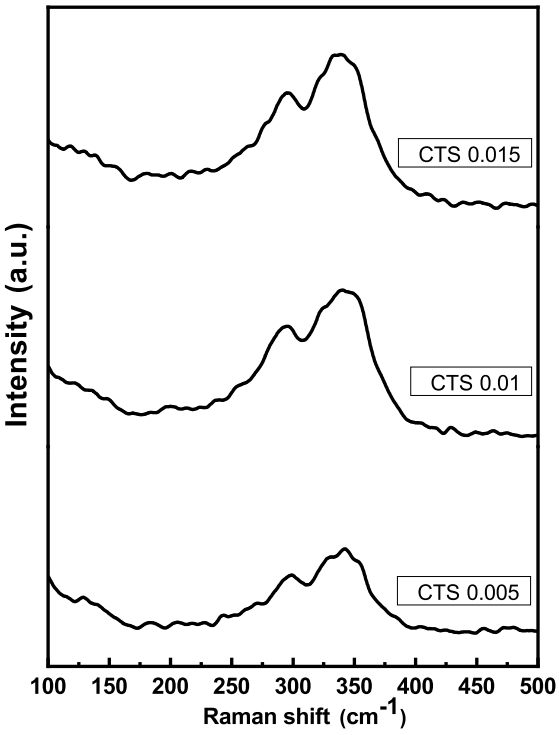

Figure 2.12: Raman scattering spectra of CTS samples (CTS 0.015, CTS 0.01 and CTS 0.005) deposited with different molarities

Table 2.4: Electrical characterization of CTS film with molarity variations

Sample Name	Carrier Concentration (cm^{-3})	Resistivity (Ωcm)	Mobility (cm^2 /Vs)
CTS 0.005	1.67×10^{21}	6.83×10^{-3}	0.55
CTS 0.0075	1.84×10^{21}	5.35×10^{-3}	0.63
CTS 0.01	1.09×10^{21}	5.44×10^{-3}	1.05
CTS 0.0125	9.92×10^{20}	9.47×10^{-3}	0.67
CTS 0.015	8.00×10^{20}	9.61×10^{-3}	0.81

2.7 Trial on junction fabrication

Solar cells were fabricated with all these molarities varied samples (i.e., from CTS 0.015 to CTS 0.005) and named as S 0.015, S 0.0125, S 0.01, S 0.0075

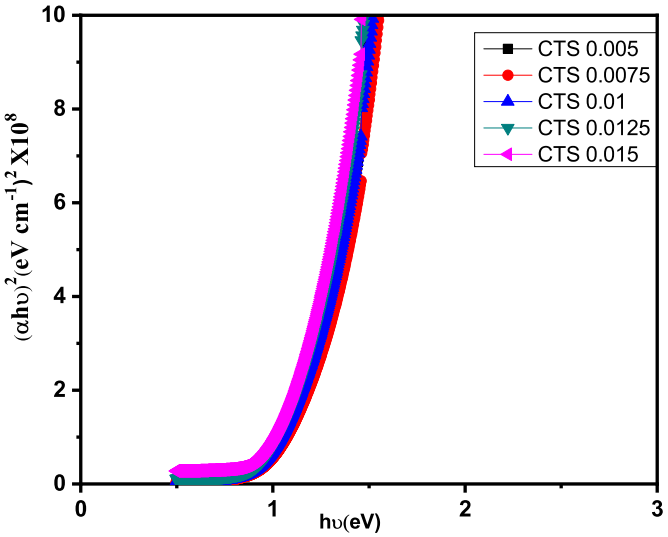

Figure 2.13: Tauc plot of CTS thin film

and S 0.005. The CTS film deposited over the ITO coated glass plate with spray rate 3 ml/min, substrate temperature 325 °C and the volume of spray 3 ml (minimum volume).As we expected, for lower molarity samples, shows light activity.

2.7.1 Error calculation

For error calculation of solar cell, 4 samples were fabricated in each case of molarity (0.005 M to 0.015 M) and each sample was deposited with nine electrodes. The electrodes were isolated from each other by scribing using doctors blade so that each electrode can act as single solar cell. On measuring the cell parameters all the electrodes in the sample show almost the same behavior. Hence cell parameters from one electrode (showing the best results) was selected from nine electrodes of each sample for error analysis.

Table 2.5 shows the photovoltaic parameters of the CTS solar cells fabricated with different molarities of the absorber layer. On comparing the activity of all these samples, slightly better light activity was obtained for samples from S 0.01 to S 0.005. The device S 0.005 (best cell shown in Figure 2.14) exhibited open circuit voltage of 261 mV, short circuit current density of 1.62 mA/cm^2, fill factor of 28% and efficiency of 0.12% [39].

Table 2.5: Photovoltaic parameters of the CTS solar cells fabricated with different molarities of absorber layer

Sample Name	V_{OC} (mV)	J_{SC} (mA/cm^2)	FF (%)	Efficiency (%)
S 0.015	No activity			
S 0.0125				
S 0.01	36±8	0.46±0.13	25±1	0.0005±0.002
S 0.0075	97±4	1.53±0.47	26±1	0.04±0.01
S 0.005	227±25	1.5±0.09	26±1	0.09±0.02

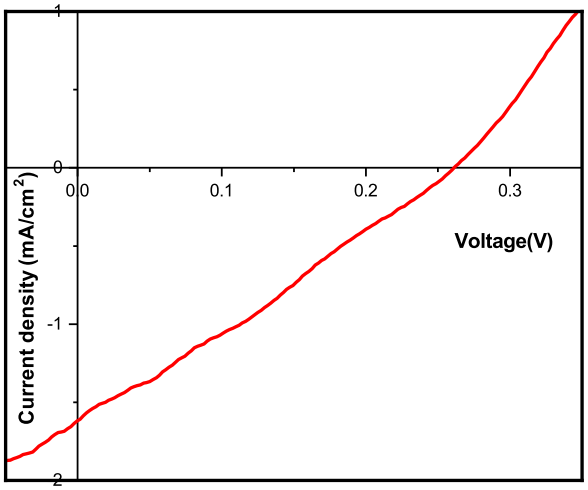

Figure 2.14: Illuminated J-V characteristics of S 0.005

For fine-tuning the thickness of the S 0.005 sample, the volume of CTS precursor solution was varied from 3 ml to 12 ml in the step of 3 ml and the samples were named as S3, S6, S9, and S12 respectively. The illuminated J-V characteristics of the solar cell (S3 to S 12) shown in Table 2.6 among these better one obtain for 6 ml. The device S 6 (best cell shown in Figure 2.15) showed an open circuit voltage of 384 mV short circuit current density of 2.32 mA/cm^2, fill factor of 28% and an efficiency of 0.25%.

Here also solar cells were fabricated with different tin and copper concentrations and in all case sulfur concentration kept constant (12); cell parameters

Table 2.6: Photovoltaic parameters of the CTS solar cells fabricated with different volumes of the absorber layer

Sample Name	V_{OC} (mV)	J_{SC} (mA/cm^2)	FF (%)	Efficiency (%)
S3	227±25	1.5±0.09	26±1	0.09±0.02
S6	374±19	2.2±0.17	26±2	0.22±0.04
S9	332±24	1.67±0.13	32±3	0.17±0.03
S12	50±30	0.88±0.28	24±1	0.01±0.0069

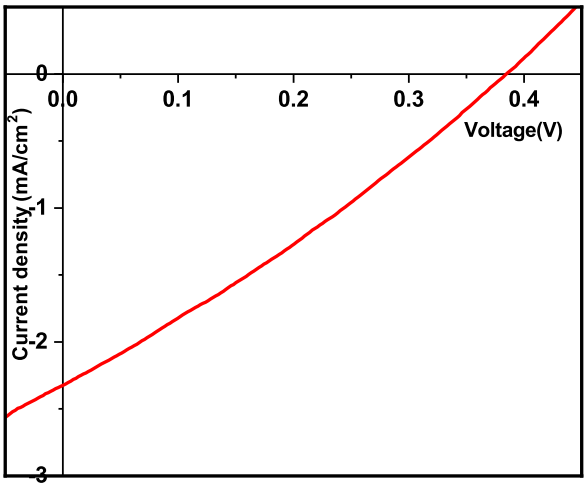

Figure 2.15: Illuminated J-V characteristics of the S 6

are given in Table 2.7. Among these cells, the one with Copper: Tin :Sulfur ratio of 1.6:0.8:12 (S 1.6 B) had better efficiency.

Table 2.7: Photovoltaic parameters of the CTS solar cells fabricated with different Tin and Copper concentration of absorber layer

Copper Concentration	Tin Concentration	Sulfur Concentration	Sample Name	V_{OC} (mV)	J_{SC} (mA/cm^2)	FF (%)	Efficiency (%)
1.2	0.4	12	S 1.2 A	18±5	1.64±0.09	25±1	0.007±0.002
	0.8	12	S 1.2 B	106±44	0.71±0.19	26±3	0.018±0.005
	1.2	12	S 1.2 C				
1.6	0.4	12	S 1.6 A	95±29	2.73±0.04	26±1	0.07±0.02
	0.8	12	S 1.6 B	374±19	2.2±0.17	26±2	0.22±0.04
	1.2	12	S 1.6 C	365±12	1.48±0.08	27±1	0.15±0.02
2	0.4	12	S 2 A	Short			
	0.8	12	S 2 B	119±14	3.3±0.13	27±.5	0.11±0.013
	1.2	12	S 2 C	229±24	1.5±0.07	25±2	0.09±0.02

2.8 Conclusion

In this chapter, the role of some of the significant spray parameters, such as substrate temperature, and molarity of precursor solution on the properties of CTS films were studied. From the substrate temperature variation studies, crystallinity was found to be increasing up to 325 °C and then decreased with further increase in temperature. Molarity variation does not change the optoelectronic properties of the film and hence it is used as an effective method for CTS sample thickness variation. Sprayed CTS/In_2S_3 solar cells were fabricated; light activity was obtained only in the case of low molarity sample. The efficiency of fabricated CTS/In_2S_3 solar cell was not improved (by Copper and Tin variation) up to our expectation; maximum efficiency obtained was 0.25%. The main reason for the low performance of solar cell might be due to the presence of HCl in the precursor solution of Tin. Since the further improvement of the solar cell was possible only by replacing the Tin precursor we replaced Stannous Chloride by Stannic Chloride and studies on those samples are presented in the following chapters.

References

[1] T. A. Kuku and O. A. Fakolujo, "Photovoltaic characteristics of thin films of cu2sns3," *Solar Energy Materials*, vol. 16, no. 1, pp. 199 – 204, 1987.

[2] T. Nomura, T. Maeda, and T. Wada, "Fabrication of cu2sns3solar cells by screen-printing and high-pressure sintering process," *Japanese Journal of Applied Physics*, vol. 53, p. 05FW01, jan 2014.

[3] M. Nakashima, J. Fujimoto, T. Yamaguchi, J. Sasano, and M. Izaki, "KF addition to cu2sns3thin films prepared by sulfurization process," *Japanese Journal of Applied Physics*, vol. 56, p. 04CS02, feb 2017.

[4] X. Liang, Q. Cai, W. Xiang, Z. Chen, J. Zhong, Y. Wang, M. Shao, and Z. Li, "Preparation and characterization of flower-like cu2sns3 nanostructures by solvothermal route," *Journal of Materials Science and Technology*, vol. 29, no. 3, pp. 231 – 236, 2013.

[5] J. Han, Y. Zhou, Y. Tian, Z. Huang, X. Wang, J. Zhong, Z. Xia, B. Yang, H. Song, and J. Tang, "Hydrazine processed cu2sns3 thin film and their application for photovoltaic devices," *Frontiers of Optoelectronics*, vol. 7, pp. 37–45, Mar 2014.

[6] M. Bouaziz, J. Ouerfelli, S. Srivastava, J. Bernde, and M. Amlouk, "Growth of cu2sns3 thin films by solid reaction under sulphur atmosphere," *Vacuum*, vol. 85, no. 8, pp. 783 – 786, 2011.

[7] Y.-X. Guo, W.-J. Cheng, J.-C. Jiang, and J.-H. Chu, "The effect of substrate temperature, cu/sn ratio and post-annealing on the phase-change and properties of cu2sns3 film deposited by ultrasonic spray pyrolysis," *Journal of Materials Science: Materials in Electronics*, vol. 27, pp. 4636–4646, May 2016.

[8] J. Koike, K. Chino, N. Aihara, H. Araki, R. Nakamura, K. Jimbo, and H. Katagiri, "Cu2sns3 thin-film solar cells from electroplated precursors," *Japanese Journal of Applied Physics*, vol. 51, p. 10NC34, oct 2012.

[9] R. Chierchia, F. Pigna, M. Valentini, C. Malerba, E. Salza, P. Mangiapane, T. Polichetti, and A. Mittiga, "Cu2sns3 based solar cell with 3% efficiency," *physica status solidi c*, vol. 13, no. 1, pp. 35–39, 2016.

[10] P. A. Fernandes, P. M. P. Salom, and A. F. da Cunha, "Cuxsnsx+1 (x = 2, 3) thin films grown by sulfurization of metallic precursors deposited by dc magnetron sputtering," *physica status solidi c*, vol. 7, no. 34, pp. 901–904, 2010.

[11] M. Nakashima, J. Fujimoto, T. Yamaguchi, and M. Izaki, "Cu2sns3thin-film solar cells fabricated by sulfurization from NaF/cu/sn stacked precursor," *Applied Physics Express*, vol. 8, p. 042303, apr 2015.

[12] A. Lokhande, K. Gurav, E. Jo, M. He, C. Lokhande, and J. H. Kim, "Towards cost effective metal precursor sources for future photovoltaic material synthesis: Cts nanoparticles," *Optical Materials*, vol. 54, pp. 207 – 216, 2016.

[13] A. Lokhande, K. Gurav, E. Jo, C. Lokhande, and J. H. Kim, "Chemical synthesis of cu2sns3 (cts) nanoparticles: A status review," *Journal of Alloys and Compounds*, vol. 656, pp. 295 – 310, 2016.

[14] L. Isac, A. Duta, A. Kriza, S. Manolache, and M. Nanu, "Copper sulfides obtained by spray pyrolysis possible absorbers in solid-state solar cells," *Thin Solid Films*, vol. 515, no. 15, pp. 5755 – 5758, 2007. Proceedings of Sympodium O on Thin Film Chalcogenide Photovoltaic Materials, EMRS 2006 Conference.

[15] P. S. Patil, "Versatility of chemical spray pyrolysis technique," *Materials Chemistry and Physics*, vol. 59, no. 3, pp. 185 – 198, 1999.

[16] R. R. Chamberlin and J. S. Skarman, "Chemical spray deposition process for inorganic films," *Journal of The Electrochemical Society*, vol. 113, no. 1, pp. 86–89, 1966.

[17] T. Sebastian, R. Jayakrishnan, C. S. Kartha, and K. P. Vijayakumar, "Characterization of spray pyrolysed cuins2 thin films," *The Open Surface Science Journal*, vol. 1, no. 3, pp. 1 – 6, 2009.

[18] D. Deepu, C. S. Kartha, and K. Vijayakumar, "How spray rate influences the formation and properties of transparent conducting sno2 thin films," *Journal of Analytical and Applied Pyrolysis*, vol. 121, pp. 24 – 28, 2016.

[19] S. Kermadi, S. Sali, F. A. Ameur, L. Zougar, M. Boumaour, A. Toumiat, N. Melnik, D. Hewak, and A. Duta, "Effect of copper content and sulfurization process on optical, structural and electrical properties of ultrasonic spray pyrolysed cu2znsns4 thin films," *Materials Chemistry and Physics*, vol. 169, pp. 96 – 104, 2016.

[20] V. Rajeshmon, C. S. Kartha, K. Vijayakumar, C. Sanjeeviraja, T. Abe, and Y. Kashiwaba, "Role of precursor solution in controlling the opto-electronic properties of spray pyrolysed cu2znsns4 thin films," *Solar Energy*, vol. 85, no. 2, pp. 249 – 255, 2011.

[21] N. Kamoun, H. Bouzouita, and B. Rezig, "Fabrication and characterization of cu2znsns4 thin films deposited by spray pyrolysis technique," *Thin Solid Films*, vol. 515, no. 15, pp. 5949 – 5952, 2007. Proceedings of Sympodium O on Thin Film Chalcogenide Photovoltaic Materials, EMRS 2006 Conference.

[22] G. Sunny, S. Vanalakar, and H. Min, "Studies on cu2sns3 thin films: Review," *Journal of Engineering and Applied Sciences*, vol. 13, pp. 4152–4159, 07 2018.

[23] M. Bouaziz, M. Amlouk, and S. Belgacem, "Structural and optical properties of cu2sns3 sprayed thin films," *Thin Solid Films*, vol. 517, no. 7, pp. 2527 – 2530, 2009. Thin Film Chalogenide Photovoltaic Materials (EMRS, Symposium L).

[24] A. Amlouk, K. Boubaker, and M. Amlouk, "A new procedure to prepare semiconducting ternary compounds from binary buffer materials and vacuum-deposited copper for photovoltaic applications," *Vacuum*, vol. 85, no. 1, pp. 60 – 64, 2010.

[25] M. Adelifard, M. M. B. Mohagheghi, and H. Eshghi, "Preparation and characterization of cu2sns3ternary semiconductor nanostructures via the spray pyrolysis technique for photovoltaic applications," *Physica Scripta*, vol. 85, p. 035603, feb 2012.

[26] U. Chalapathi, Y. Jayasree, S. Uthanna, and V. Sundara Raja, "Effect of annealing temperature on the properties of spray deposited cu2sns3 thin films," *physica status solidi (a)*, vol. 210, no. 11, pp. 2384–2390, 2013.

[27] U. Chalapathi, B. Poornaprakash, and S. Park, "Influence of cu/sn ratio on the structural, micrsostructural and optical properties of spray depositied cu2sns3 thin films," *Chalcogenide Letters*, vol. 13, no. 7, pp. 325–330, 2016.

[28] Z. Jia, Q. Chen, J. Chen, T. Wang, Z. Li, and X. Dou, "The photovoltaic properties of novel narrow band gap cu2sns3 films prepared by a spray pyrolysis method," *RSC Adv.*, vol. 5, pp. 28885–28891, 2015.

[29] V. V. Brus, I. S. Babichuk, I. G. Orletskyi, P. D. Maryanchuk, V. O. Yukhymchuk, V. M. Dzhagan, I. B. Yanchuk, M. M. Solovan, and I. V. Babichuk, "Raman spectroscopy of cu-sn-s ternary compound thin films prepared by the low-cost spray-pyrolysis technique," *Appl. Opt.*, vol. 55, pp. B158–B162, Apr 2016.

[30] J. Bougnot, S. Duchemin, and M. Savelli, "Chemical spray pyrolysis of cuinse2 thin films," *Solar Cells*, vol. 16, pp. 221 – 236, 1986.

[31] U. Chalapathi, B. Poornaprakash, and S.-H. Park, "Effect of thiourea concentration on the growth and properties of cu3sns4 thin films prepared by spray pyrolysis," *Journal of Materials Science: Materials in Electronics*, vol. 28, pp. 2954–2961, Feb 2017.

[32] T. S. Reddy, R. Amiruddin, and M. S. Kumar, "Deposition and characterization of cu2sns3 thin films by co-evaporation for photovoltaic application," *Solar Energy Materials and Solar Cells*, vol. 143, pp. 128 – 134, 2015.

[33] G. Sunny, C. S. Kartha, and K. P. Vijayakumar, "Tuning of optoelectronic properties of cu2sns3 thin films through variation of stoichiometry," *AIP Conference Proceedings*, vol. 1591, no. 1, pp. 1750–1752, 2014.

[34] M. Ortega-Lpez and A. Morales-Acevedo, "Characterization of cuins2 thin films for solar cells prepared by spray pyrolysis," *Thin Solid Films*, vol. 330, no. 2, pp. 96 – 101, 1998.

[35] Y. K. Kumar, P. U. Bhaskar, G. S. Babu, and V. S. Raja, "Effect of copper salt and thiourea concentrations on the formation of cu2znsns4 thin films by spray pyrolysis," *physica status solidi (a)*, vol. 207, no. 1, pp. 149–156, 2010.

[36] A. S. Cherian, T. Abe, Y. Kashiwaba, C. S. Kartha, and K. Vijayakumar, "Cuins2/in2s3 cells using a cost-effective technique: Significance of precursor ratios on cell parameters," *Energy Procedia*, vol. 15, pp. 283 – 290, 2012. International Conference on Materials for Advanced Technologies 2011, Symposium O.

[37] M. Santhosh, D. Deepu, C. S. Kartha, K. R. Kumar, and K. Vijayakumar, "All sprayed ito-free cuins2/in2s3 solar cells," *Solar Energy*, vol. 108, pp. 508 – 514, 2014.

[38] M. S. Sreejith, D. R. Deepu, C. S. Kartha, K. Rajeevkumar, and K. P. Vijayakumar, "Tuning the properties of sprayed cuzns films for fabrication of solar cell," *Applied Physics Letters*, vol. 105, no. 20, p. 202107, 2014.

[39] G. Sunny, T. Thomas, D. Deepu, C. S. Kartha, and K. Vijayakumar, "Thin film solar cell using earth abundant cu2sns3 (cts) fabricated through spray pyrolysis: Influence of precursors," *Optik*, vol. 144, pp. 263 – 270, 2017.

Chapter 3

Characterization of CTS film Prepared using Stannic Chloride precursor

Contents

3.1 Introduction

Solar cell fabricated with the structure of ITO/CTS/In_2S_3/Ag did not show light activity up to our expectation, as explained/observed in the previous chapter. In the previous chapter for the deposition of CTS film, stannous chloride was used as the tin precursor. In this case, HCl was required for dissolving stannous chloride in demineralized water. Presence of HCl may be the reason for low performance of the solar cells prepared using this type of CTS films. it is observed that presence of higher quantity of HCl reduces the cell performance of CZTS based solar cell [1]. To avoid presence of larger quantity of HCl in the precursor solution, we replaced the tin precursor with stannic chloride; it has high solubility in water as compared to stannous chloride and hence it does not need HCl to dissolve in water. This chapter deals with preparation of CTS films prepared using stannic chloride as the tin precursor and characterisation of these films through structural, electrical and optical techniques. This chapter also deals with thickness variation of the new CTS films due to molarity variation as well as optimization of the spray parameters such as substrate temperature and spray rate for this new set of films.

3.2 CTS film deposition using Stannic Chloride precursor

For the deposition of this new set of CTS films, same precursors were used for copper and sulfur as in the case of the previous chapter (i.e., copper chloride ($CuCl_2.2H_2O$) and thiourea ($SC(NH_2)_2$) dissolved in demineralized water). Here we used stannic chloride ($SnCl_4.5H_2O$) instead of stannous chloride ($SnCl_2.2H_2O$) as tin precursor. The stock solutions of copper and sulfur were prepared in the same way as explained in the previous chapter. The stock solution of 1 M stannic chloride was prepared by dissolving 17.5299 g of salt in 50 ml demineralized water. Solution with desired molarity for spray was obtained by modifying/diluting required volume of the stock solution as per the Equation 2.1 in chapter 2. CTS film was deposited with Cu:Sn:S ratio of 1.6:0.8:12 with molarity 0.015. The quantities of copper, tin, and thiourea salt solutions (stock solution) taken for preparing the spray solution of 30 ml were 0.72, 0.36 and 5.4 ml respectively. The precursor solution was sprayed onto cleaned and preheated glass substrates, (maintained at 325 °C), using compressed air as the carrier gas. For the deposition of this set of films too, spray rate and volume of spray solution were maintained at 3 ml/min, and 30 ml respectively and the deposited film was named as CTS-Cl4.

3.2.1 Structural studies

Figure 3.1 illustrates the XRD pattern of sample CTS-Cl4. From literature, Cu_2SnS_3 films crystallize in different crystal structures such as cubic [2, 3] [4], tetragonal [5, 6], hexagonal [7], monoclinic [8, 9] or triclinic [10, 11]. XRD analysis of the deposited film gave the same result as in the case of CTS films deposited with stannous chloride tin precursor. The peaks obtained here were corresponding to (112), (200), (220), and (312) planes of Cu_2SnS_3 having tetragonal structure(ICDD card number- 089-4714) [5, 12, 13]. No significant variation in the structural properties was observed on changing the tin precursor; similarly, peaks corresponding to any other impurity phase were not detected in XRD analysis.

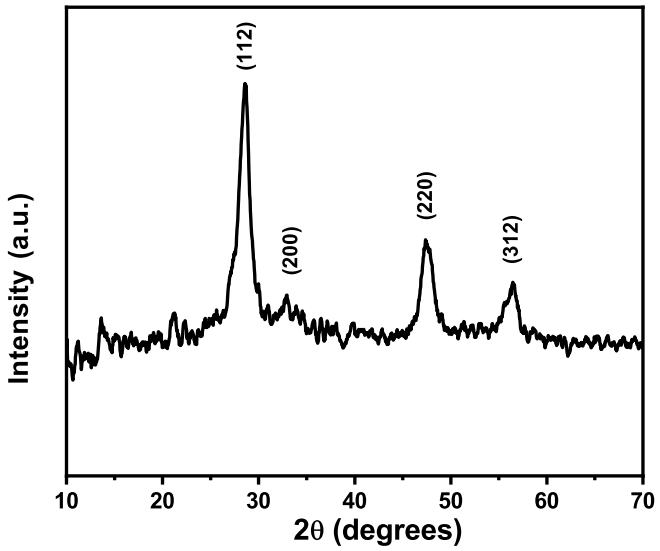

Figure 3.1: XRD patterns of CTS-Cl4 film

3.2.2 Electrical properties

Electrical properties of sample CTS-Cl4 were analyzed using Hall measurement, which disclosed the p-type nature of the film, with carrier concentration, mobility, and resistivity as 1.2×10^{21} cm^{-3}, 1.03 cm^2/Vs, and 4.77×10^{-3} Ωcm respectively. Electrical properties of the samples also did not show any significant variation on changing tin precursor to stannic chloride.

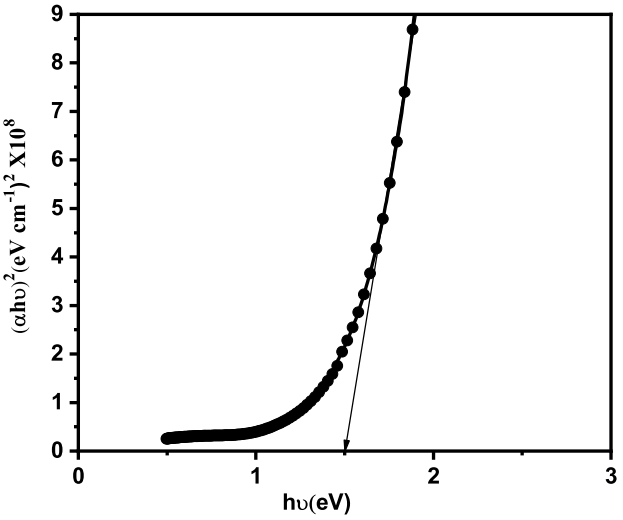

Figure 3.2: Tauc plot of deposited CTS-Cl4 film

3.2.3 Optical characterization

$(\alpha h\nu)^2$ versus $h\nu$ plot (Tauc plot) of sample CTS-Cl4 is shown in Figure 3.2. Optical analysis indicated bandgap of 1.5 eV; here also there was no evidence for any other impurity phase. However, the samples CTS-Cl4 deposited with stannic chloride precursor have higher band gap compared to those prepared using stannous chloride precursor. The same behaver was observed in the case of CZTS thin films too [14].

3.2.4 XPS analysis

Composition and stoichiometry of the film were analyzed using X-ray photoelectron spectroscopy (XPS). XPS spectra are obtained by irradiating the surface of a sample with x-rays resulting in emission of photoelectrons. Binding energy of the emitted electrons can be calculated using the equation

$$\mathrm{E}_{\text{ binding}} = \mathrm{E}_{\text{ photon}} - (\mathrm{E}_{\text{ kinetic}} + \phi) \tag{3.1}$$

where
$\mathrm{E}_{\text{ binding}}$: binding energy (BE) of the electron,
$\mathrm{E}_{\text{ photon}}$: the energy of irradiating X-ray,
$\mathrm{E}_{\text{ kinetic}}$: kinetic energy (KE) of electrons and ϕ: work function.

In the present study, XPS spectra were recorded using Kratos Analytical AMICUS spectrometer. XPS measurements figure out the atomic composition and chemical state of the elements present in the sample. To analyze elemental concentration across thickness of the film depth profile analysis was done using argon ion etching (2 KV and 20 mA). Figure 3.3 represents the atomic concentration of elements (Cu, Sn, O, Na, Cl, and S) vs etching time (i.e., film thickness). From the depth profile analysis, copper and tin atomic concentration maintain almost stoichiometric ratio throughout the film and the concentration of chlorine throughout the film is less than 1%. Sulfur content in CTS film is low which may be due to the high volatile nature of sulfur at high temperature. From the XPS depth profile, concentration of copper, tin, and sulfur was found to be constant throughout the thickness of the film.

Figure 3.4 illustrates core level peaks of Cu 2p; binding energies of corresponding to Cu $2p_{1/2}$ and Cu $2p_{3/2}$ are 952.4 eV and 932.6 eV, with separation

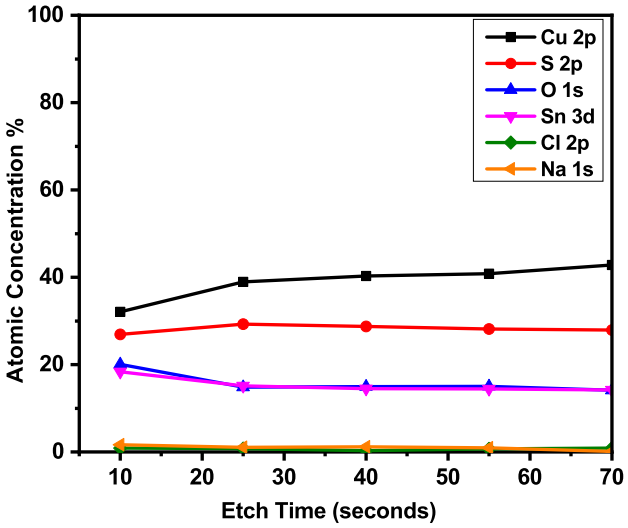

Figure 3.3: Depth profile of CTS-Cl4

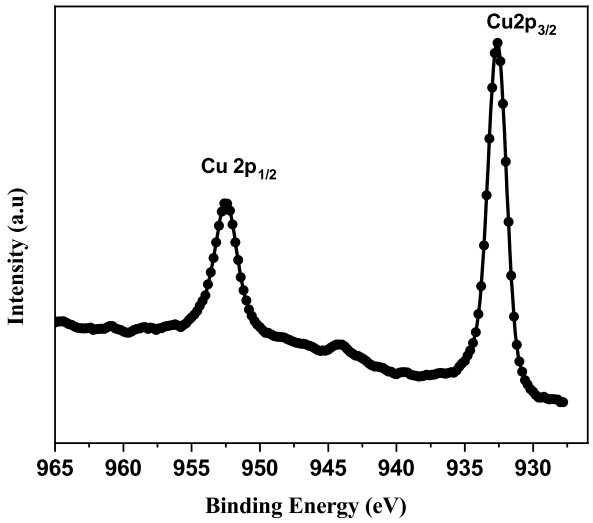

Figure 3.4: XPS core level peaks of Cu 2p

of 19.8 eV. Hence it can be concluded that it is +1 oxidation state of copper in the compound (Cu^{+} state) [10, 15] Figure 3.5 shows the Sn 3d core-level spectrum; the spectra illustrate binding energies at 494.7 and 486.4 eV corresponding to Sn $3d_{5/2}$ and $3d_{3/2}$ respectively and this confirms existence of tin in Sn^{4+} state. No other peak corresponding to Sn^{2+} was observed [16]. From Figure 3.6 one can see peaks corresponding to S $2p_{3/2}$ and S $2p_{1/2}$ (binding energies 162.7 eV and 161.6 eV respectively), which proved that sulfur existed in S^{2-} state [10].

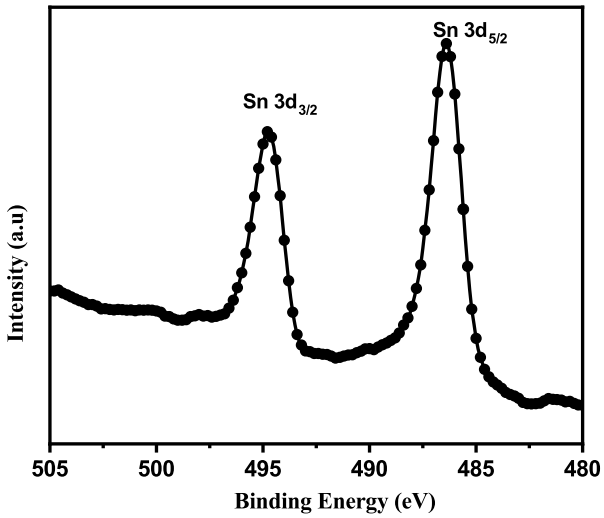

Figure 3.5: XPS core level peaks of Sn 3d

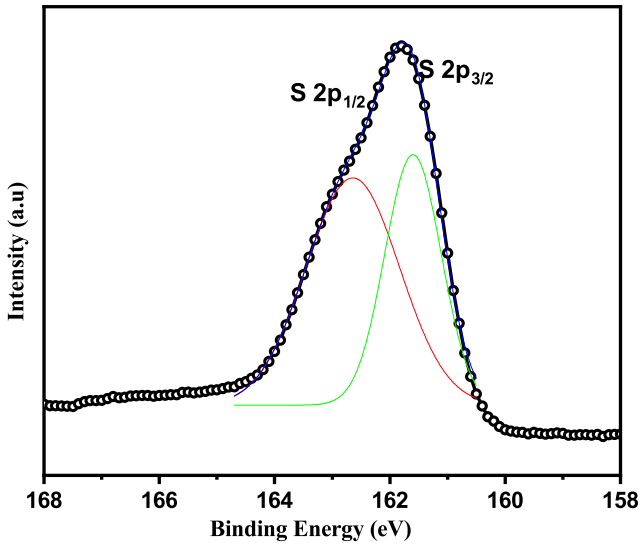

Figure 3.6: XPS core level peaks of S 2p

3.3 Thickness variation of CTS film due to molarity variation

In solar cells, thickness of absorber layer plays an important role in determining its efficiency. From the previous chapter, we knew that molarity variation is an effective method for thickness variation of CTS film. Here also thickness

variation takes place with molarity variation of the precursor solution. Usually, in chemical spray pyrolysis, thickness variation of the film is achieved by varying deposition time [17].

3.3.1 Experimental details

For the CTS film fabrication, precursor used for copper, tin and sulfur are copper chloride ($CuCl_2.2H_2O$), stannic chloride ($SnCl_4.5H_2O$) and thiourea ($SC(NH_2)_2$) which were dissolved in demineralized water (in the same way as described earlier). To study variation in optoelectronic properties as well as thickness of the samples with molarity of the precursor solution, molarity of precursor solution was varied from 0.015 to 0.005 in steps of 0.0025. Cu:Sn:S ratio in the precursor solution was maintained as 1.6:0.8:12 in all cases. Substrate temperature, volume of spray and spray rate were fixed at 325 °C, 30 ml and 3 ml/min respectively. These samples were named as Cl4 0.015M. Cl4 0.0125M, Cl4 0.001M, Cl4 0.0075M and Cl4 0.005M.

Table 3.1: Thickness measurements of CTS films with different molarities.

Sample Name	Thickness(nm)
Cl4 0.015M	1100±50
Cl4 0.0125M	740±35
Cl4 0.01M	580±40
Cl4 0.0075M	370±30
Cl4 0.005M	200±35

3.3.2 Thickness measurements

Thickness values of the sample measured using stylus thickness profiler (Dektak-6 M) are given in Table 3.1. As anticipated, the thickness of the films decreased with a decrease in the molarity of the precursor solution.

3.3.3 Structural properties

3.3.3.1 XRD analysis

XRD measurements were done on all these films (Cl4 0.015M to Cl4 0.005M) and the results are shown in Figure 3.7. The peaks obtained are compared with standard data (ICDD card number- 089-4714)and the peaks are corresponding to (112), (200), (220), and (312) planes of Cu_2SnS_3 with tetragonal structure [12, 18]. Peaks indicating any impurity phases were not detected. As in the case of CTS film deposited using stannous chloride, film prepared using this precursor with lower molarity, (CTS 0.005) appears to be amorphous, which may be due to low thickness of the deposited film. On increasing the volume of spray solution to 75 ml for this sample, the XRD pattern (Figure 3.8) developed all peaks corresponding to the tetragonal structure of CTS.

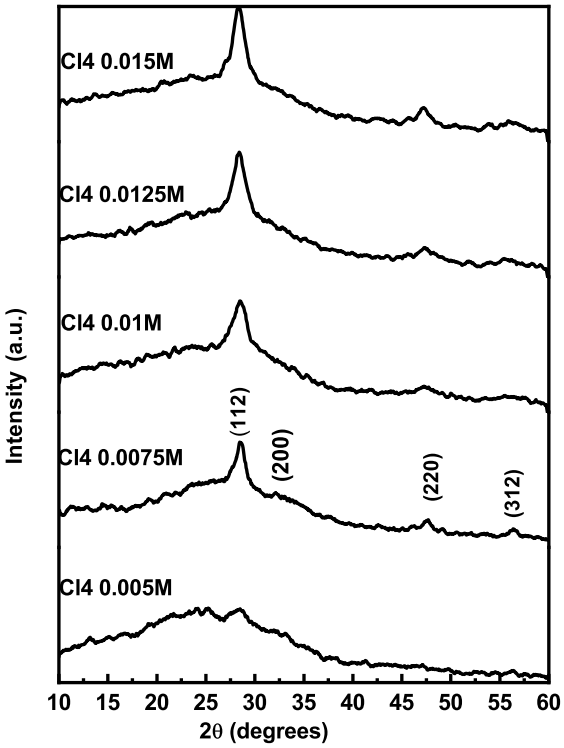

Figure 3.7: XRD patterns of CTS films deposited at different molarities

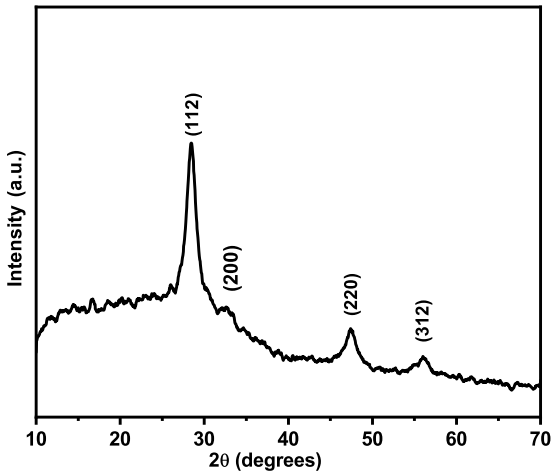

Figure 3.8: XRD patterns of CTS film deposited at a molarity of 0.005M and precursor volume of 75ml

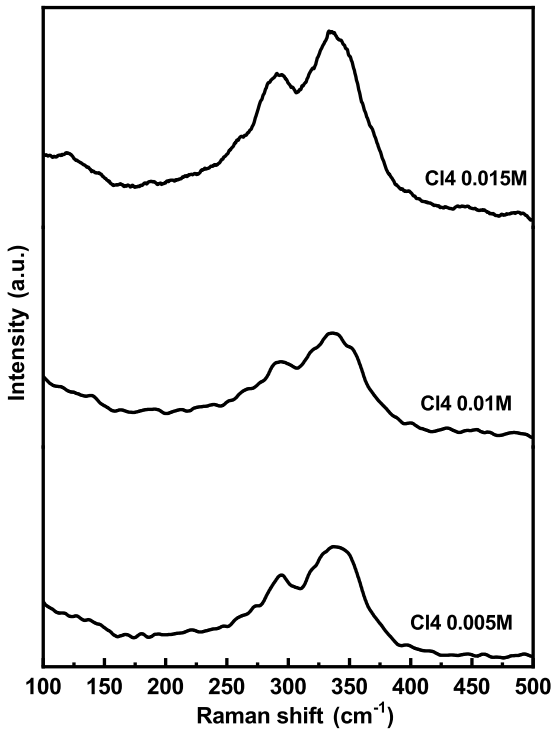

Figure 3.9: Raman analysis of CTS films deposited at different molarities

3.3.3.2 Raman analysis

Figure 3.9 shows Raman spectra of the samples Cl4 0.005M, Cl4 0.01M, and Cl40.015M. The most intense mode at 337 cm^{-1} and weaker peak at 294

cm^{-1}correspond to the tetragonal CTS phase. It was reported earlier that for tetragonal CTS phase, the intense mode is at 335-337 cm^{-1} along with two low intense peaks at 297 and 351 cm^{-1} [18, 19]. The peak at 351 was not observed in the sample this may be due to either negligible height or low-intensity peak merged with the high-intensity peak of 337 cm^{-1}

Table 3.2: Electrical characterizations of CTS films with different molarity.

Sample Name	Carrier Concentration (cm^{-3})	Resistivity (Ωcm)	Mobility (cm^2 /Vs)
Cl4 0.005M	1.06×10^{21}	4.46×10^{-3}	1.31
Cl4 0.0075M	1.84×10^{21}	5.35×10^{-3}	0.63
Cl4 0.01M	1.09×10^{21}	5.44×10^{-3}	1.05
Cl4 0.0125M	9.92×10^{20}	9.47×10^{-3}	0.67
Cl4 0.015M	1.27×10^{21}	4.77×10^{-3}	1.03

3.3.4 Electrical properties

Results of Hall measurements are shown in Table 3.2 and this proved beyond doubt that all the samples are p-type in nature and mobility values are comparable with that of other absorber materials like CZTS and CIS deposited by CSP technique [14, 20]. Electrical properties of these samples do not show any significant change due to the variation molarity of the precursor. Hence molarity variation can be effectively used for the thickness variation of the films.

3.3.5 Optical characterization

$(\alpha h\nu)^2$ versus $h\nu$ plot of the CTS thin films deposited with different molarities are shown in Figure 3.10. Optical band gap does not show any variation with change molarity of the precursor solution, and have a band gap of $\sim$ 1.5 eV.

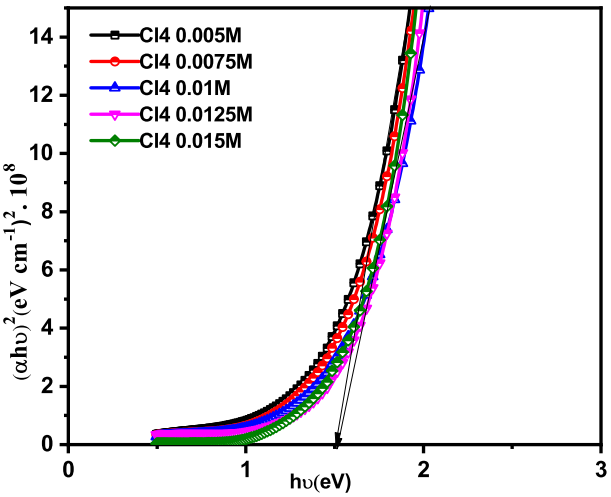

Figure 3.10: Tauc plot of deposited CTS film

Table 3.3: AFM analysis of CTS films with different molarity.

Sample Name	Roughness (nm)
Cl4 0.005M	74
Cl4 0.01M	84
Cl4 0.015M	88

3.3.6 Morphological characterization

Surface morphology is one of the important parameters in determining the solar cell performance, especially for Extremely Thin Absorber (ETA) type solar cells. In this case, high roughness of the film can result in creating shunting path for the minority carriers and thereby reducing the cell performance. Surface morphology of films with different molarities was studied with the help of atomic force microscopy (AFM). In the present study, the scanning was done with Nanosurf Easyscan 2 tabletop model AFM. The results indicated that the root mean square (RMS) value of roughness of the samples decreased with decrease in the molarity. AFM analysis of the sample Cl4 0.005M, Cl40.01M and Cl4 0.015M are shown in Figure 3.11.

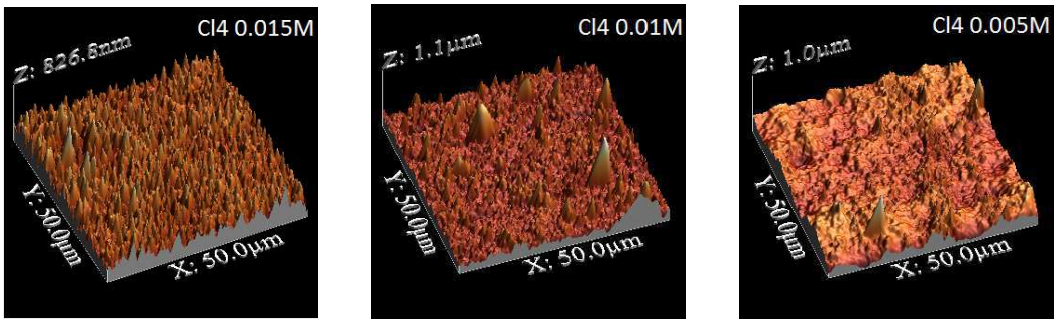

(a) *(b)* *(c)*

Figure 3.11: AFM image of the CTS sample with molarity (a). 0.015, (b). 0.01 and (c). 0.005

3.3.7 Solar cell fabrication

Solar cells were fabricated with varied molarity (0.005 to 0.015 M). Here Cu:Sn:S ratio, the volume of the precursor solution and spray rate were taken as 1.6:0.8:12, 6 ml and 3 ml/min respectively. Solar cells fabricated with molarity (0.005 to 0.015 M) were named as s0.005, s0.0075, s0.01, s0.0125 and s0.015 respectively. Quantities of copper, tin and sulfur salt solutions required for the deposition of solar cells are given in Table 3.4. Illuminated solar cell parameters are given in Table 3.5. Error calculations were done in the same way as in the previous chapter 2 (2.7.1 Error calculation).

Sample s0.005 exhibited better performance, similar to the case of solar cells fabricated using stannous chloride as tin precursor. From the morphological characterization (Section 3.3.6), this type of samples showed minimum roughness; this may be the reason for better performance of the cell. Cell parameters of the best cell are open circuit voltage of 359 mV, short circuit current density of 5.9 mA/cm^2, fill factor of 40% and efficiency of 0.84%.

Table 3.4: Preparation of precursor solution with different molarity for solar cell fabrication

Sample Name	The volume of the precursor solution to be sprayed (ml)	Amount of 1M copper chloride solution added to the spray solution (ml)	Amount of 1M tin chloride solution added to the spray solution (ml)	Amount of 1M thiourea solution added to the spray solution (ml)
s0.005	6	0.048	0.024	0.36
s0.0075	6	0.072	0.036	0.54
s0.01	6	0.096	0.048	0.72
s0.0125	6	0.12	0.06	0.9
s0.015	6	0.144	0.072	1.08

Table 3.5: Photovoltaic parameters of the device fabricated with different molarity of CTS film.

Sample Name	V_{OC} (mV)	J_{SC} (mA/cm^2)	FF (%)	Efficiency (%)
s0.005	350±18	5.85±0.28	40±1	0.82±0.02
s0.0075	318±4	4.72±0.11	33±1	0.495±0.01
s0.01	197±8	3±0.11	37±3	0.22±0.02
s0.0125	95±29	2.73±0.05	26±0.5	0.07±0.02
s0.015	No light activity			

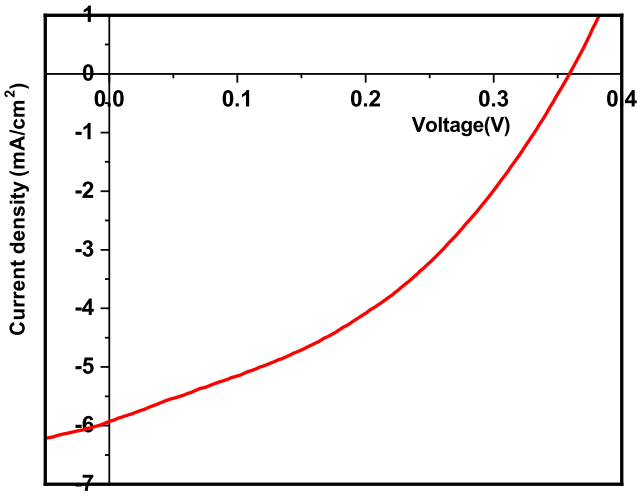

Figure 3.12: J-V characteristics of solar cell s0.005 (best among cells fabricated).

3.4 Substrate temperature variation

In the present work, precursors were copper chloride ($CuCl_2.2H_2O$), stannic chloride ($SnCl_4.5H_2O$) and thiourea (CH_4N_2S) in the ratio 1.6:0.8:12 (Cu: Sn: S) which were dissolved in demineralized water. Ultrasonically cleaned micro glass slides were used as substrate with area 2 cm^2 and thickness 1.2 mm. In the case of CSP technique, substrate temperature plays critical role in forming well adherent, pinhole free, uniform good quality film. From the literature review, deposition temperature for spray pyrolysis of CTS film was found to be between 285 - 360 °C [18, 21–23]. In order to optimize this parameter, films were deposited at different substrate temperatures, varying from 275 to 375 °C, in steps of 25 °C while the other parameters like Cu:Sn:S ratio, spray rate and volume of solution sprayed were kept constant as 1.6:0.8:12, 3 ml/min and 75 ml respectively; these samples were named as CTS 275, CTS 300, CTS 325, CTS 350, and CTS 375.

3.4.1 Structural characterization

Samples CTS 275 to CTS 375 depicted X-ray diffraction peaks (Figure 3.13) corresponding to the (112), (220), and (312) planes which are characteristics of CTS films with tetragonal structure (ICDD 089-4714). Preferential orientation was along (112) plane. Peaks in the XRD pattern became more intense

up to the substrate temperature of 325 °C. However further increase in substrate temperature resulted in the decrease of peak intensity. Film growth was dominant at lower substrate temperature (i.e., up to 325 °C) while at higher substrate temperature, probably evaporation is taking place and this might be the reason for reduction in the intensity of XRD peaks. But it is to be noted here that there is no secondary phase formation anywhere in this temperature range.

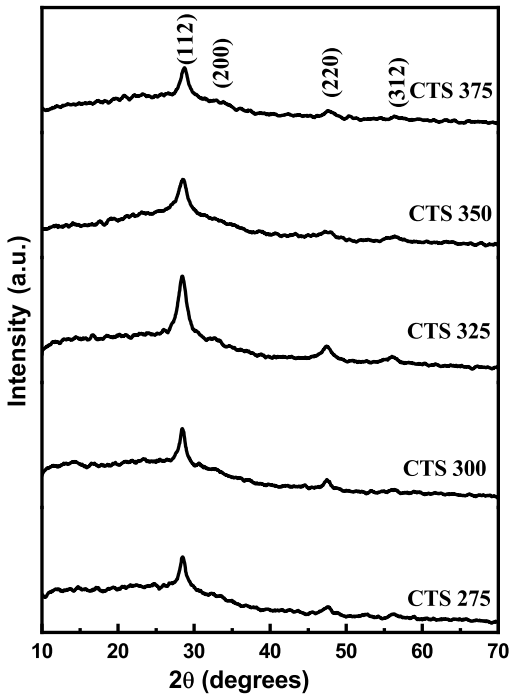

Figure 3.13: XRD patterns of samples CTS 275 to CTS 375

3.4.2 Optical characterization

Effect of substrate temperature on optical properties of CTS thin films was studied by measuring optical absorption spectra in the wavelength range 190-2500 nm. Optical band gap was calculated by plotting (hν) vs $(\alpha h\nu)^2$ graphs (Figure 3.14). Thickness of the film measured using stylus profiler proved that there was decrease of thickness with increase in temperature (from 1.4 to 0.8m). Optical studies disclosed that samples possess band gap of $\sim$ 1.5 eV (band gap slightly decreased from 1.54 to 1.49 eV with increase in substrate temperature).

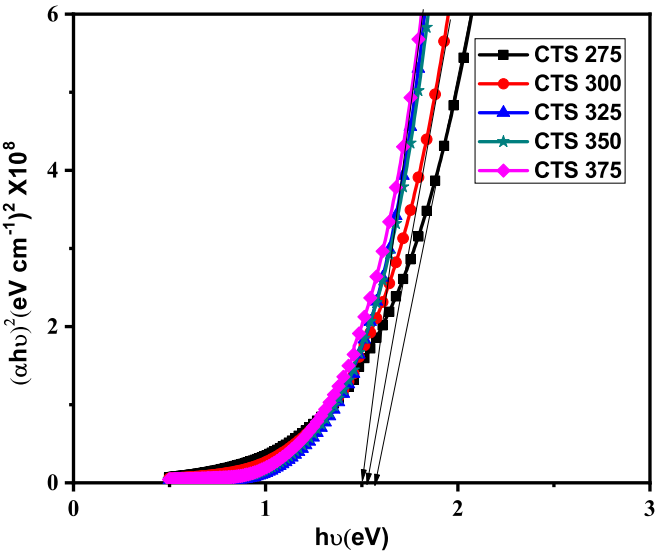

Figure 3.14: Tauc plot of samples CTS 275 to CTS 375.

3.4.3 Electrical characterization

Electrical properties (such as resistivity, mobility and carrier concentration) of all samples are presented in Table 3.6. All samples were found to be p-type from both hot probe and Hall measurement methods. Here the samples had almost the same mobility with slight increase for those prepared at substrate temperature 325 °C (CTS 325) and this may be due to better crystallization of the films at this temperature. Hence this substrate temperature was selected for further work.

Table 3.6: Electrical characterization of samples CTS 275 to CTS 375.

Sample Name	Carrier Concentration (cm^{-3})	Resistivity (Ωcm)	Mobility (cm^2/Vs)
CTS 275	3.15×10^{20}	2.52×10^{-2}	0.79
CTS 300	4.17×10^{20}	1.35×10^{-2}	1.11
CTS 325	9.64×10^{20}	4.80×10^{-3}	1.35
CTS 350	1.01×10^{21}	6.22×10^{-3}	1
CTS 375	7.39×10^{20}	8.31×10^{-3}	1.02

3.5 Spray rate variation

In order to optimize the spray rate, samples were prepared with different spray rates using the same precursor as copper chloride ($CuCl_2.2H_2O$), stannic chloride ($SnCl_4.5H_2O$) and thiourea (CH_4N_2S). substrate temperature was fixed at 325 °C and Cu:Sn:S ratio was taken as 1.6:0.8:12; volume of solution sprayed was 75 ml, while spray rate of the sample was varied from 3 ml/min to 9 ml/min in steps of 2 ml/min. These samples were named according to spray rate as CTS 3, CTS 5, CTS 7 and CTS 9. On decreasing the spray rate below 3 ml/min, film formation was not proper.

3.5.1 Structural characterization

Figure 3.15 depicts XRD data of all the deposited films and the films have diffraction peaks corresponding to (112), (220) and (312) planes of CTS. These are characteristic peaks of tetragonal structured Cu_2SnS_3 with preferential orientation along (112) plane (ICDD 089-4714), as explained earlier. Very interestingly (and unlike in earlier cases) formation of Cu_xS_x impurity phase, in addition to CTS peak, began for higher spray rate and this secondary phase became prominent with increase in spray rate. The peak intensity of the CTS phase decreased with increase in spray rate. This can be explained in the following way: At higher spray rate, large quantity of precursor solution falls on the substrate, making the pyrolysis reaction of the first layer incomplete when the next layer is deposited, leading to the formation of impurity or amorphous phase [24]. From the XRD peak at $2\theta = 46.7°$, it is clear that the peak broadens at the spray rate of 5 ml/min, and on further increasing the spray rate, this peak splits in to two; the peak at $2\theta = 46.7°$ corresponds to CTS phase and the other peak at $2\theta = 46.2°$ corresponds to Cu_9S_5 impurity phase [25]. Intensity of the impurity phase increases with further increase in spray rate. Study based on XRD measurements also hints that the film showing the best crystallinity was obtained at the spray rate of 3 ml/min (CTS 3) in which impurity phases were totally absent. Raman analysis of the sample CTS 3 was already done (Figure 3.9 sample name Cl4 0.005M) and from this result also it is clear that the CTS 3 sample crystalizes in tetragonal phase with no impurity phase formation.

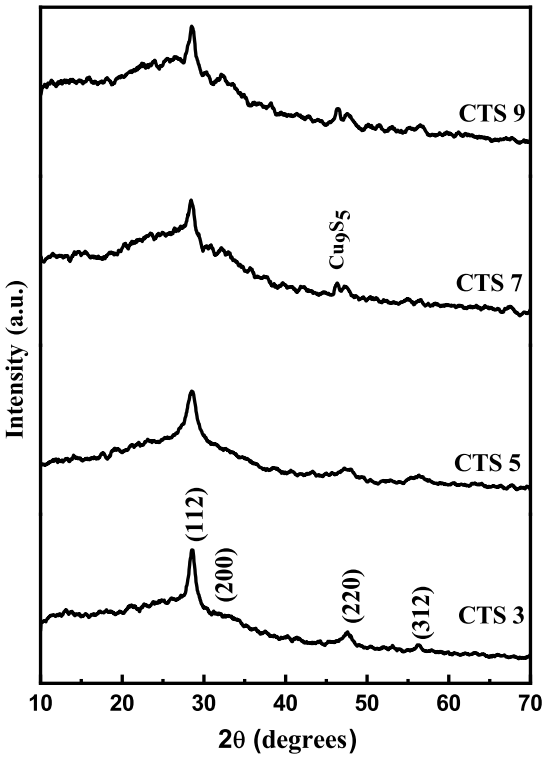

Figure 3.15: XRD patterns of CTS 3 to CTS 9.

3.5.2 Optical characterization

To estimate optical band gap of the samples prepared with different spray rates, again Tauc's approximation was used. As seen in Figure 3.16, there is no variation in the band gap with the variation of spray rate of the precursor solution for samples from CTS 3 to CTS 7. Band gap is $\sim$ 1.5 eV which is suitable for absorber layer in photovoltaic energy conversion. But in the case of highest spray rate (9 ml/min; CTS 9), higher band gap of 1.62 eV is observed which may be due to the formation of the impurity phase.

3.5.3 Morphological characterizations

Surface morphology is very important in developing device quality thin film and the surface morphologies of the deposited films (CTS 3 to CTS 9) were determined using AFM (Figure 3.17). AFM images show the direct relationship between surface roughness and spray rate. Surface roughness increased

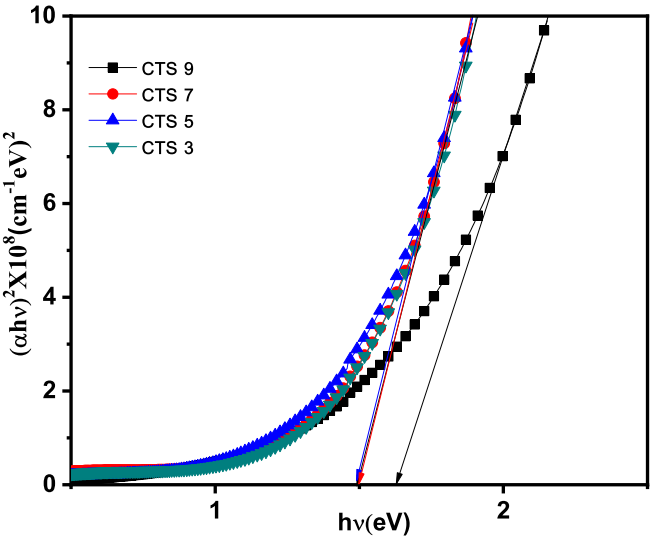

Figure 3.16: Tauc plot of samples CTS 3 to CTS 9

with increase in spray rate. This result is generally anticipated in CSP technique. From Figure 3.17, it is clear that, with increase in spray rate, cluster formation increases. With the increase in spray rate, higher quantity of precursor solution falls on the substrate from the nozzle resulting in incomplete pyrolytic reaction of the precursor as well as lowering of substrate temperature. Here lowering the substrate temperature can lead to variation in nature of film growth leading to changes in surface roughness. With the increase in spray rate, droplet size of the spray also increases which can cause the formation of large cluster. In device fabrication, cluster formation usually leads to poor performance of the cell. RMS roughness of the samples deposited with different spray rate is shown in Table 3.7. Morphological characterizations point out that lower spray rates are preferred for the formation of uniform films without much roughness.

3.5.4 Electrical characterization

Electrical properties of the samples are studied using Hall measurement at the temperature of 300 K (Table 3.8). All the samples showed p-type conductivity; carrier concentration, resistivity, and mobility are in good agreement with other published reports [26]. Resistivity of the samples is low in general and there is slight increase with increase in spray rate. This may be due to the fact

Table 3.7: RMS roughness of samples CTS 3 to CTS 9.

Sample Name	Roughness (nm)
CTS 3	74
CTS 5	135
CTS 7	285
CTS 9	368

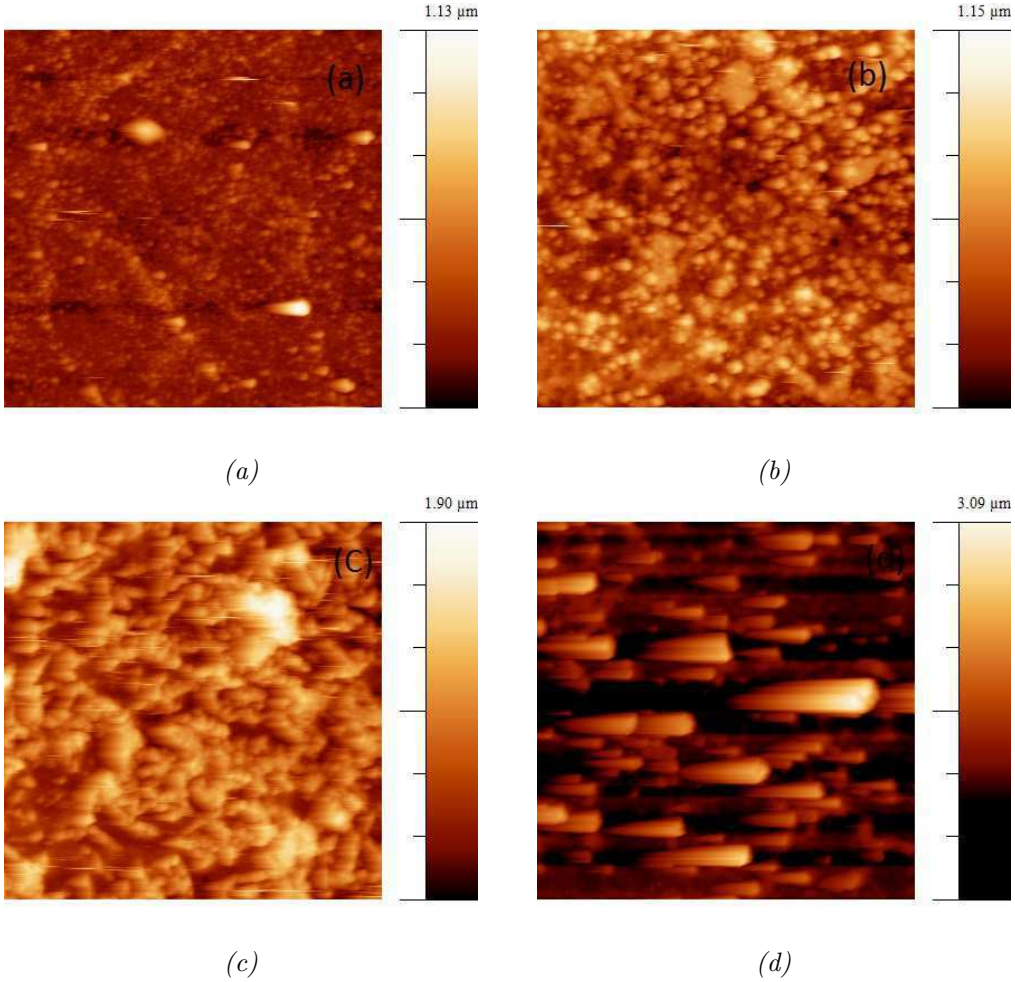

(a) *(b)*

(c) *(d)*

Figure 3.17: AFM (two-dimensional) image of (a) CTS 3, (b) CTS 5, (c) CTS 7 and (d) CTS 9.

Table 3.8: Electrical characterizations of sample CTS 3 to CTS 9.

Sample Name	Carrier Concentration (cm^{-3})	Resistivity (Ωcm)	Mobility (cm^2/Vs)
CTS 3	9.64×10^{20}	4.80×10^{-3}	1.35
CTS 5	8.37×10^{20}	5.53×10^{-3}	1.35
CTS 7	5.7×10^{20}	9.77×10^{-3}	1.12
CTS 9	3.60×10^{20}	1.42×10^{-2}	1.22

that at higher spray rate, film formation is not uniform and crystallinity of the film also declines. Moreover, electrical resistivity increases with increase in the surface roughness, as observed by Tang et.al [27].

3.5.5 Solar cell fabrication

Solar cells were fabricated with all these samples (CTS 3 to CTS 9). The deposition parameters such as substrate temperature, and Cu:Sn:S ratio were taken as 325 °C, and 1.6:0.8:12 respectively. To check constancy of the cell, 4 samples were fabricated in each case of spray rate (spray rate 3 ml to 9 ml) and each sample was deposited with nine electrodes. The electrodes were isolated from each other by scribing using doctors blade so that each electrode can act as single solar cell. On measuring the cell parameters all the electrodes in the sample show almost the same behavior. Hence cell parameters from one electrode (showing the best results) was selected from nine electrodes of each sample for error analysis.

The solar cell parameters are tabulated in Table 3.9. Performance of solar cells shows decreasing nature with increase in spray rate. The poor performance of solar cell at higher spray rate may be due to the increased roughness of the film or due to the formation of the impurity phase as we saw in the characterization results of these films. Solar cell with lower spray rate showed better light activity. The best among the solar cell fabricated using CTS sample S3 (with low spray rate) had open circuit voltage of 359 mV, short circuit current density of 5.9 mA/cm^2, fill factor of 40% and efficiency of 0.84%.

Table 3.9: Photovoltaic parameters of the device fabricated with different spray rate precursor solution of CTS film.

Solar Cell Name	V_{OC} (mV)	J_{SC} (mA/cm^2)	FF (%)	Efficiency (%)
S 3	350±18	5.85±0.28	40±1	0.82±0.02
S 5	346±3	4.78±0.1	38±0.8	0.625±0.01
S 7	267±10	3.4±0.44	35±6	0.31±0.04
S 9	30±29	1.24±0.19	25±2	0.009±0.01

3.6 Conclusion

Structural and electronic properties did not show significant variation with change in tin precursor solution. But optical characterization proved that, on changing the tin precursor, band gap of the deposited film increased to 1.5 eV. Molarity variation study showed that there was no variation in structural or optoelectronic properties of the film with change in molarity of the precursor solution; the only variation observed was in the case of surface morphology of the film. The studies revealed that spray rate and temperature had significant role in controlling the uniformity and phase purity of the films. Good quality CTS films were obtained when the spray rate was minimum (3 ml/min) at substrate temperature of 325 °C. Solar cell fabricated with stannic chloride precursor showed almost four times enhancement in cell efficiency in comparison with cell fabricated using stannous chloride precursor. The best among the solar cell fabricated with stannic chloride precursor had efficiency of 0.84%.

References

[1] V. G. Rajeshmon, *Prospects of Sprayed CZTS Thin Film Solar Cells from the Perspective of Material Characterization and Device Performance.* PhD thesis, Cochin University of Science and Technology, 2013.

[2] H. Zhang, M. Xie, S. Zhang, and Y. Xiang, "Fabrication of highly crystallized cu2sns3 thin films through sulfurization of sn-rich metallic precursors," *Journal of Alloys and Compounds*, vol. 602, pp. 199 – 203, 2014.

[3] Y. Dong, J. He, L. Sun, Y. Chen, P. Yang, and J. Chu, "Effect of sulfurization temperature on properties of cu2sns3 thin films and solar cells prepared by sulfurization of stacked metallic precursors," *Materials Science in Semiconductor Processing*, vol. 38, pp. 171 – 176, 2015.

[4] V. Robles, J. Trigo, C. Guilln, and J. Herrero, "Copper tin sulfide (cts) absorber thin films obtained by co-evaporation: Influence of the ratio cu/sn," *Journal of Alloys and Compounds*, vol. 642, pp. 40 – 44, 2015.

[5] K. Chino, J. Koike, S. Eguchi, H. Araki, R. Nakamura, K. Jimbo, and H. Katagiri, "Preparation of cu2sns3 thin films by sulfurization of cu/sn stacked precursors," *Japanese Journal of Applied Physics*, vol. 51, p. 10NC35, oct 2012.

[6] D. Tiwari, T. K. Chaudhuri, T. Shripathi, U. Deshpande, and R. Rawat, "Non-toxic, earth-abundant 2tetragonal films direct-coated from single metal-organic precursor solution," *Solar Energy Materials and Solar Cells*, vol. 113, pp. 165 – 170, 2013.

[7] C. Wu, Z. Hu, C. Wang, H. Sheng, J. Yang, and Y. Xie, "Hexagonal cu2sns3 with metallic character: Another category of conducting sulfides," *Applied Physics Letters*, vol. 91, no. 14, p. 143104, 2007.

[8] D. M. Berg, R. Djemour, L. Gtay, G. Zoppi, S. Siebentritt, and P. J. Dale, "Thin film solar cells based on the ternary compound cu2sns3," *Thin Solid Films*, vol. 520, no. 19, pp. 6291 – 6294, 2012.

[9] D. M. Berg, R. Djemour, L. Gtay, S. Siebentritt, P. J. Dale, X. Fontane, V. Izquierdo-Roca, and A. Prez-Rodriguez, "Raman analysis of monoclinic cu2sns3 thin films," *Applied Physics Letters*, vol. 100, no. 19, p. 192103, 2012.

[10] B. Li, Y. Xie, J. Huang, and Y. Qian, "Synthesis, characterization, and properties of nanocrystalline cu2sns3," *Journal of Solid State Chemistry*, vol. 153, no. 1, pp. 170 – 173, 2000.

[11] D. Avellaneda, M. T. S. Nair, and P. K. Nair, "Cu2sns3 and cu4sns4 thin films via chemical deposition for photovoltaic application," *Journal of the Electrochemical Society*, vol. 157, no. 6, pp. D346–D352, 2010.

[12] P. A. Fernandes, P. M. P. Salomé, and A. F. da Cunha, "A study of ternary cu2sns3and cu3sns4thin films prepared by sulfurizing stacked metal precursors," *Journal of Physics D: Applied Physics*, vol. 43, p. 215403, may 2010.

[13] N. Aihara, A. Kanai, K. Kimura, M. Yamada, K. Toyonaga, H. Araki, A. Takeuchi, and H. Katagiri, "Sulfurization temperature dependences of photovoltaic properties in cu2sns3-based thin-film solar cells," *Japanese Journal of Applied Physics*, vol. 53, p. 05FW13, apr 2014.

[14] V. Rajeshmon, C. S. Kartha, K. Vijayakumar, C. Sanjeeviraja, T. Abe, and Y. Kashiwaba, "Role of precursor solution in controlling the opto-electronic properties of spray pyrolysed cu2znsns4 thin films," *Solar Energy*, vol. 85, no. 2, pp. 249 – 255, 2011.

[15] S. Vanalakar, G. Agawane, A. Kamble, C. Hong, P. Patil, and J. Kim, "Fabrication of cu2sns3 thin film solar cells using pulsed laser deposition technique," *Solar Energy Materials and Solar Cells*, vol. 138, pp. 1 – 8, 2015.

[16] Y. Dong, J. He, X. Li, W. Zhou, Y. Chen, L. Sun, P. Yang, and J. Chu, "Synthesis and optimized sulfurization time of cu2sns3 thin films obtained from stacked metallic precursors for solar cell application," *Materials Letters*, vol. 160, pp. 468 – 471, 2015.

[17] T. P. Rao and M. Santhoshkumar, "Effect of thickness on structural, optical and electrical properties of nanostructured zno thin films by spray pyrolysis," *Applied Surface Science*, vol. 255, no. 8, pp. 4579 – 4584, 2009.

[18] U. Chalapathi, Y. Jayasree, S. Uthanna, and V. Sundara Raja, "Effect of annealing temperature on the properties of spray deposited cu2sns3 thin films," *physica status solidi (a)*, vol. 210, no. 11, pp. 2384–2390, 2013.

[19] P. A. Fernandes, P. M. P. Salom, and A. F. da Cunha, "Cuxsnsx+1 (x = 2, 3) thin films grown by sulfurization of metallic precursors deposited by

dc magnetron sputtering," *physica status solidi c*, vol. 7, no. 34, pp. 901–904, 2010.

[20] M. Santhosh, D. Deepu, C. S. Kartha, K. R. Kumar, and K. Vijayakumar, "All sprayed ito-free cuins2/in2s3 solar cells," *Solar Energy*, vol. 108, pp. 508 – 514, 2014.

[21] M. Adelifard, M. M. B. Mohagheghi, and H. Eshghi, "Preparation and characterization of cu2sns3ternary semiconductor nanostructures via the spray pyrolysis technique for photovoltaic applications," *Physica Scripta*, vol. 85, p. 035603, feb 2012.

[22] Y.-X. Guo, W.-J. Cheng, J.-C. Jiang, and J.-H. Chu, "The effect of substrate temperature, cu/sn ratio and post-annealing on the phase-change and properties of cu2sns3 film deposited by ultrasonic spray pyrolysis," *Journal of Materials Science: Materials in Electronics*, vol. 27, pp. 4636–4646, May 2016.

[23] V. V. Brus, I. S. Babichuk, I. G. Orletskyi, P. D. Maryanchuk, V. O. Yukhymchuk, V. M. Dzhagan, I. B. Yanchuk, M. M. Solovan, and I. V. Babichuk, "Raman spectroscopy of cu-sn-s ternary compound thin films prepared by the low-cost spray-pyrolysis technique," *Appl. Opt.*, vol. 55, pp. B158–B162, Apr 2016.

[24] D. Deepu, C. S. Kartha, and K. Vijayakumar, "How spray rate influences the formation and properties of transparent conducting sno2 thin films," *Journal of Analytical and Applied Pyrolysis*, vol. 121, pp. 24 – 28, 2016.

[25] M. Chen, J. Zhao, and X. Zhao, "Scanning electrochemical microscopy studies of micropatterned copper sulfide (cuxs) thin films fabricated by a wet chemistry method," *Electrochimica Acta*, vol. 56, no. 14, pp. 5016 – 5021, 2011.

[26] T. S. Reddy, R. Amiruddin, and M. S. Kumar, "Deposition and characterization of cu2sns3 thin films by co-evaporation for photovoltaic application," *Solar Energy Materials and Solar Cells*, vol. 143, pp. 128 – 134, 2015.

[27] W. Tang, Y. Chao, X. Weng, L. Deng, and K. Xu, "Optical property and the relationship between resistivity and surface roughness of indium tin oxide thin films," *Physics Procedia*, vol. 32, pp. 680 – 686, 2012. The 18th International Vacuum Congress (IVC-18).

Chapter 4

Tuning optoelectronic properties of CTS film for improving cell parameters

Contents

4.1 Introduction

In this chapter stoichiometry related route is used to improve conjoint structural, electrical, optical and morphological properties of CTS thin film for solar cell application. As CTS is compound intended for solar cell application, it is imperative to know how its properties change with stoichiometric variations. This chapter is totally devoted for presenting results of these studies and is divided into two parts: first part discusses about structural, electrical, optical, morphological and compositional properties of CTS film with variation in copper, sulfur and tin concentrations and in each case, solar cells were also fabricated. The second part discusses improvement of solar cell parameters by introducing a transparent buffer layer between ITO and CTS layer.

4.2 Copper variation

In this section, influence of Cu concentration on optoelectronic properties of CTS films has been analyzed. A number of research groups so far studied significance of Cu concentration on properties of CTS thin films and these studies

indicate that copper concentration plays vital role in determining structure and optoelectronic properties of CTS films [1–4]

4.2.1 Experimental

In order to study optoelectronic and structural properties, the films were deposited over ultrasonically cleaned soda lime glass substrates, at 325 °C. Film deposition was done using the same precursors as those of the previous chapter (copper chloride ($CuCl_2.2H_2O$), stannic chloride ($SnCl_4.5H_2O$) and thiourea (CH_4N_2S) for Cu, Sn and S respectively). The precursor solution was uniformly sprayed over the glass substrate at the rate of 3 ml/min. For varying copper concentration in the precursor solution, the stoichiometric ratio (Cu:Sn:S) in the precursor solution was taken as x:0.8:12 and the value of x (copper concentration) was varied from 0.8 to 2.8 with increment step of 0.4, keeping sulfur and tin concentrations the same. These samples were named Cu0.8, Cu1.2, Cu1.6, Cu2, Cu2.4, and Cu2.8 respectively with copper variation.

4.2.2 Structural studies

4.2.2.1 Structural studies using X-ray diffraction (XRD)

All these films were analyzed using XRD and results are shown in Figure 4.1. On varying copper concentration in the precursor solution, there is chance for developing secondary phases in the final product [5] and that was the major issue analyzed here. XRD studies proved that films were polycrystalline in nature with tetragonal structure, having characteristic planes (112), (200), (220) and (312) of tetragonal structure, with preferential orientation along (112) plane. On increasing copper concentration in spray solution, new peak originated at 46.38° (denoted by #) belonging to $Cu_{(2-x)}S$ phase [6]. However, intensity of the new phase was negligible. XRD analysis also revealed that peak intensity of CTS phase increased as Cu concentration increased up to 1.6; further increase in copper concentration resulted in stagnation of peak height. This observation concluded that increase in copper concentration assists CTS film growth up to some limit and after this, unwanted/impurity phase formation takes place. The same behavior was also reported in CTS and CZTS thin

films [7] [8]. At lower copper concentration, samples did not give any XRD peak and this may be due to the amorphous nature of the formed film.

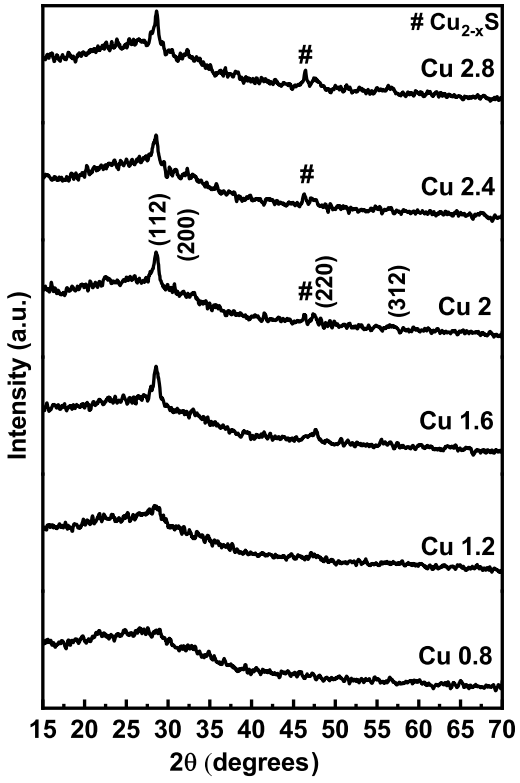

Figure 4.1: XRD patterns of CTS films deposited at different copper concentrations

4.2.2.2 Structural studies using Raman spectra

Raman analysis of samples Cu 0.8, Cu 1.6 and Cu 2.8 were done and the results were presented in Figure 4.2. From the Raman spectra, significant peaks are observed at 294, 337 and 475 cm^{-1}. Intense peak at 337 cm^{-1} and low intense peak at 294 cm^{-1} correspond to CTS with tetragonal structure [9]. The peak at 475 (denoted by #) corresponds to binary impurity phase of copper [10].

4.2.3 Electrical characterization

All samples showed p-type conductivity in hot probe and Hall measurement. From Hall measurement, electrical resistivity decreased with increase in copper concentration. Same behavior was also reported by Guo et al for CTS

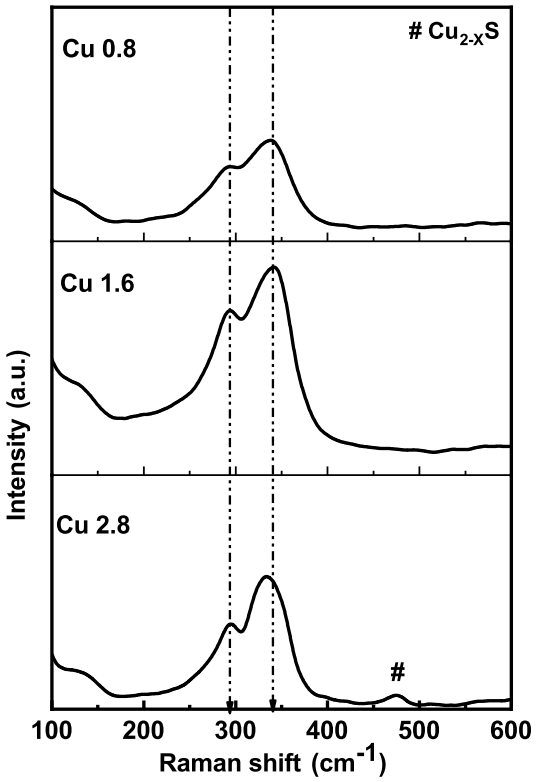

Figure 4.2: Raman analysis of CTS films deposited at different copper concentrations

Table 4.1: Electrical characterizations of CTS films with different copper concentration.

Sample Name	Carrier Concentration (cm^{-3})	Resistivity (Ωcm)	Mobility (cm^2/Vs)
Cu0.8	1.90×10^{20}	2.76×10^{-2}	1.19
Cu1.2	6.54×10^{20}	7.83×10^{-3}	1.22
Cu1.6	1.04×10^{21}	4.46×10^{-3}	1.35
Cu2	1.33×10^{21}	3.49×10^{-3}	1.35
Cu2.4	1.63×10^{21}	3.41×10^{-3}	1.13
Cu2.8	4.09×10^{21}	1.73×10^{-3}	0.88

thin film [2]. Low resistivity and high carrier concentration at high copper

concentration may be due to creation of more acceptors and hence production of more holes with increase in copper concentration.

4.2.4 Optical properties

Optical band gap was deduced from Tau plot (Figure 4.3) and band gap decreased with increase in copper concentration up to 1.6 (Cu1.6); the decrease in band gap may be due to increase in the crystallinity of the film [9]. On increasing copper above 1.6 (Cu2, Cu2.4 and Cu2.8) there is again increase in the band gap and this increase is possibly due to the presence secondary phase of copper [11].

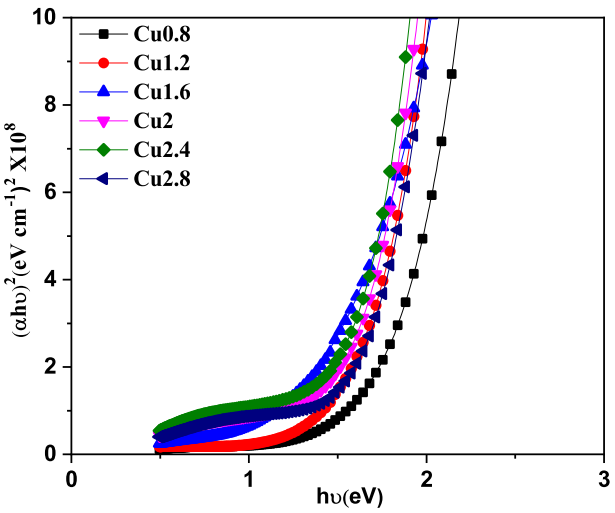

Figure 4.3: Tauc plot of samples with different copper concentration

4.2.5 Morphological characterization

Figure 4.4 shows AFM image of samples Cu2.8, Cu1.6 and Cu0.8. From this, it is observed that CTS films completely cover substrate surface. RMS roughness of samples increases with increase in copper concentration in precursor solution. Surface of samples having high copper concentration was not smooth; this uneven surface is not suitable for solar cell fabrication because this may result in formation of shunting path for the photo-generated carriers.

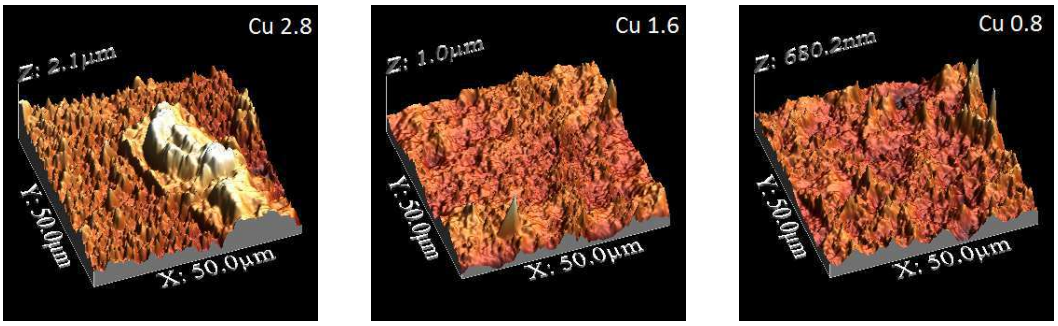

(a) *(b)* *(c)*

Figure 4.4: AFM image of samples (a). Cu 2.8,(b). Cu 1.6 and (c). Cu 0.8

4.2.6 Compositional analysis

It is very important to know how atomic concentration of each element varied with variation of copper concentration in the precursor solution. Depth profile analysis of the sample was done using Argon ion etching to get elemental concentration of samples from surface to bulk of the film using XPS. Figure 4.5 represents atomic concentration of elements (Cu, Sn, S and O) vs etch time of samples (a) Cu 0.8, (b) Cu 1.6 and (c) Cu 2.8. For lower copper concentration sample (Cu 0.8) oxygen content in the films was very high and excess oxygen in films replaced sulfur, leading to low sulfur concentration in the film. Copper concentration in the films increased with increase in the precursor solution. In all samples copper concentration at the surface of the film was low as compared to the bulk of the film. But in the case of tin, atomic concentration was high at the surface as compared to the bulk of the film. Sulfur concentration of the samples was found to be lower than of stoichiometric samples and this may be due to high volatile nature of sulfur at higher temperature. After a few etch cycles, atomic concentration of copper, tin and sulfur became stable throughout the thickness of the film.

4.2.7 Solar cell fabrication

Characterization studies of samples (Cu0.8 to Cu2.8) shows that optical, electrical and structural properties can be tuned with copper concentration. To evaluate how copper concentration affected photoelectric properties, solar cells were fabricated using the structure of ITO/CTS/In_2S_3/Ag, and the cells were

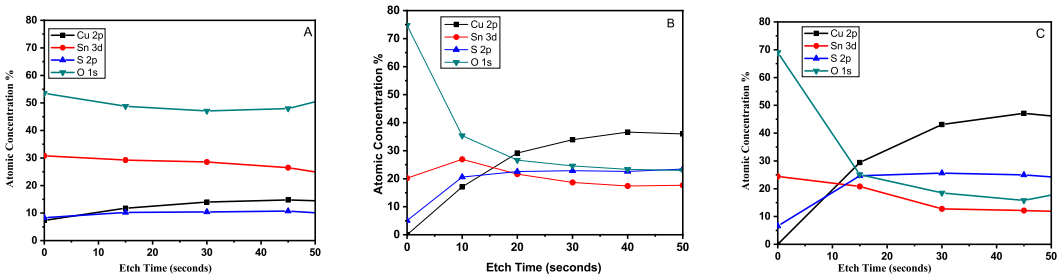

(a) *(b)* *(c)*

Figure 4.5: Compositional analysis of (a). Cu0.8,(b). Cu1.6 and (c). Cu2.8

Table 4.2: Photovoltaic parameters of the samples S 0.8 to S 2.8

Sample Name	V_{OC} (mV)	J_{SC} (mA/cm^2)	FF (%)	Efficiency (%)
S 0.8	No activity			
S 1.2	135±24	1.9±0.21	47±5	0.12±0.04
S 1.6	350±18	5.85±0.28	40±1	0.82±0.02
S 2	270±10	7.28±0.49	36±4	0.70±0.02
S 2.4	245±3	7.69±0.11	35±1	0.66±0.02
S 2.8	short			

named as S 0.8, S 1.2, S 1.6, S 2, S 2.4 and S 2.8 respectively. CTS film deposited with spray rate, volume of spray, substrate temperature and molarity are 3 ml/min, 30 ml, 325 °C and 0.005 M respectively. Here In_2S_3 (InS), was used as buffer layer; it was deposited over the CTS layer using same CSP method with In:S ratio as 1.2:12, and substrate temperature at 350 °C. Spray rate was 4 ml/min [12]. Vacuum evaporated Ag electrodes with area of 0.03 cm^2 were deposited above the In_2S_3 layer in order to make the front contact.

Table 4.2 shows photovoltaic parameters of solar cells S 0.8 to S 2.8 with error limit. The error calculation was done in the same as described in chapter 2 (2.7.1 Error calculation). Among the cells S1.6 showed better efficiency (same as that in the case of previous chapter); here copper concentration of the CTS film was 1.6. For further increase in copper concentration, there was decrease in the open circuit voltage. But short circuit current density showed

increasing nature with copper concentration; this may be due to the decrease in resistance of the layer with increase in copper concentration.

4.3 Sulfur variation

XPS analysis (Figure 4.5) pointed out that atomic concentration of sulfur in the sample was not up to the stoichiometry, due to it volatile nature. Commonly sulfurization in sulfur vapors and H_2S gas are used for increasing sulfur content of films [13, 14]. Sulfurization using H_2S gas is the easiest method but the process can be done in specialized equipment due to its toxicity; compared to H_2S gas, elemental sulfur is safe, but controlling atomic concentration in the film was difficult. Hence we used a simple method for increasing sulfur concentration: we increased sulfur concentration of precursor solution in order to increase the sulfur content of the film.

4.3.1 Experimental details

The precursors used for film deposition were copper chloride ($CuCl_2.2H_2O$), stannic chloride ($SnCl_4.5H_2O$) and thiourea (CH_4N_2S) for Cu, Sn and S respectively. Here also films were deposited over ultrasonically cleaned soda lime glass at 325 °C with spray rate of 3 ml/min. In order to understand effect of sulfur concentration on film properties, films were deposited with different sulfur concentrations while copper and tin concentrations were kept constant. For film deposition, Cu:Sn:S ratio of precursor solution was taken as 1.6:0.8:x where value of x (sulfur concentration) varies from 12 to 28 with increment of 8 and the samples were named as 12 TU, 20 TU and 28 TU respectively

4.3.2 Structural studies

4.3.2.1 Structural studies using X-ray diffraction (XRD)

Results of XRD analysis are shown in Figure 4.6. From the XRD data the peaks corresponding to (112), (200), (220), and (312) planes of Cu_2SnS_3 with tetragonal structure were seen. Structural properties of the sample have no

variations with change in sulfur concentration in samples. With sulfur concentration variation any peak corresponding to impurity phase was not detected from XRD; also there was no change in peak with sulfur variation.

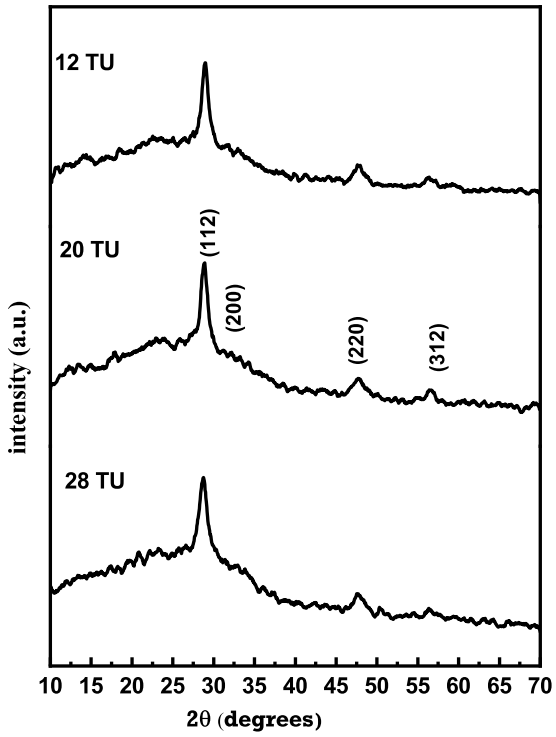

Figure 4.6: XRD patterns of CTS films deposited with different sulfur concentration

4.3.2.2 Structural studies using Raman analysis

In order to confirm phase formation, Raman analysis was done. From the Raman spectra (Figure 4.7) Raman shift corresponding to tetragonal structure of CTS was observed. In addition to CTS phase, sample 28TU showed peak corresponding to $Cu_{(2-x)}S$ phase also. At higher thiourea concentration in the precursor solution, there is a tendency for the formation of secondary phase. But from the XRD analysis the impurity phase could not be detected; this may be either due to the amorphous nature of the impurity phase or due to the minute quantity of the formed phase.

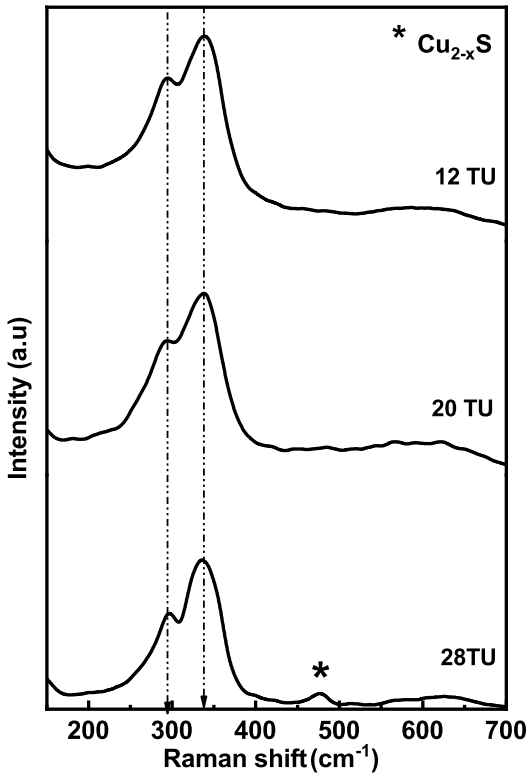

Figure 4.7: Raman analysis of CTS films deposited at different sulfur concentrations

4.3.3 Electrical properties

Hall measurement data of samples are tabulated in Table 4.3. All samples showed p-type conductivity as proved from both Hall measurement and hot probe analysis. Carrier concentration, resistivity and mobility of the samples do not show any significant variation with sulfur variation.

4.3.4 Optical properties

Absorption spectra of all samples were recorded in the range of 190 - 2500 nm. From the Tauc plot, band gap was calculated (Figure 4.8). From the Tauc plot all sample showed band gap of 1.5 eV. Sulfur concentration does not affect optical properties of the films.

Table 4.3: Electrical characterizations of CTS films with different sulfur concentration.

Sample Name	Carrier Concentration (cm^{-3})	Resistivity (Ωcm)	Mobility (cm^2/Vs)
12 TU	$1.04x10^{21}$	$4.46x10^{-3}$	1.35
20 TU	$1.23x10^{21}$	$4.50x10^{-3}$	1.13
28 TU	$5.24x10^{20}$	$8.30x10^{-3}$	1.44

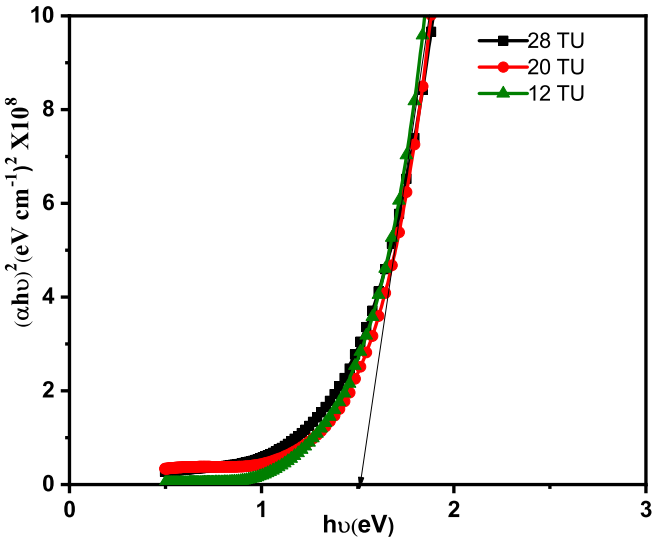

Figure 4.8: Tauc plot of samples with different sulfur concentrations

4.3.5 Compositional analysis

To recognize how atomic concentration of sulfur in the film varied with increase the sulfur concentration in the precursor solution, XPS analysis of sample with higher sulfur concentration (28 TU) was done. Figure 4.9 represents atomic concentration of elements (Cu, Sn, S and O) vs etch time of sample CTS 28 TU. Comparing with sample having sulfur concentration of 12 (Figure 4.5) there is slight increase in atomic concentration of sulfur.

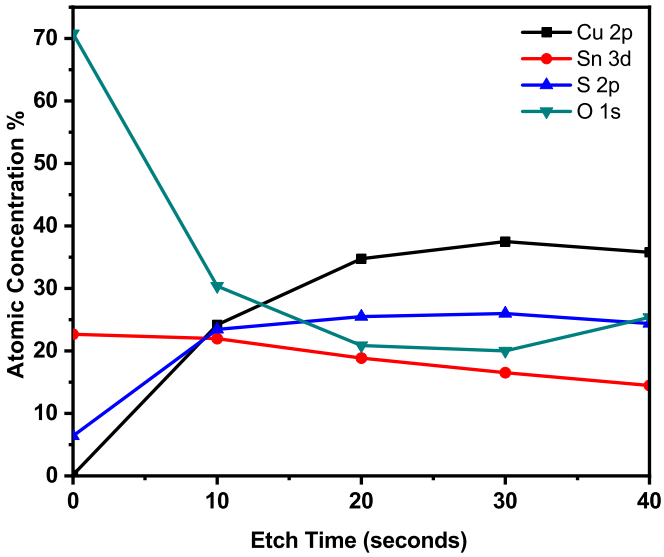

Figure 4.9: Compositional analysis of CTS films sample CTS 28 TU

Table 4.4: Photovoltaic parameters of the device S 12, S 20 and S 28 with error limit

Sample Name	V_{OC} (mV)	J_{SC} (mA/cm^2)	FF (%)	Efficiency (%)
S 12	350±18	5.85±0.28	40±1	0.82±0.02
S 20	348±9	5.7±0.22	40±1	0.79±0.01
S 28	380±4	5.63±0.04	32	0.68±0.003

4.3.6 Solar cell fabrication

Solar cells were fabricated with 12 TU, 20 TU and 28 TU samples to assess consequence of sulfur concentration on photoelectric properties. Solar cells fabricated using the same structure of ITO/CTS/In_2S_3/Ag and these were named as S 12, S 20 and S 28 respectively. The deposition condition for CTS film are spray rate 3 ml/min, volume of spray 6 ml, and deposition temperature 325 °C. Table 4.4 shows photovoltaic parameters of solar cells (S 12 to S 28). From the illuminated J-V characteristics it becomes clear that increase in sulfur concentration does not affect the cell parameters and this also points out that excess oxygen (in the place of sulfur) in the CTS film has no role in carrier transport. Hence sulfur concentration of 12 was selected for

further studies.

4.4 Tin variation

Here, we focus on relationship of crystal structure, electrical properties and optical properties with tin concentration. Solar cells were also fabricated in order to find the relationship between photoelectric properties with tin variation.

4.4.1 Experimental details

Films were deposited over ultrasonically cleaned soda lime glass at substrate temperature of 325 °C and spray rate of 3 ml/min. Here also precursors used were copper chloride ($CuCl_2.2H_2O$), stannic chloride ($SnCl_4.5H_2O$) and thiourea (CH_4N_2S) for Cu, Sn and S respectively. In order to study variation in optoelectronic properties of CTS films with tin concentration, samples were prepared by varying tin concentration in the precursor solution. Cu:Sn:S ratio in the precursor solution was taken as 1.6:y:12 where value of y (tin concentration) varies from 0.2 to 1.2 with a step of 0.2. The samples were named as Sn 0.2, Sn 0.4, Sn 0.6, Sn 0.8, Sn 1 and Sn 1.2 respectively.

4.4.2 Structural studies

4.4.2.1 Structural studies using X-ray diffraction (XRD)

Figure 4.10 illustrates XRD pattern of samples with different tin concentrations. Sample Sn 0.4 to sample Sn 1.2 have preferential orientation along (112) plane with low intense plane (200), (220) and (312) which correspond to tetragonal phase of Cu_2SnS_3. Along with the CTS phase, sample Sn 1.2 shows additional peak at 15° which corresponds to impurity phase of SnS_2 [15]. However, sample Sn 0.2 (with lowest tin concentration) shows peaks corresponding to CuS phase [16] [17]. On increasing tin concentration, CuS phase vanishes and CTS phase becomes more prominent, up to sample Sn 0.8. Further increase in tin concentration resulted in diminished CTS phase and appearance

of SnS_2 binary phase. This phase of tin, along with the CTS phase, is unwanted since SnS_2 being an n type semiconductor this may be undesirable for hetero junction nature of the prepared device.

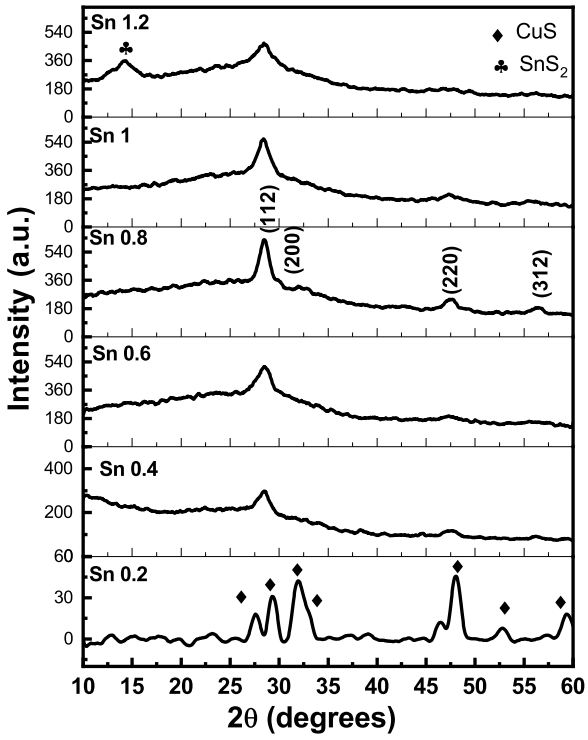

Figure 4.10: XRD patterns of CTS films with different tin concentration

4.4.2.2 Structural studies using Raman analysis

Even though XRD analysis gives details of phases present in the samples, it does not throw any light on the phases with amorphous nature, if present. In order to confirm exact details of phases that are present in the samples, Raman analysis was carried out. Figure 4.11 depicts Raman analysis results of the of CTS films with different tin concentration. Raman shifts at 294 cm^{-1} and 337 cm^{-1} are corresponding to the tetragonal structure of CTS; hence it is clear that samples Sn 0.6 to Sn 1 consist of tetragonal phase of Cu_2SnS_3 only. For Sn 0.4 sample, along with CTS phase an additional shift is observed at 474 $cm^{-1}$and this confirms presence of CuS binary phase [18] [19]. In the case of sample Sn 0.2, peak at 474 cm^{-1} corresponding to the CuS phase, is the prominent one. But for this sample in both XRD and Raman,

no peak corresponding to the CTS phase is observed. Here, in addition to CuS phase, another peak is observed at 326 cm^{-1} whose cause of origin is not clear. Also in sample Sn 1.2 an additional peak at 226 cm^{-1} is present this peak corresponds to impurity phase of tin [20].

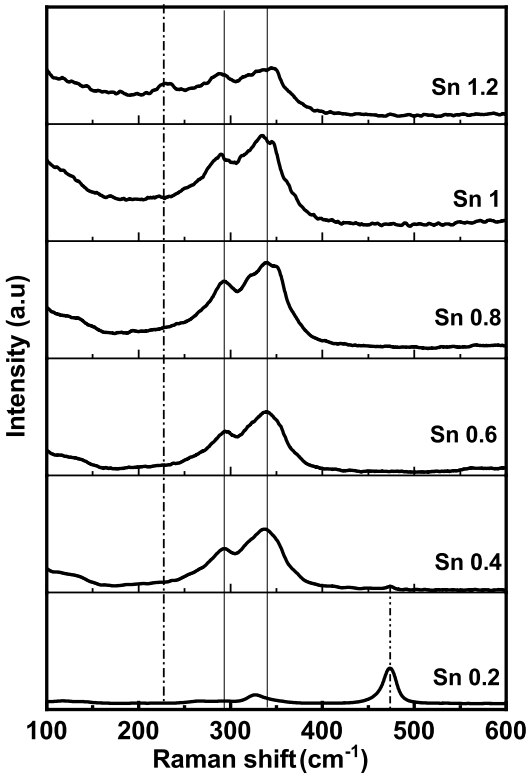

Figure 4.11: Raman spectrum of CTS films with different tin concentration

4.4.3 Optical characterization

Absorption spectra of samples (Sn 0.2 to Sn 1.2) were recorded in the wavelength range 190 - 2500 nm and band gaps were calculated by plotting ($h\nu$) vs $(\alpha h\nu)^2$ graph were is the absorption coefficient of the material. Figure 4.12 points out that majority of the samples possess band gap around 1.5 eV. It is clearly seen that on increasing the tin concentration, the band gap initially decreases (up to Sn 1) and on further increase in tin concentration (Sn 1.2) the band gap increased. Optical band gap values of the samples are given in the Table 4.5. The samples possess two band gaps; one around 2 eV and the other near 1.5 eV. Among these, the higher one exists in samples Sn

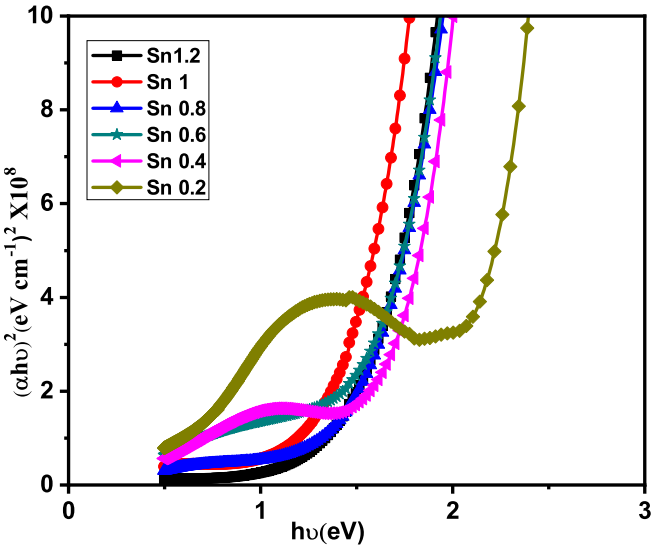

Figure 4.12: $h\nu$ vs $(\alpha h\nu)^2$ plot of CTS film with different tin concentration

Table 4.5: Band gap of CTS film with different tin concentration

Sample Name	Band Gap (eV)
Sn 0.2	2.1
Sn 0.4	1.68
Sn 0.6	1.5
Sn 0.8	1.5
Sn 0.1	1.45
Sn 1.2	1.5

0.2 which have low tin concentration. Hence naturally this can be attributed to the copper Sulfide phase as indicated by the XRD results (Figure 4.10) and Raman analysis (Figure 4.11). In the case of Sn 0.4, the higher band gap almost vanishes making it approximately equal to 1.68 eV. Similarly the prominence of higher band gap decreases considerably, as we go to the sample with higher tin concentration. In addition to higher band gap an absorption in the low energy region is observed for low tin concentration sample (Sn 0.2 to Sn 0.6), this is due to formation of two phases CTS and CuS; in the case of Sn 0.2 and Sn 0.4 sample it is very clear, as CuS is very prominent there (with weak CTS phase). But for other samples with higher tin concentration (Sn

Table 4.6: Electrical characterization of CTS films

Sample Name	Carrier Concentration (cm^{-3})	Resistivity (Ωcm)	Mobility (cm^2/Vs)
Sn 0.2	5.6x 10^{21}	1.14 x 10^{-3}	9.75x 10^{-1}
Sn 0.4	2.4x 10^{21}	3x 10^{-3}	8.84 x 10^{-1}
Sn 0.6	1.55 x 10^{21}	4.12 x 10^{-3}	9.77 x 10^{-1}
Sn 0.8	1.04 x 10^{21}	4.46 x 10^{-3}	1.35 x 10^{0}
Sn 1	3.72 x 10^{20}	6.32 x 10^{-2}	2.65 x 10^{-1}
Sn 1.2	1.71 x 10^{20}	2.11 x 10^{-1}	1.73 x 10^{-1}

0.6) instead of CuS, the copper is present as a defect creating the absorption; this happens as a result of having not enough tin in the sample. For samples having higher tin concentration (from Sn 0.8 onwards) this is totally absent indicating that whole Cu is used for forming CTS.

4.4.4 Electrical characterization

Electrical properties of the samples are tabulated in the Table 4.6. All samples showed p-type conductivity. Carrier concentration was 5.6×10^{21} cm^{-3} for sample Sn 0.2 and on increasing tin concentration, carrier concentration decreased to 1.71×10^{20} cm^{-3} (for Sn 1.2 sample). The decrease in the carrier concentration may be due to reduction in defect due to Cu and CuS phase with increase in tin concentration. Resistivity of the samples shows considerable variation with tin concentration. In the case of the sample Sn 0.2, resistivity is 1.14×10^{-3} Ωcm, and the resistivity increased by two orders (2.11×10^{-1} Ωcm) on increasing tin concentration (Sn 1.2).

4.4.5 Compositional analysis

XPS analysis was carried out for sample Sn 0.4, Sn 0.8 and Sn 1.2. The relative atomic concentrations of each element vs. sputtering cycles/thickness of CTS sample are presented in Figure 4.13. It can be understood that surface

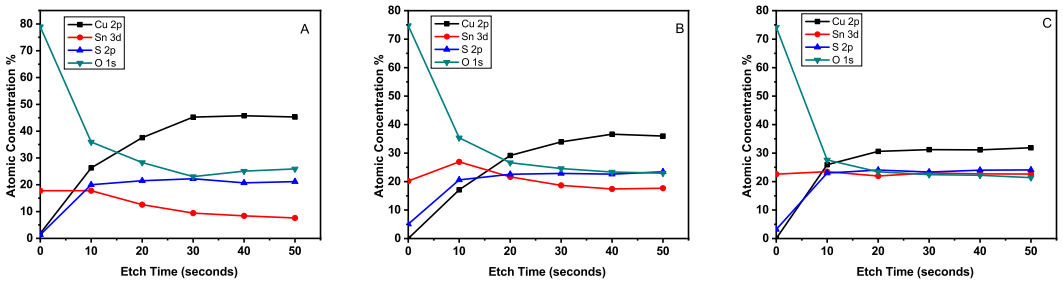

(a) *(b)* *(c)*

Figure 4.13: Compositional analysis of samples (a). Sn 0.4,(b). Sn 0.8 and (c). Sn 1.2

atomic composition of each sample is different from its bulk composition. In all samples, atomic concentration ratio of copper to tin was maintained almost the same as in precursor solution. Sulfur has high volatile nature at higher temperature and this may be the reason for the lower sulfur content in CTS film. Atomic concentration of tin in the surface of the film is higher than that of bulk which is also observed in CZTS thin film [21]. In the case of lower tin concentration the copper concentration in the film is higher and more tin is seen in the surface of the film than that of bulk (Sn 0.4 and Sn 0.8); but in the case higher tin concentration samples, tin concentration throughout the film was almost constant. Tin is probably expelled to surface of the sample in the case of sample with higher Cu/Sn ratio.

4.4.6 Solar cell fabrication

For understanding photovoltaic properties of these thin films, solar cells were fabricated using these samples as absorber layers with the structure ITO/CTS/In_2S_3/Ag. The devices were named as S 0.2, S 0.4, S 0.6, S 0.8, S 1 and S 1.2 respectively. Solar cell parameters are tabulated in Table 4.7. In_2S_3, was deposited over the CTS layer which acted as the buffer layer. Deposition of In_2S_3 layer was also carried out through CSP technique. Here Indium to sulfur ratio was taken as 1.2:12 in precursor solution. Vacuum evaporated Ag electrode with area of 0.03 cm^2 was given above the In_2S_3 layer as the front contact.

Table 4.7: Cell parameters of CTS solar cells having different tin concentrations

Tin Concentration	V_{OC} (mV)	J_{SC} (mA/cm^2)	FF (%)	Efficiency (%)
S 0.2	292±55	8.07±1.03	31±9	0.76±0.4
S 0.4	376±2	8.47±0.03	44±1	1.39±0.01
S 0.6	354±1	6.9±0.07	45±1	1.09±0.02
S 0.8	350±18	5.85±0.28	40±1	0.82±0.02
S 1	335±12	4.52±0.15	36±2	0.54±0.04
S 1.2	260±2	3.77±0.08	30±1	0.3±0.01

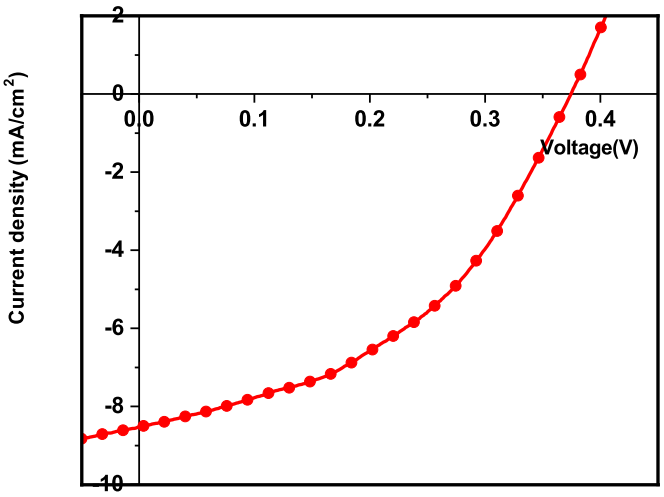

Figure 4.14: J-V characteristics of the CTS solar cell S 0.4 (under illumination)

Increasing tin concentration leads to formation of SnS_2 binary phase in the film and this may be the reason for reduction in cell performance. Needless to say that presence of n type SnS_2 semiconductor impurity phase in the p type absorber layer is detrimental for solar cell functioning. The best device fabricated was S 0.4 having Efficiency (η) 1.4, fill factor (FF) 44, open circuit voltage (V_{OC}) 0.374 V and short circuit current density (J_{SC}) 8.5 mA/cm^2. From the structure analysis it was found that Sn 0.4 is a mixture of CTS and CuS phase. It is also reported that small quantity of CuS impurity phase improve the solar cell parameters [22].

4.5 Improvement of solar cell parameters by introducing interlayer between ITO and CTS

In the previous section, solar cells were fabricated with CTS using the structure glass/ITO/CTS/ In_2S_3/Ag. Cu, Sn and S concentration of CTS films were varied to see how it affected solar cell performance; from this, better efficiency was obtained for solar cells with Cu:Sn:S ratio of 1.6:0.4:12. However many of the early reports on solar cells fabricated with CTS absorber layer showed current density greater than 30 mA/cm^3. Low current density in the present case may be due to the interface loss between ITO and CTS layer. In thin film solar cells or such other electronic devices, interface between the collection point and the device play significant role in the performance of the device. Here the device fabricated is extremely thin (300 nm) and only small quantity of precursor solution is used for cell fabrication (6 ml for CTS) which makes thickness very small. Hence interface should be smooth. In spray pyrolysed CTS thin film the initial layer of the film formed over the ITO surface may be irregular leading to rough interface between ITO and CTS which may significantly limit the carrier collection. In order to improve interface between the ITO and the CTS layer thin layer of ZnO layer was given between ITO and CTS layer.

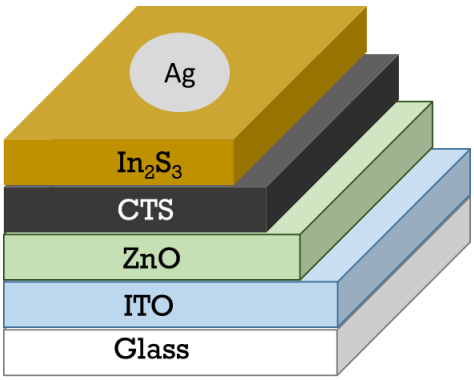

Figure 4.15: Schematic diagram of solar cell

4.5.1 Experimental

ZnO thin film was deposited on ITO coated soda-lime glass substrates using the same CSP technique. Zinc acetate dihydrate (Zn $(CH_3COO)_2.2H_2O$) was used as source of zinc and the solvent was mixture of demineralized water and isopropyl alcohol (1:1 ratio). The solution for spray was prepared by dissolving (Zn $(CH_3COO)_2.2H_2O$) in the solvent solution and few drops of acetic acid also was added to the solution to prevent precipitation due to hydroxide formation. Molarity, substrate temperature and spray rate are taken as 0.1 M, 350 °Cand 3 ml/min respectively. To optimize the thickness of the ZnO layer volume of precursor solution was varied from 3 ml to 12 ml in steps of 3 ml. The absorber layer (CTS) of solar cell was deposited using same precursor and deposition conditions were similar to above cases with Cu:Sn:S ratio taken as 1.6:0.4:12 (optimized from previous study).

Solar cells were fabricated using structure (ITO/ZnO /CTS/In_2S_3/Ag). These were named as S 3, S 6, S 9 and S 12 respectively. Schematic diagram of fabricated solar cell is shown in Figure 4.15.

Table 4.8: Cell parameters of CTS solar cell (S3 to S12)

Sample Name	V_{OC} (mV)	J_{SC} (mA/cm^2)	FF (%)	Efficiency (%)
S 3	378±6	8.4±0.03	43	1.38±0.03
S 6	387±3	8.3±0.04	44±1	1.44±0.02
S 9	422±10	5.93±0.43	48±1	1.19±0.08
S 12	423±4	5.88±0.24	34±1	.84±0.03

Illuminated photovoltaic parameters of fabricated solar cells with various ZnO layer thicknesses (by varying the volume of the spray solution) are tabulated in the Table 4.8. The error calculation was done in same way as described in chapter 2 (2.7.1). Among the solar cells fabricated, S 6 showed better efficiency and the J-V characteristics of best one is shown in the Figure 4.16. The best device was having Efficiency (η) of 1.46, fill factor (FF) of 45,

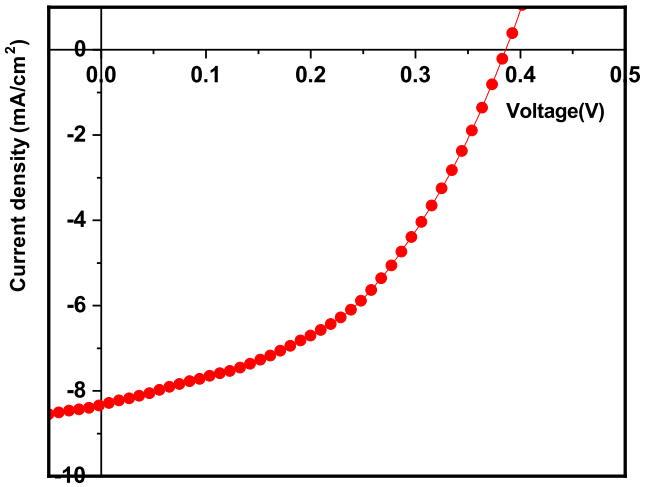

Figure 4.16: J-V characteristics of the CTS solar cell S 6 (under illumination)

open circuit voltage (V_{OC}) of 0.386 V and short circuit current density (J_{SC}) of 8.32 mA/cm^2. From the illuminated solar cell parameters, open circuit voltage (V_{OC}) had increasing nature with increase in the ZnO thickness; but short circuit current density exhibited decreasing nature with ZnO thickness. This may be either due to the higher resistance of the ZnO layer and/or low light transmittance with increased thickness of ZnO layer. In our own research group, ZnO is well studied material and resistance of ZnO can be reduced by Al doping [23]. Solar cells were fabricated using the structure ITO/ZnO:Al /CTS/In_2S_3/Ag as shown in the schematic diagram (Figure 4.17).Here also solar cells were fabricated with thickness was varied for ZnO:Al layer; for this the precursor volume of ZnO:Al was varied from 3 ml to 12 ml in steps of 3 ml same as in the earlier case. These cells were named as Al 3, Al 6, Al 9 and Al 12 respectively. Here also the error calculation was done in same way as described in chapter 2 (section 2.7.1).

Figure 4.18 represent SEM image of ITO coated over the glass plate and Figure 4.19 represent ZnO:Al deposited over the ITO. From the SEM image (Figure 4.19) it is understood that depositing ZnO:Al over ITO makes the surface smooth.

From the illuminated J-V curve (Figure 4.20) it becomes clear that current density of the solar cell improved significantly. Reason for the increased J_{SC}

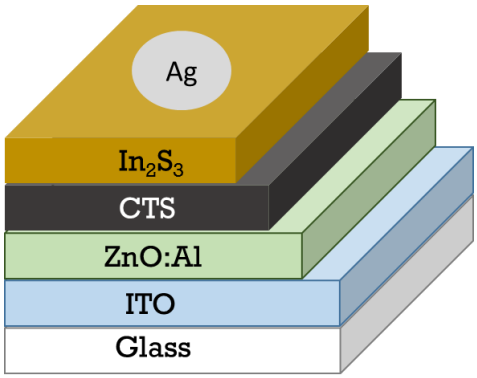

Figure 4.17: Schematic diagram of solar cell

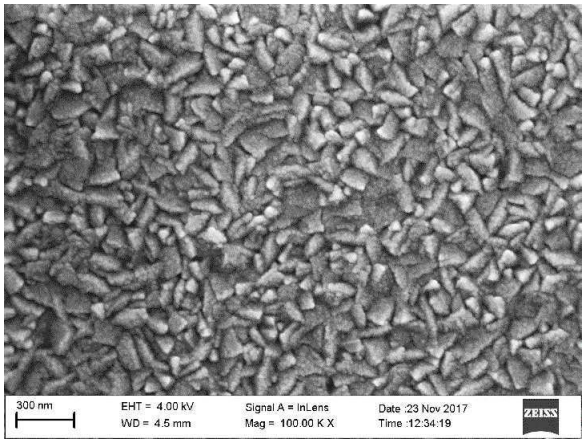

Figure 4.18: SEM image of ITO deposited over glass plate

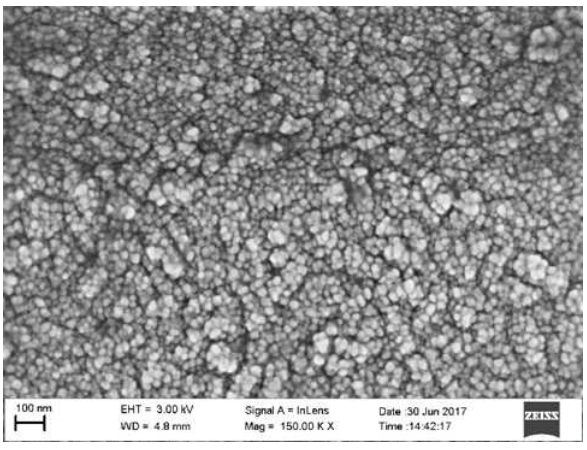

Figure 4.19: SEM image of ZnO:Al deposited over ITO

Table 4.9: Cell parameters of CTS solar cell with different ZnO:Al thickness

Sample Name	V_{OC} (mV)	J_{SC} (mA/cm^2)	FF (%)	Efficiency (%)
Al 3	3804	9.20.24	401	1.420.01
Al 6	41014	9.660.38	472	1.880.05
Al 9	5254	6.640.49	462	1.60.06
Al 12	5317	6.350.12	412	1.370.06

can be mainly due to improvement in the interface between ITO and CTS by the deposition of ZnO:Al layer. Thin layer of ZnO:Al layer probably reduced shunting path which resulted in improvement in the cell parameters.

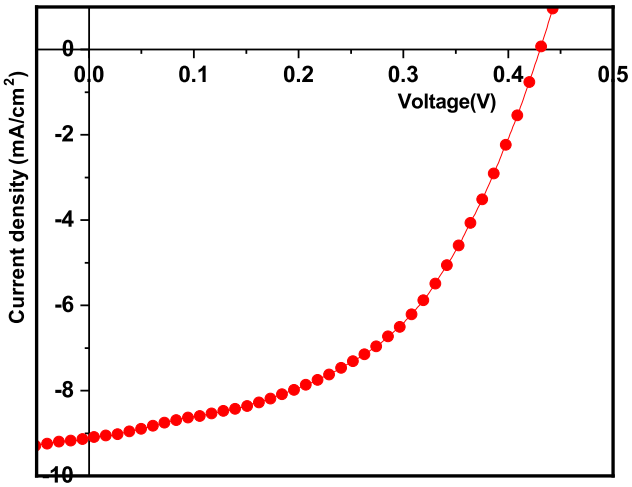

Figure 4.20: J-V characteristics of the CTS solar cell Al 6 (under illumination)

ZnO:Al plays critical role in cell fabrication; generally open circuit voltage of CTS based solar cell lays in the range of 300 mV. But on introducing ZnO:Al layer, the open circuit voltage increased significantly. The cells were fabricated with different ZnO:Al thickness (by varying precursor volume); among these, cell Al 6 shows better efficiency and the illuminated J-V characteristics of best one is shown in the Figure 4.20. The best device fabricated having an Efficiency (η) of 1.93, fill factor (FF) of 49, open circuit voltage (V_{OC}) of 0.430 V and short circuit current density (J_{SC}) of 9.1 mA/cm^2

4.6 Conclusion

Semiconductors with tunable composition and band gaps are of great interest for photovoltaic and photocatalytic application. Our studies point out that optoelectronic properties of CTS thin films can be tuned by varying copper, and tin concentration. Solar cells were fabricated with these CTS absorber layers having structure ITO/CTS/In_2S_3/Ag. Enhancement in solar cell parameters was recognized for Cu:Sn:S ratio of 1.6:0.4:12 which exhibited maximum power conversion efficiency of 1.4. Trials on further improvement of solar cell parameters were done initially by introducing interlayer of ZnO between ITO and CTS and the device showed efficiency of 1.46. On replacing the ZnO layer with ZnO:Al, the efficiency (η) could be improved to 1.93, with fill factor (FF) of 49, open circuit voltage (V_{OC}) of 0.430 V and short circuit current density (J_{SC}) of 9.1 mA/cm^2. It is the highest reported efficiency of CTS based solar cell deposited fully (absorber and buffer layer) by employing CSP technique.

References

[1] V. Robles, J. Trigo, C. Guilln, and J. Herrero, "Copper tin sulfide (cts) absorber thin films obtained by co-evaporation: Influence of the ratio cu/sn," *Journal of Alloys and Compounds*, vol. 642, pp. 40 – 44, 2015.

[2] Y.-X. Guo, W.-J. Cheng, J.-C. Jiang, and J.-H. Chu, "The effect of substrate temperature, cu/sn ratio and post-annealing on the phase-change and properties of cu2sns3 film deposited by ultrasonic spray pyrolysis," *Journal of Materials Science: Materials in Electronics*, vol. 27, pp. 4636–4646, May 2016.

[3] M. Adelifard, M. M. B. Mohagheghi, and H. Eshghi, "Preparation and characterization of cu2sns3ternary semiconductor nanostructures via the spray pyrolysis technique for photovoltaic applications," *Physica Scripta*, vol. 85, p. 035603, feb 2012.

[4] M. He, A. Lokhande, I. Y. Kim, U. Ghorpade, M. Suryawanshi, and J. H. Kim, "Fabrication of sputtered deposited cu2sns3 (cts) thin film

solar cell with power conversion efficiency of 2.39 %," *Journal of Alloys and Compounds*, vol. 701, pp. 901 – 908, 2017.

[5] N. T. Hiep, F. Shotaro, H. Takashi, C. Jakapan, M. akashi, N. Shuji, and I. Shigeru, "Impact of precursor compositions on the structural and photovoltaic properties of spray-deposited cu2znsns4 thin films," *ChemSusChem*, vol. 9, no. 17, pp. 2414–2420, 2016.

[6] M. Wang, F. Xie, W. Li, M. Chen, and Y. Zhao, "Preparation of various kinds of copper sulfides in a facile way and the enhanced catalytic activity by visible light," *J. Mater. Chem. A*, vol. 1, pp. 8616–8621, 2013.

[7] J. Zhen, C. Qinmiao, C. Jin, W. Tingting, L. Zhenqing, and D. Xiaoming, "The photovoltaic properties of novel narrow band gap cu2sns3 films prepared by a spray pyrolysis method," *RSC Adv.*, vol. 5, pp. 28885–28891, 2015.

[8] V. Rajeshmon, M. R. Menon, C. S. Kartha, and K. Vijayakumar, "Effect of copper concentration and spray rate on the properties cu2znsns4 thin films deposited using spray pyrolysis," *Journal of Analytical and Applied Pyrolysis*, vol. 110, pp. 448 – 454, 2014.

[9] U. Chalapathi, Y. Jayasree, S. Uthanna, and V. Sundara Raja, "Effect of annealing temperature on the properties of spray deposited cu2sns3 thin films," *physica status solidi (a)*, vol. 210, no. 11, pp. 2384–2390, 2013.

[10] A. Cuevas, R. Romero, D. Leinen, E. Dalchiele, J. Ramos-Barrado, and F. Martin, "Effect of the stoichiometry of cuxs thin films on the optical and electrical properties and the solar thermal performance," *Solar Energy Materials and Solar Cells*, vol. 134, pp. 199 – 208, 2015.

[11] P. Vas-Umnuay, K.-J. Kim, D.-H. Kim, and C.-H. Chang, "Conformal growth of copper sulfide thin films on highly textured surface via microreactor-assisted solution deposition," *CrystEngComm*, vol. 17, pp. 2827–2836, 2015.

[12] M. Santhosh, D. Deepu, C. S. Kartha, K. R. Kumar, and K. Vijayakumar, "All sprayed ito-free cuins2/in2s3 solar cells," *Solar Energy*, vol. 108, pp. 508 – 514, 2014.

[13] M. Nakashima, T. Yamaguchi, H. Itani, J. Sasano, and M. Izaki, "Cu2sns3 thin film solar cells prepared by thermal crystallization of evaporated cu/sn precursors in sulfur and tin atmosphere," *physica status solidi c*, vol. 12, no. 6, pp. 761–764, 2015.

[14] K. Moriya, K. Tanaka, and H. Uchiki, "Cu2znsns4thin films annealed in h2s atmosphere for solar cell absorber prepared by pulsed laser deposition," *Japanese Journal of Applied Physics*, vol. 47, pp. 602–604, jan 2008.

[15] I. B. Kherchachi, H. Saidi, A. Attaf, N. Attaf, A. bouhdjar, H. bendjdidi, youcef Benkhetta, R. Azizi, and M. Jlassi, "Influence of solution flow rate on the properties of sns2 films prepared by ultrasonic spray," *Optik*, vol. 127, no. 8, pp. 4043 – 4046, 2016.

[16] M. R. Kim, H. A. Hafez, X. Chai, L. V. Besteiro, L. Tan, T. Ozaki, A. O. Govorov, R. Izquierdo, and D. Ma, "Covellite cus nanocrystals: realizing rapid microwave-assisted synthesis in air and unravelling the disappearance of their plasmon resonance after coupling with carbon nanotubes," *Nanoscale*, vol. 8, pp. 12946–12957, 2016.

[17] J. Kundu and D. Pradhan, "Influence of precursor concentration, surfactant and temperature on the hydrothermal synthesis of cus: structural, thermal and optical properties," *New J. Chem.*, vol. 37, pp. 1470–1478, 2013.

[18] S. L. L. Milekhin A G, Yeryukov N A and D. T. A, "Combination of surface- and interference-enhanced raman scattering by cus nanocrystals on nanopatterned au structures," *Beilstein J. Nanotechnol.*, vol. 6, pp. 749–754, 2015.

[19] U. Chalapathi, Y. Jayasree, S. Uthanna, and V. Sundara Raja, "Effect of annealing temperature on the properties of spray deposited cu2sns3 thin films," *physica status solidi (a)*, vol. 210, no. 11, pp. 2384–2390, 2013.

[20] G. G. Ninan, C. S. Kartha, and K. Vijayakumar, "On the preparation of n-type sns:cu using chemical spray pyrolysis for photovoltaic application: Effect of annealing," *Solar Energy Materials and Solar Cells*, vol. 157, pp. 229 – 233, 2016.

[21] D. R. Deepu, V. G. Rajeshmon, C. S. Kartha, and K. P. Vijayakumar, "Xps depth profile study of sprayed czts thin films," *AIP Conference Proceedings*, vol. 1591, no. 1, pp. 1666–1668, 2014.

[22] M. Santhosh, C. S. Kartha, K. R. Kumar, and K. Vijayakumar, "Thin film solar cells with extremely thin absorber layer having multiple absorption bands: A novel attempt," *Solar Energy*, vol. 122, pp. 712 – 717, 2015.

[23] T. Vimalkumar, *Highly conductive and transparent ZnO thin film using Chemical Spray Pyrolysis technique: Effect of doping and deposition parameters*. PhD thesis, Cochin University of Science and Technology, 2011.

Chapter 5

Fabrication of CTS based photovoltaic hetero-junction in superstrate structure

Contents

5.1 Introduction

Usually in the case of solar cells fabricated entirely using CSP technique (absorber and buffer layer deposition), superstrate structure (ITO/In_2S_3/ABSORBER/Ag)

is found to be inefficient to give photovoltaic activity in the case of absorbers like CIS,CTS,CZTS and CZS [1–4]; hence in the present work, in earlier chapters, we described characterization and fabrication having structure (ITO/ (CTS)/ In_2S_3/Ag). CTS is one of the novel absorber material and hence research works on CTS based solar cell is in preliminary stage. Also, there is no reported work on cell fabrication in superstrate structure completely using CSP technique; in this chapter, we describe in detail, the efforts for fabricating CTS based solar cells in superstrate structure to check the possibility of this structure.

5.2 Selection of electrode

The interface between semiconductor and metal become very significant since it affects electrical properties/carrier transport of the device [5]. In ideal case, junction should be ohmic without any defects or there should be no significant variation in its properties due to inter-diffusion at the interface. Making junction close to ideal one is a challenging task since most of the material has defects and interdiffusion between two different solids at higher temperature is unavoidable (especially for solar cells kept in open sunlight) at the junction.

According to work function of metal and semiconductor, the junction formed between metal and semiconductor can either be rectifying (Schottky junction) or non-rectifying (ohmic contact). The Schottky junction is a unidirectional system conducting current only in one direction and hence it can be used as rectifiers in high power circuits. In the case of solar cell fabrication formation of Schottky barrier damages open-circuit voltage at the interface. Nonrectifying contact has negligible resistance irrespective of the polarity of the applied voltage. This type of interface is called Ohmic contact. Ohmic contact is needed to create connections to other devices in an electronic system. In solar cells, role of metal contact is charge collection and hence ohmic contact is desired. According to the Schottky contact model, work function plays critical role in determining the characteristics of junction formed (the difference between the metal work function (ϕ) and the semiconductor Fermi level). Metal with deep work function can give Ohmic contact with p-type semiconductor

while for shallow work function metal, Schottky barrier is formed with p-type semiconductor. Solar cell parameters of these devices such as open circuit voltage (V_{OC}) and short circuit current density (J_{SC}) are limited by the selection of metal contact used. On a careful review of the research history of CTS, it becomes clear that it is in the embryonic stage and hence the suitable metal electrode for cell fabrication is not yet examined.

5.2.1 Experimental Procedure

CTS thin films were deposited as usual, over ITO coated glass plate, using precursors copper chloride ($CuCl_2.2H_2O$), stannic chloride ($SnCl_4.5H_2O$) and thiourea ($SC(NH_2)_2$). Cu:Sn:S ratio in the precursor solution was taken as 1.6:0.8:12. The substrate temperature and the spray rate were 325 °C and 3 ml/min respectively. This aqueous solution was sprayed onto glass substrates using compressed air as a carrier gas. In order to optimize the top metal

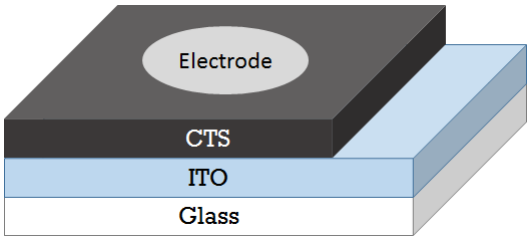

Figure 5.1: Schematic diagram of junction fabrication of semiconductor and metal electrode

electrode, metals with different work functions shown in Table 5.1 [6] (Ag, In, Al, Sn, Cu, and Au) were coated over CTS film deposited on ITO; electrodes were having same area (0.03 cm^2) and thickness (50 nm). Electrode deposition was done using vacuum evaporation technique and the samples were named as Ag, In, Al, Sn, Cu, and Au.

Figure 5.2 shows the J-V characteristics of different electrodes with a bias voltage applied to it. All devices with electrodes except Sn, In and Al had linear J-V curves, indicating that ohmic contacts were formed with Au, Ag and Cu. (Sn, In and Al had non-linear curves probably due to Schottky junction formed with CTS film). According to the Schottky contact model, hole

Table 5.1: Work function and resistivity of different metallic elements

Element	Work Function (eV)	Resistivity (Ωm)
Aluminum	4.06 - 4.26	2.82×10^{-8}
Silver	4.26 - 4.74	1.59×10^{-8}
Copper	4.53 - 5.10	1.68×10^{-8}
Indium	4.09	8×10^{-8}
Tin	4.42	1.09×10^{-7}
Gold	5.10 - 5.47	2.3×10^{-8}

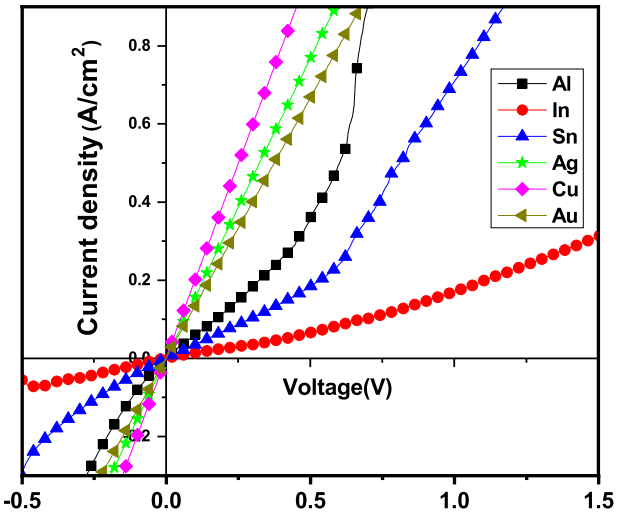

Figure 5.2: J-V characteristics of the CTS thin film with different electrode

extraction efficiency is highly influenced by anode work function. Only metals with deep work function exhibit ohmic contact with the semiconductor. But in case of Silver electrode, its work function is lower than that of all other electrodes selected here; however, it shows ohmic nature with the semiconductor [7]. This strange behavior of Silver electrode may be due to the formation of a thin layer of silver oxide (Ag_2O) at the interface. Interestingly Ag_2O is a p-type semiconductor with enhanced work function [8]. Even though Ag, Au, and Cu show ohmic contact Ag is better choice for the cell fabrication because from our observation Cu has higher diffusion coefficient as compared

to Ag electrode and Au electrode was not economical.

5.3 Selection of buffer layer

Schematic diagram of solar cell fabricated in superstrate structure is shown in Figure 5.3. Different types of buffer layer were used for thin film solar cell fabrication such as CdS, ZnS, ZnO, In_2S_3, In_2Se_3, SnS etc. Generally, CdS

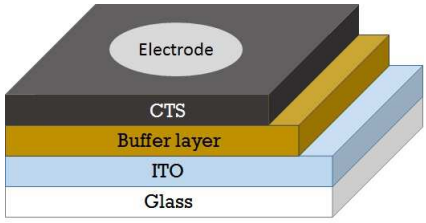

Figure 5.3: Schematic diagram of solar cell fabrication

is used as buffer layer for CTS solar cell fabrication [9–13] since it has high transparency, direct band gap and shows n-type conductivity [14, 15]. Also it is one of the best material used for fabricating CIGS, CIS, and CZTS solar cells [16–18]. However, the main drawbacks of CdS thin film are absorption in the blue part of the spectrum and toxicity of the material Cd. Other materials used for CTS solar cell fabrication are ZnO and In_2S_3 [19, 20]. These two materials also have high transparency in the visible region and both are n-type in conductivity [21, 22]. Solar cells were fabricated using these three materials to select the better buffer material.

CdS buffer layer deposited over ITO coated glass substrate employing Chemical Bath Deposition using precursors Cadmium Sulfate, Sodium hydroxide, Ammonia, Triethylamine and Thiourea. After deposition of CdS layer the sample was washed with demineralized water to remove loosely sticking particles. Then the film was dried to remove excess moisture. After drying, the CdS layer deposited on the back side of the film was removed with HCl. CTS layer was then deposited over the CdS layer using CSP with Cu:Sn:S in the ratio of 1.6:0.4:12 (total volume of CTS precursor for spray was 6 ml, spray rate was 3 ml/min and molarity was 0.005 M as optimized from the previous chapter). But on depositing CTS layer over the CdS layer, there was

re-evaporation of CdS layer and I-V measurement showed failure of junction formation due to re-evaporation. Hence further trials using CdS were avoided.

ZnO thin films were deposited over the ITO coated glass using CSP technique; precursors were (Zn $(CH_3COO)_2.2H_2O$) dissolved in the solvent (a mixture of demineralized water and propanol in 1:1 volume ratio) and few drops of acetic acid also were added to the solution to prevent precipitation. The substrate temperature was 450 °C and molarity of precursor solution taken was 0.3 M and spray rate of 7 ml/min. CTS film of Cu:Sn:S ratio of 1.6:0.4:12 (total volume of of CTS precursor for spray 6 ml, spray rate of 3 ml/min and molarity 0.005 M as optimized from the previous chapter) was deposited over the ZnO layer. But the solar cell fabricated with structure ITO/ZnO/CTS/Ag did not have any light activity.

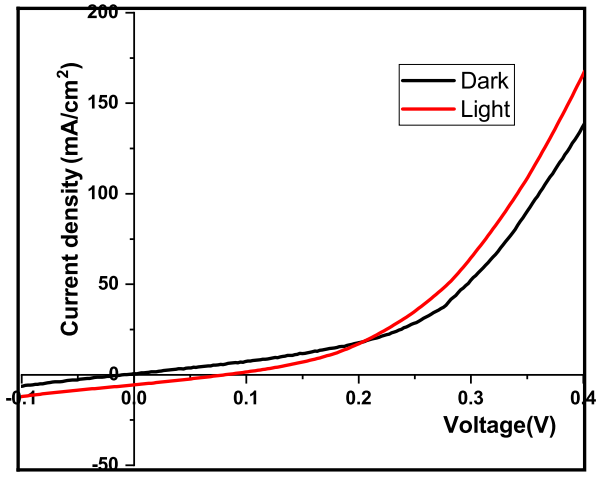

Figure 5.4: Illuminated J-V characteristics of the In_2S_3/CTS solar cell

In the next set of cells fabricated, In_2S_3 thin films were deposited over ITO substrates using CSP technique. An aqueous solution containing indium chloride and thiourea was used as precursors. Indium to sulfur ratio in the precursor solution was 1.2:12 (same as used in the previous chapter). Film deposition was at substrate temperature of 350 °C and spray rate of 4 ml/min and compressed air was used as carrier gas. Here also CTS films were deposited with Cu:Sn:S ratio of 1.6:0.4:12 (total volume of CTS precursor for spray 6 ml, spray rate of 3 ml/min and molarity 0.005 M as optimized from second

chapter). Fabricated solar cell exhibited very small light activity and the illuminated J-V characteristics shown in Figure 5.4.

5.4 Solar cell fabrication using ITO/In_2S_3/CTS structure: Trials for improvement

Absorber layer plays critical role in cell performance since it absorbs light and transfers the electromagnetic energy to the electron-hole pair. From previous chapter, it was observed that photovoltaic properties of CTS film vary with stoichiometric variations and hence solar cells were fabricated with different copper and tin concentrations. Sulfur concentration was always kept constant (12) for all trials and the deposition conditions for CTS film were also the same as in earlier cases. Indium sulfide was the buffer layer, prepared using In:S ratio as 1.2:12 with spray rate of 4 ml/min, the volume of indium sulfide precursor solution to be spayed 16 ml and a substrate temperature of 350 °C.

Table 5.2: Solar cell parameters with different tin and copper concentration

Copper Concentration	Tin Concentration	V_{OC} (mV)	J_{SC} (mA/cm^2)	FF (%)	Efficiency (%)
1.2	0.4	27±16	1.81±0.28	25±1	0.01±0.01
	0.8	70±44	0.71±0.19	25±3	0.01±0.01
	1.2	Noise			
1.6	0.4	94±29	2.73±0.04	26±1	0.07±0.02
	0.8	117±6	2.97±0.5	26±2	0.09±0.01
	1.2	100±24	1.7±0.07	25±2	0.06±0.02
2	0.4	Short			
	0.8				
	1.2	135±32	1.64±0.38	24±4	0.04±0.01

All the solar cells fabricated with different Copper and Tin concentrations had only slight activity as compared to the cases described in the previous chapter. Among these, the cell having copper concentration of 1.6 and tin concentration of 0.8 exhibited small improvement in activity as compared to the other cases which prompted us to have this ratio (1.6:0.8:12) for Cu:Sn:S for further works.

5.5 Optimization of buffer layer thickness

The buffer layer thickness should be optimum for better performance of solar cell. At lower thickness of buffer layer, junction formation is not proper due to diffusion of highly mobile copper atoms from absorber layer and this leads to shorting of device. For the higher thickness of buffer layer, light reaching the junction is restricted; along with this, high resistance of buffer layer also results in poor performance of the cell. In order to find out the optimum thickness of buffer layer, volume of the precursor solution was varied from 8 ml to 20 ml, in steps of 4 ml and the fabricated solar cell named as S8, S12, S16 and S20. Here the volume of spray solution of absorber layer (CTS) was kept constant (same as 6 ml as optimized). Four samples (each with six electrodes) were fabricated for each spray volume of the buffer layer and the photovoltaic parameters are shown in Table 5.3.

Table 5.3: Solar cell parameters with different Indium Sulfide thickness

Sample Name	V_{OC} (mV)	J_{SC} (mA/cm^2)	FF (%)	Efficiency (%)
S8	22±3	4.9±1.49	24±1	0.03±0.01
S12	83±11	5.95±0.35	26±2	0.125±0.01
S16	117±6	2.97±0.5	26±2	0.09±0.01
S20	122±27	1.73±0.34	31±6	0.06±0.01

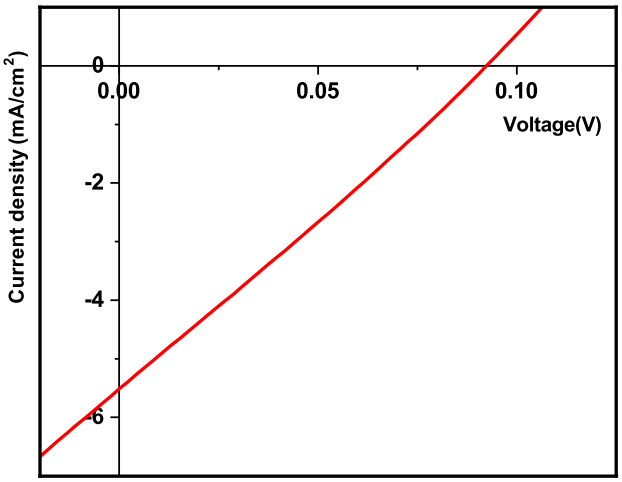

Figure 5.5: Illuminated J-V characteristics of the sample S12

From the thickness variation of buffer layer, better cell performance was obtained for buffer layer deposited with precursor volume of 12 ml (S12) and the device shows V_{OC} of 92 mV, J_{SC} of 5.49 mA/cm^2, fill factor of 28% and efficiency of 0.14%. Even though the voltage is slightly lower, this cell has better value for short circuit current. Illuminated J-V characteristic of the best-fabricated device is shown in Figure 5.5.

5.6 Optimization of buffer layer stoichiometry

In/S ratio was varied by changing the concentration of indium chloride in the precursor solution while the concentration of sulfur was kept constant (as four times higher than the required quantity) in order to compensate loss of Sulfur due to the volatile nature. Here the indium chloride concentration varied from 1 to 2.5 keeping deposition condition of absorber layer the same. For all concentrations of indium, four samples (each with six electrodes) were fabricated. All the six (isolated) electrodes in a single sample showed almost same efficiency and hence from among the six electrodes the best one was selected for error calculations. The photovoltaic parameters are shown in Table 5.4. By varying indium concentration from 1 to 2.5 (above and below

Table 5.4: Photovoltaic parameters of the CTS solar cells fabricated with different Indium Sulfide ratio

In:S Ratio	Sample Name	V_{OC} (mV)	J_{SC} (mA/cm^2)	FF (%)	Efficiency (%)
1:12	S1	42±4	6.19±0.14	25±1	0.06±0.01
1.2:12	S1.2	83±11	5.95±0.35	26±2	0.13±0.01
2:12	S2	118±23	2.47±0.55	28±2	0.08±0.01
2.5:12	S2.5	139±35	1.64±0.38	29±4	0.06±0.01

1.2), there was no appreciable enhancement in the cell efficiency/parameters.

5.7 Optimization of absorber layer thickness

Solar cell performance is usually controlled by thickness of absorber layer too. Lower thickness of absorber layer reduces the light absorption and high thickness of the absorber layer reduces the carrier collection. Thickness of the absorber layer was varied by varying the volume of spray solution of CTS. Here the volume of precursor solution varied from 3 ml to 12 ml in steps of 3 ml and the samples named as S3, S6, S9 and S12. The other deposition condition was kept the same as Cu:Sn:S ratio 1.6:0.8:12, spray rate at 3 ml/min and substrate temperature at 325 °C. The deposition conditions for the buffer layer were fixed as those of the earlier studies.

The photovoltaic parameters for solar cell fabricated with different absorber layer thickness are there in Table 5.5. Better cell performance was obtained for absorber layer deposited with precursor volume of 9ml. The optimized absorber layer precursor volume is different for superstrate structure comparing with the structure used in the previous chapter. And the device had V_{OC} = 94 mV, J_{SC} = 7.49 mA/cm^2, fill factor = 26% and efficiency = 0.18%. Illuminated J-V characteristics of best fabricated device is shown in Figure 5.6.

Table 5.5: Photovoltaic parameters of the CTS solar cells fabricated with different absorber layer thickness

Sample Name	V_{OC} (mV)	J_{SC} (mA/cm^2)	FF (%)	Efficiency (%)
S3	27±16	1.81±0.28	25±1	0.01±0.01
S6	83±11	5.95±0.35	26±2	0.125±0.01
S9	86±8	7.16±0.27	26±1	0.16±0.02
S12	122±11	3±0.49	27±2	0.01±0.01

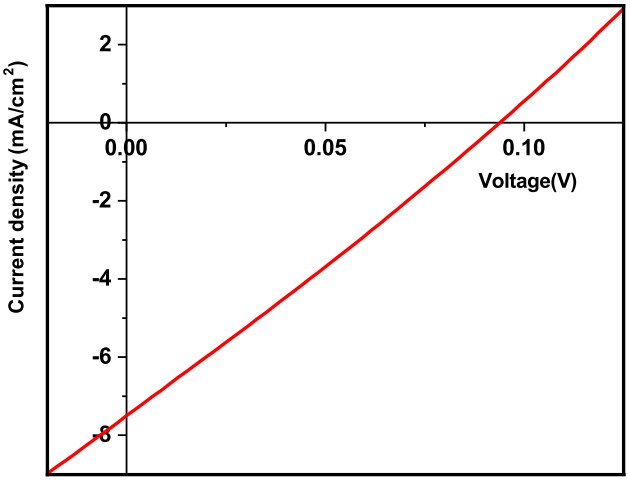

Figure 5.6: Illuminated J-V characteristics of the sample S9

5.8 Improvement of cell parameters

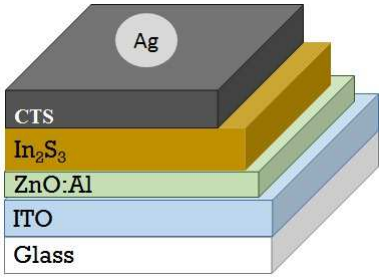

Figure 5.7: Schematic diagram of solar cell fabrication

Table 5.6: Photovoltaic parameters of the CTS solar cells fabricated with different window layer thickness

Sample Name	V_{OC} (mV)	J_{SC} (mA/cm^2)	FF (%)	Efficiency (%)
Z3	155±3	10.51±0.13	28±1	0.45±0.01
Z6	171±9	12.84±0.49	27±1	0.6±0.03
Z9	226±5	6.02±0.07	30±1	0.41±0.02
Z12	273±35	2.42±0.18	29±3	0.19±0.01

The window layer is a transparent thin layer usually deposited between buffer and transparent conducting layers. In general ZnO:Al, i-ZnO or combination of ZnO:Al, i-ZnO layer is used along with buffer layer in CIGS solar cell [23]. The main role of window layer is to block the shunting path and this makes improvements in solar cell performance; together with this, window layer can reduce surface recombination too. Here we deposited ZnO:Al of different thickness (the volume of the precursor solution varied from 3 to 12 ml in steps of 3 ml and the sample named as Z3, Z6, Z9 and Z12) as window layer and fabricated solar cells with absorber and buffer layer properties as optimized from the studies.

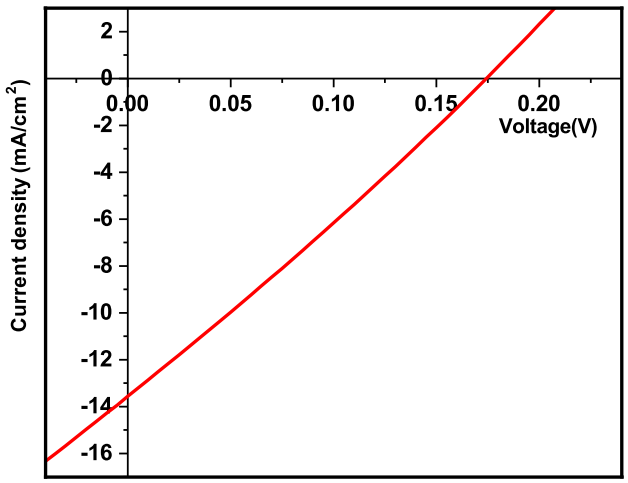

Figure 5.8: Illuminated J-V characteristics of the sample Z6

On introduction of ZnO:Al between ITO and In_2S_3 layer a drastic increase in short circuit current density was observed. The open circuit voltage increased with increase in the thickness of ZnO:Al; but the short circuit current density decreased after the volume of 6ml. Solar cell fabricated with window layer deposited with precursor volume of 6 ml (Z6) had V_{OC} = 174 mV, J_{SC} = 13.57 mA/cm^2, fill factor = 27% and efficiency = 0.63%. Illuminated J-V characteristics of the best fabricated device are shown in Figure 5.8.

5.9 Conclusion

In the present chapter, results of parametric studies on CTS based solar cell deposited using superstrate structure are reported; details of different steps were taken to improve the cell fabricated in this structure are also included. Optimization of the top electrode, buffer layer, Copper to Tin ratio of CTS layer, thickness of In_2S_3 layer, ratio of In_2S_3 layer and thickness of CTS layer were done. But the solar cell fabricated using superstrate structure showed poor cell performance. Finally, a trial was also done by introducing a window layer of ZnO:Al between ITO and In_2S_3 (buffer) layer, which improved the short circuit current density considerably; but the efficiency of this cell also was only 0.63%. Hence it can be concluded that in all trials, the superstrate structured cell showed poor cell parameters.

References

[1] T. John, C. Kartha, K. Vijayakumar, T. Abe, and Y. Kashiwaba, "Modification in cell structure for better performance of spray pyrolysed cuins2/in2s3 thin film solar cell," *Applied Physics A*, vol. 82, pp. 703–707, Mar 2006.

[2] M. Santhosh, D. Deepu, C. S. Kartha, K. R. Kumar, and K. Vijayakumar, "All sprayed ito-free cuins2/in2s3 solar cells," *Solar Energy*, vol. 108, pp. 508 – 514, 2014.

[3] V. Rajeshmon, C. S. Kartha, K. Vijayakumar, C. Sanjeeviraja, T. Abe, and Y. Kashiwaba, "Role of precursor solution in controlling the opto-

electronic properties of spray pyrolysed cu2znsns4 thin films," *Solar Energy*, vol. 85, no. 2, pp. 249 – 255, 2011.

[4] S. M. S., D. D. R., S. C., R. K., and V. K. P., "Improvement of sprayed cuzns/in2s3 solar cell efficiency by making multiple band gap nature more prominent," *Journal of Renewable and Sustainable Energy*, vol. 8, no. 2, p. 023502, 2016.

[5] T. Mori, T. Kozawa, T. Ohwaki, Y. Taga, S. Nagai, S. Yamasaki, S. Asami, N. Shibata, and M. Koike, "Schottky barriers and contact resistances on ptype gan," *Applied Physics Letters*, vol. 69, no. 23, pp. 3537–3539, 1996.

[6] H. B. Michaelson, "The work function of the elements and its periodicity," *Journal of Applied Physics*, vol. 48, no. 11, pp. 4729–4733, 1977.

[7] J. B. Kim, C. S. Kim, Y. S. Kim, and Y.-L. Loo, "Oxidation of silver electrodes induces transition from conventional to inverted photovoltaic characteristics in polymer solar cells," *Applied Physics Letters*, vol. 95, no. 18, p. 183301, 2009.

[8] M. R. Menon, M. Maheshkumar, K. Sreekumar, C. S. Kartha, and K. Vijayakumar, "Inverted polymer solar cells with indium sulfide electron selective layer," *Solar Energy Materials and Solar Cells*, vol. 94, no. 12, pp. 2212 – 2217, 2010.

[9] Y. Dong, J. He, X. Li, W. Zhou, Y. Chen, L. Sun, P. Yang, and J. Chu, "Synthesis and optimized sulfurization time of cu2sns3 thin films obtained from stacked metallic precursors for solar cell application," *Materials Letters*, vol. 160, pp. 468 – 471, 2015.

[10] J. Koike, K. Chino, N. Aihara, H. Araki, R. Nakamura, K. Jimbo, and H. Katagiri, "Cu2sns3 thin-film solar cells from electroplated precursors," *Japanese Journal of Applied Physics*, vol. 51, p. 10NC34, oct 2012.

[11] S. Vanalakar, G. Agawane, A. Kamble, C. Hong, P. Patil, and J. Kim, "Fabrication of cu2sns3 thin film solar cells using pulsed laser deposition technique," *Solar Energy Materials and Solar Cells*, vol. 138, pp. 1 – 8, 2015.

[12] N. Aihara, A. Kanai, K. Kimura, M. Yamada, K. Toyonaga, H. Araki, A. Takeuchi, and H. Katagiri, "Sulfurization temperature dependences of photovoltaic properties in cu2sns3-based thin-film solar cells," *Japanese Journal of Applied Physics*, vol. 53, p. 05FW13, apr 2014.

[13] R. Chierchia, F. Pigna, M. Valentini, C. Malerba, E. Salza, P. Mangiapane, T. Polichetti, and A. Mittiga, "Cu2sns3 based solar cell with 3% efficiency," *physica status solidi c*, vol. 13, no. 1, pp. 35–39, 2016.

[14] H. Moualkia, S. Hariech, and M. Aida, "Structural and optical properties of cds thin films grown by chemical bath deposition," *Thin Solid Films*, vol. 518, no. 4, pp. 1259 – 1262, 2009. Transparent Conductive Oxides.

[15] K. S. Ramaiah, A. K. Bhatnagar, R. D. Pilkington, A. E. Hill, and R. D. Tomlinson, "The effect of sulfur concentration on the properties of chemical bath deposited cds thin films," *Journal of Materials Science: Materials in Electronics*, vol. 11, pp. 269–277, Apr 2000.

[16] Y. Hashimoto, N. Kohara, T. Negami, N. Nishitani, and T. Wada, "Chemical bath deposition of cds buffer layer for gigs solar cells," *Solar Energy Materials and Solar Cells*, vol. 50, no. 1, pp. 71 – 77, 1998.

[17] N. Moritake, Y. Fukui, M. Oonuki, K. Tanaka, and H. Uchiki, "Preparation of cu2znsns4 thin film solar cells under non-vacuum condition," *physica status solidi c*, vol. 6, no. 5, pp. 1233–1236, 2009.

[18] A. Ennaoui, M. Lux-Steiner, A. Weber, D. Abou-Ras, I. Ktschau, H.-W. Schock, R. Schurr, A. Hlzing, S. Jost, R. Hock, T. Vo, J. Schulze, and A. Kirbs, "Cu2znsns4 thin film solar cells from electroplated precursors: Novel low-cost perspective," *Thin Solid Films*, vol. 517, no. 7, pp. 2511 – 2514, 2009. Thin Film Chalogenide Photovoltaic Materials (EMRS, Symposium L).

[19] D. Tiwari, T. K. Chaudhuri, T. Shripathi, U. Deshpande, and R. Rawat, "Non-toxic, earth-abundant 2tetragonal films direct-coated from single metal-organic precursor solution," *Solar Energy Materials and Solar Cells*, vol. 113, pp. 165 – 170, 2013.

[20] Q. Chen, X. Dou, Y. Ni, S. Cheng, and S. Zhuang, "Study and enhance the photovoltaic properties of narrow-bandgap cu2sns3 solar cell by pn junction interface modification," *Journal of Colloid and Interface Science*, vol. 376, no. 1, pp. 327 – 330, 2012.

[21] M. A. Mughal, R. Engelken, and R. Sharma, "Progress in indium (iii) sulfide (in2s3) buffer layer deposition techniques for cis, cigs, and cdte-based thin film solar cells," *Solar Energy*, vol. 120, pp. 131 – 146, 2015.

[22] T. Vimalkumar, N. Poornima, C. S. Kartha, and K. Vijayakumar, "Effect of precursor medium on structural, electrical and optical properties of sprayed polycrystalline zno thin films," *Materials Science and Engineering: B*, vol. 175, no. 1, pp. 29 – 35, 2010.

[23] C. E. Chang, C. Ji-Hyun, J. Duk-Young, and H. Byungyou, "Structural, electrical, and optical properties of zno film used as buffer layer for cigs thin-film solar cell," *Journal of Nanoscience and Nanotechnology*, vol. 16, no. 5, pp. 5087–5091, 2016.

Chapter 6

Summary and future prospects

Nonsilicon thin film solar cell such as Cu(In, Ga)Se_2 (CIGS), GaAs and CdTe, have undertaken rapid growths over the past times. But, these materials composed of scarce (In, Ga) and toxic (Cd) element so extensive consumption of these materials not possible. Therefore, a serious search for an alternative material need, which is economical, non-toxic earth-abundant and the deposition can be done in low-cost technique. CTS has been considered to be one of such material that full fill all these conditions and the deposition can be done with low-cost CSP technique. In the present study, CTS used as absorber material for solar cell fabrication.

First CTS absorber layer deposited using the precursor copper chloride ($CuCl_2.2H_2O$), stannous chloride ($SnCl_2.2H_2O$) and thiourea ($SC(NH_2)_2$) as a source of copper, tin, and sulfur respectively. It was observed that 325 °C be the optimum temperature for film deposition. The optoelectronic properties of the film do not change with molarity variation of precursor solution hence it is an effective method for thickness variation of CTS film. CTS solar cells were fabricated using In_2S_3 as a buffer layer, among the cell fabricated low molarity samples only shows the light activity. Different optimization work was done to improve the solar cell parameters like Copper and Tin concentration variation but it does not enhance the efficiency of the solar cell up to our expectation; maximum efficiency obtained was 0.25% for Cu:Sn:S ratio of 1.6:0.8:12. HCl in the precursor solution of tin might be the main reason for the low performance of the solar cell. Since the further work the tin precursor we replaced stannous chloride by stannic chloride.

Structural and electronic properties do not show significant variation with stannic chloride tin precursor but the optical band gap of the deposited film increase to 1.5 eV. Here also the solar cell fabricated with low molarity sample only shows light activity. From the optimization of deposition parameters,

Good quality CTS films were obtained when the spray rate of the precursor solution was minimum (3 ml/min) at a substrate temperature of 325 °C. Solar cell fabricated with structure ITO/CTS/In_2S_3/Ag and shows almost four times enhancement in cell efficiency in comparison with cell fabricated using stannous chloride precursor. The best among the solar cell fabricated has an efficiency of 0.84%.

Tuning of optoelectronic properties of the CTS film done by varying copper, and tin concentration. Improvement in solar cell parameters was observed for Cu:Sn:S ratio of 1.6:0.4:12 which shown maximum power conversion efficiency of 1.4%. Further improvement of solar cell parameters done initially by introducing interlayer of ZnO between ITO and CTS and the device showed an efficiency of 1.46%. On replacing the ZnO layer with ZnO:Al, the efficiency (η) could be improved to 1.93%, with fill factor (FF) of 49%, open circuit voltage (V_{OC}) of 0.430 V and short circuit current density (J_{SC}) of 9.1 mA/cm^2.

Finally, CTS based solar cell fabricated also using superstrate structure, optimization work was done to improve the cell parameters are; the top electrode, buffer layer, copper to tin ratio of CTS layer, the thickness of In_2S_3 layer, indium to sulfur ratio of In_2S_3 layer and thickness of CTS layer. But then again the superstrate structure displays poor cell performance. Finally, introducing a window layer of ZnO:Al between ITO and In_2S_3 (buffer) layer, which enhanced the short circuit current density considerably; but the efficiency of this cell moreover was only 0.63%. Hence in all trials, the superstrate structured cell showed poor cell parameters.

Future Prospects

The main research work on CTS based solar cell started in 2012 now it attain an efficiency of 4.63% within a short interval of time. Here also using CSP we get an efficiency of 1.93%. So there is a good chance for improvement of cell efficiency in the coming years. So CTS one of the promising material for cell fabrication in the future.

Low short circuit current density is the main challenge for CTS based solar cell prepared using the CSP technique. The short circuit current density can be improved by reducing the series resistance of the solar cell. Series resistance can be reduced by enhancing the conductivity of In_2S_3 (doping) or by depositing a highly conductive layer over In_2S_3 layer.

Annealing in the sulfur atmosphere can improve the grain growth and electrical transport of the carrier thereby enhancing the photovoltaic parameters of the device.

In the current work, solar cell fabrication done over sputtered ITO coated glass substrate. If we replace the costly sputtered ITO back contact with spray deposited FTO the cost of the solar cell can be reduced further reduction in the cost of the solar cell can be achieved by replacement of buffer layer(In_2S_3), with another low-cost non-toxic earth abundant wide band gap material.

List of publications

Journals:

1. Gincy Sunny, Titu Thomas, D.R. Deepu, C. Sudha Kartha and K.P. Vijayakumar, "*Thin film solar cell using earth abundant Cu_2SnS_3 (CTS) fabricated through spray pyrolysis: Influence of precursors*", Optik, vol. 144, 263 - 270, 2017.

2. Ho Soonmin, Gincy Sunny and Sharadrao A. Vanalakar, "*STUDIES ON Cu_2SnS_3 THIN FILMS: REVIEW*", ARPN Journal of Engineering and Applied Sciences, vol.13 (13), 2018.

3. Gincy Sunny, C. Sudha Kartha, and K. P. Vijayakumar, "*Tuning of opto-electronic properties of Cu_2SnS_3 thin films through variation of stoichiometry*", AIP Conference Proceedings 1591, 1750 (2014).

4. Gincy Sunny, C. Sudha Kartha, and K. P. Vijayakumar, "*Preparation of Cu_2SnS_3 thin film through Chemical Spray Pyrolysis: optimization of spray parameters*", (to be communicated ...)

5. Gincy Sunny, C. Sudha Kartha, and K. P. Vijayakumar, "*Nontoxic, facile and economical route for solar cell fabrication using Cu_2SnS_3 thin film: Tuning optoelectronic properties by variation in tin concentration*", (to be communicated ...)

Conferences:

1. Gincy Sunny, C. Sudha Kartha, and K. P. Vijayakumar, "*Effect of deposition temperature on the opto electronic properties of Cu_2SnS_3 thin film*", International conference on Energy Harvesting, Storage and Conversion (IC-EEE) 2015, 5^{th} - 7^{th} February, Organized by CUSAT, Cochin-22. *(International Conference)*

2. Gincy Sunny, C. Sudha Kartha, and K. P. Vijayakumar, "*Effect of Thickness Variation of CTS Thin Films by Chemical Spray Pyrolysis*", ASCII-2018, 14^{th} - 17^{th} February, Organized by CUSAT, Cochin-22. *(National Conference)*